2023-12-01

Preliminary assessment for Critical Minerals in the Terlingua Quicksilver District, Texas and Tres Marias Mine, Chihuahua, Mexico

Eduardo Lee Zuniga
University of Texas at El Paso

PRELIMINARY ASSESSMENT FOR CRITICAL MINERALS IN THE TERLINGUA QUICKSILVER DISTRICT, TEXAS, AND TRES MARIAS MINE, CHIHUAHUA, MEXICO

EDUARDO LEE ZUNIGA

Master's Program in Geological Sciences

APPROVED:

Philip Goodell, Ph.D., Chair

Richard Langford, Ph.D.

Raed Aldouri

Stephen L. Crites, Jr., Ph.D.
Dean of the Graduate School

Dedication

TO THE PILLARS OF MY WORLD,

TO MY PARENTS, WHOSE UNWAVERING ENCOURAGEMENT AND BOUNDLESS SUPPORT HAVE BEEN THE GUIDING LIGHTS THROUGHOUT MY ACADEMIC JOURNEY. YOUR BELIEF IN MY ABILITIES HAS BEEN MY GREATEST SOURCE OF STRENGTH.

TO MY BROTHER, A STEADFAST COMPANION ON THIS INTELLECTUAL ADVENTURE. YOUR SUPPORT AND SHARED MOMENTS OF LAUGHTER MADE THE CHALLENGES BEARABLE AND THE VICTORIES SWEETER.

TO ERIKA, WHOSE UNWAVERING ENCOURAGEMENT AND UNDERSTANDING HAVE BEEN A SOURCE OF INSPIRATION. YOUR BELIEF IN MY DREAMS AND THE COUNTLESS MOMENTS OF ENCOURAGEMENT PROPELLED ME FORWARD.

THIS THESIS STANDS AS A TESTAMENT TO THE LOVE, SUPPORT, AND UNDERSTANDING I HAVE RECEIVED FROM EACH OF YOU. THANK YOU FOR BEING MY CONSTANT ANCHORS, CHEERING ME ON DURING THE HIGHS AND PROVIDING SOLACE DURING THE LOWS. THIS ACHIEVEMENT IS AS MUCH YOURS AS IT IS MINE.

WITH HEARTFELT GRATITUDE,

EDDIE ZUNIGA

PRELIMINARY ASSESSMENT FOR CRITICAL MINERALS IN THE TERLINGUA QUICKSILVER DISTRICT, TEXAS, AND TRES MARIAS MINE, CHIHUAHUA, MEXICO

by

EDUARDO LEE ZUNIGA, B.S

THESIS

Presented to the Faculty of the Graduate School of

The University of Texas at El Paso

in Partial Fulfillment

of the Requirements

for the Degree of

MASTER OF SCIENCE

Departments of Earth, Environmental and Resource Sciences

THE UNIVERSITY OF TEXAS AT EL PASO

December 2023

Table of Contents

List of Tables

List of Figures

Abstract

Preliminary Assessment for Critical Minerals in the Terlingua Quicksilver District and Tres Marias Mine

The Terlingua Quicksilver district was discovered around the 1880s and was a mercury-producing district from 1900 through 1946. The most productive years were during World War one and two. From 1900-1946 the Terlingua Quicksilver District (TQD) produced 150,000 flasks; 80% came from three mines: the Rainbow-Chisos, Mariposa, and Study Butte mines. The structural controls of the Mercury mineralization within these mines are breccia pipes and fractures, often located near igneous intrusions. This study will assess the potential for Critical Minerals and Rare Earth Elements in the Terlingua Quicksilver District. Fifty-five samples have been collected and analyzed for forty-four different chemicals. Univariant, bivariant, and multivariant analyses have been applied to these data. Geochemical families identified are 1) REEs, 2) Y with LREE, 3) Zr-Hf-Nb-Ta, 4) Rb-Cs, 5) As-Sb, 6) Hg (As). The special distributions have been placed on a map, which shows the locations of three significant hydrothermal systems that have been enriched in CM and REEs, which are Black Mesa, Rainbow-Chisos mine, and Cigar Mountain. Future exploration should be directed at these sites.

1: Introduction

The city of Terlingua is in Brewster County. Situated between Big Bend Ranch State Park to the west and Big Bend National Park to the southeast. The Terlingua Quicksilver District is located near the Rio Grande, close to Lajitas, TX and Study Butte, TX. Terlingua is part of the Trans-Pecos region and the Chihuahuan Desert. The climate is arid with sparse vegetation. The topography is mountainous terrain characterized by rugged sierras, high plateaus, and gently sloping plains. The Terlingua Quicksilver district was first discovered in the late 19th century and was a producing district from 1900 through 1946 (Yates & Thompson, 1959). The most productive years were during both World Wars. However, the Native Americans of the region used the bright red cinnabar for pigment in pictographs and face-painting long before miners started removing quicksilver from this region.

Many studies followed the discovery of quicksilver in the district. Most were economic studies and surveys to understand the area more thoroughly and locate more quicksilver deposits. During the beginning of the 20th- century interest in the area increased to support the war efforts during World War One and Two. The Terlingua Quicksilver District (TQD) spans 20 miles east to west (Yates & Thompson, 1959). Most of the district is in Brewster County, TX yet the western boundary lies in Presidio County, Tx. In the end, the district had over twenty mines, the top 3 producing mines, Rainbow-Chisos, Mariposa, and Study Butte, produced about 90% of the Quicksilver (Yates & Thompson, 1959). The area was discovered in the late 1880s and produced about 150,000 flasks of Quicksilver from 1900 to 1946 (Yates & Thompson, 1959). The term Quicksilver refers to the mercury mined from the district. The primary ore mined from the TQD is cinnabar, a mercury sulfide (HgS), but other mineral ore were also producing mercury.

Approximately 10 miles south of Terlingua, Tx is the Tres Marias mine. The mine is part of the Manuel Benavides Municipality in Norther Chihuahua, MX. The Tres Marias mine is a carbonate hosted Pb, Zn deposit (Megaw, 2001). Mined intermittently from 1949 and finally closing in 1992; due to environmental issues forcing the smelter processing the oxide ores to close (Megaw, 2001). Like TQD, the Tres Marias mine is also a breccia pipe, in the Georgetown, Del Rio, Buda, and Boquillos formations (Ostendorf, Henjes-Kunst, Schneider, Melcher, & Gutzmer, 2017; Saini-Eidukat, Leoben, & Goettlicher, 2016; Megaw, 2001).

With increasing demand on critical minerals for use in technology, and with current global-political relations between Russia, China, and South America being rough, the need to obtain locally sourced critical minerals and Rare Earth Elements is an increasing necessity. In revisiting the mines, and Terlingua Quicksilver District we hope to gain a better understanding of the mineralization of the area. Quicksilver (mercury) trace elements can be used as an exploration tool to understand critical minerals and rare earth elements in the area. There are structural similarities between the TQD and Tres Marias Mine. Zn and Ge are both critical minerals. This study's intent is to investigate what other critical minerals can be found in the areas previously mined for Quicksilver. In addition, investigating critical minerals, the study hopes to understand the structural components leading to mineralization within breccia pipes.

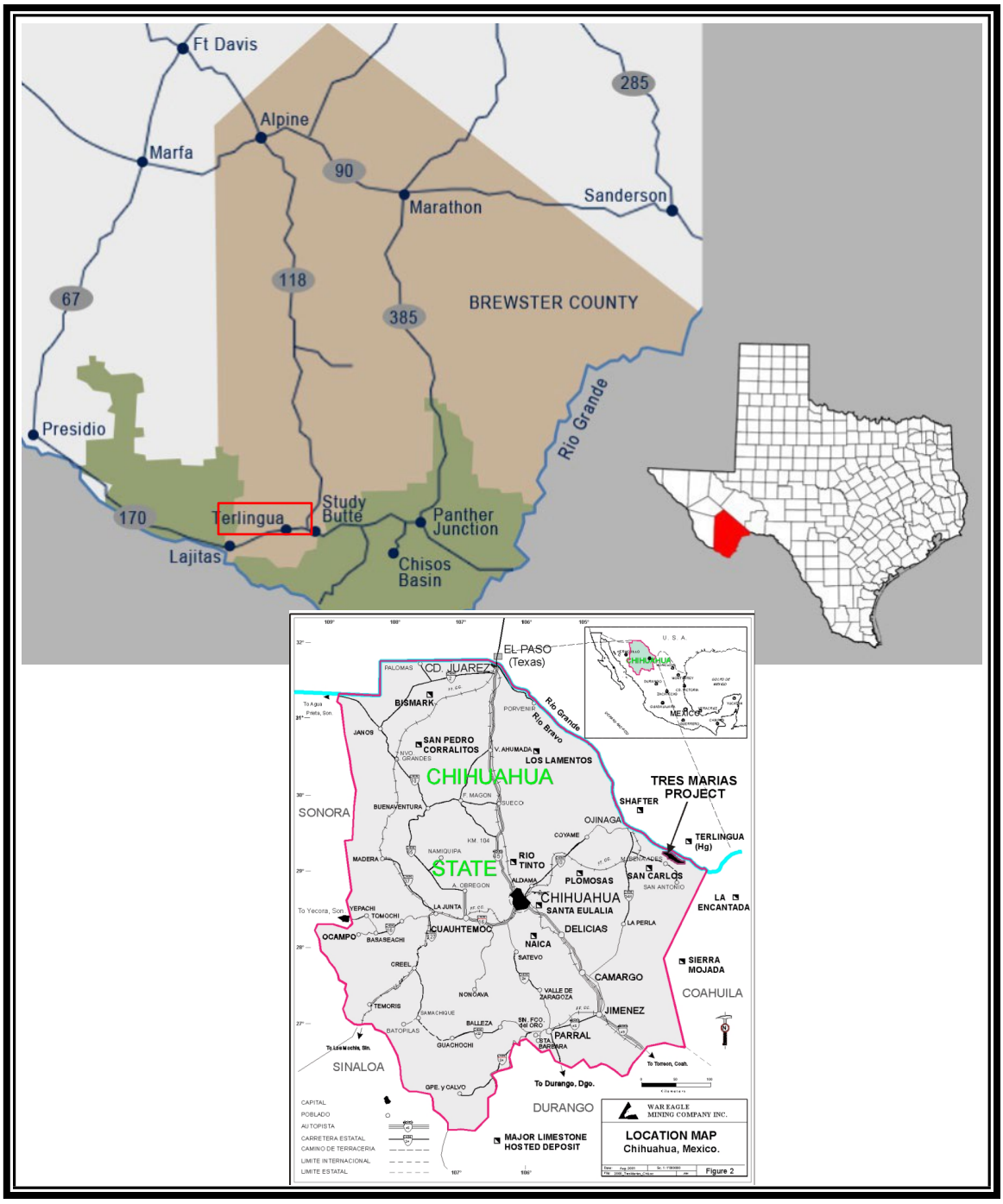

FIGURE 1: FIGURE 1 OVERALL LOCATION OF THE TERLINGUA QUICKSILVER DISTRICT AND TRES MARIAS MINES. TQD OUTLINED IN RED

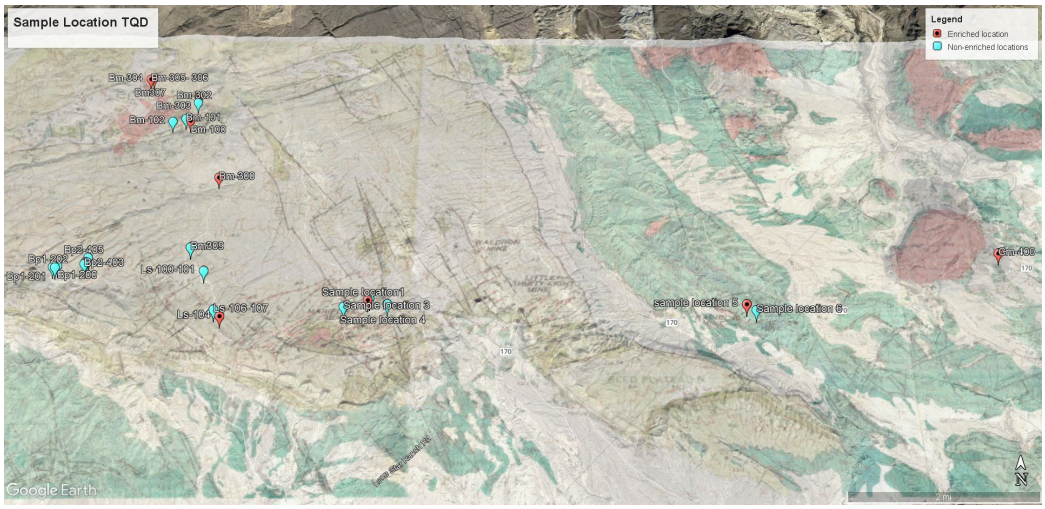

FIGURE 2: GEOLOGICAL MAP OF THE TERLINGUA QUICKSILVER DISTRICT SHOWING THE SAMPLE LOCATION IN LIGHT BLUE AND ENRICHMENT LOCATIONS IN RED. REFER TO THE CATALOG FOR SAMPLE LOCATION NAMES. GEOLOGIC OVERLAY FROM (YATES AND THOMPSON 1959) OVERSIZE VERSION LOCATED IN THE APPENDIX.

			Udden (1907a, p. 21–60)	Sellards, Adkins, and Plummer (1933)	Names used in this report	
Rocks of Tertiary age			Surface flows	Volcanic rocks	Chisos volcanics	
			Burro gravel and tuff			
Upper Cretaceous	Navarro group	Gulf series	Crown conglomerate	Crown conglomerate		
			Chisos beds	Chisos beds		
			Tornillo clays	Tornillo formation	Tornillo clay	
	Taylor group		Rattlesnake beds	Aguja formation	Aguja formation	
	Austin group		Terlingua beds	Taylor formation	Terlingua clay	
				Terlingua formation (restricted)	Boquillas flags	Upper member
	Eagle Ford group		Boquillas flags	Boquillas flags		Lower member
	Washita group	Comanche series	Buda limestone	Buda limestone	Buda limestone	
			Del Rio clay	Grayson formation	Grayson formation	
Lower Cretaceous	Fredericksburg group		Not differentiated in the Terlingua district	Georgetown limestone	Devils River limestone	
				Edwards limestone		

FIGURE 3: STRATIGRAPHIC COLUMN FROM YATES (1959) COLUMN FROM YATES IS TITLED "NAMES USED IN THIS REPORT" DEVILS RIVER LIMESTONE IS ALSO KNOWN AS SANTA ELENA LIMESTONE OR GEORGETOWN/EDWARDS LIMESTONE. THE GRAYSON FORMATION FROM YATES AND THOMPSON (1959) IS ALSO KNOWN AS DEL RIO CLAY

2: Geology of the area

Geological Setting

The Big Bend region has rocks from Paleozoic to Tertiary. However, almost all the stratified rocks in Terlingua quicksilver district (TQD) are Cretaceous age (Yates & Thompson, 1959). The TDQ rocks all fall with in distinct lithological units and are easily distinguishable in the field. Yates describes the cretaceous rocks as all sedimentary, from limestone to shaly sandstone, there are also tertiary igneous rocks in the area (Yates & Thompson, 1959). From oldest to youngest, the stratigraphic units (figure3) are Devil River limestone lower cretaceous this is a thick sequence of uniformed limestone beds resistant to weathering, this is the most abundant rock in the district; Conformably over laying the Devil Rivers limestone is the Grayson formation, consisting of Del Rio Clay it is structureless clay and easily eroded. Buda is an upper Cretaceous limestone conformably over the Grayson Formation. it is a white, massive, well-bedded, and well jointed limestone; Boquillos Flags formation is a flaggy limestone and shale, made up of two members: the upper member is more shale, while the lower member is dominant limestone layer with a thin layer of limey-shale; Terlingua Clay is soft structureless gray clay, that weathers a dirty yellow; Aguja formation, previously known as Rattlesnake beds, was changed because Rattlesnake beds is a name in another unrelated formation (Lehman, 1985). Aguja is widely, yet irregularly distributed in TQD a sandstone and clay with tuffaceous bed between the Aguja and tornillo clay; Tornillo clay consist largely of clay, locally with in the TDQ it is sandy with gypsum (Yates & Thompson, 1959).

The volcanic rocks in the area are upper cretaceous to tertiary and have caused much of the deformation in the area. According to Sharpe 1980 “Magmatic activity in Trans-Pecos Texas began about 48 million years ago with deposition of tuffs” and continued up to 20 million years

ago. Most igneous units of the Trans-Pecos region were deposited 31 to 37 million years ago (Sharp, 1980). They range from lava flow to intrusions (Yates & Thompson, 1959), or as shallow dikes, sills, laccoliths, and stocks (Sharp, 1980). The volcanic rock can be separated into two groups; based on the presence of the mineral analcite and the other using conventional nomenclature based on grain size and phenocryst composition (Sharp, 1980).

The first volcanic rock in the area are the Chisos Volcanics a group of lava flows and clastic rocks, the principal occurrence is in the Fresno mine in the west end of the district, here they unconformably overlap Boquillas (Yates & Thompson, 1959). Evidence of this unit is left over in breccia pipes and other similar collapsed structures within the TQD lead Yates & Thompson (1959) to believe Chisos lava flow once extended throughout the district. The intrusive igneous rocks of the TQD are alkalic igneous rocks (Yates & Thompson, 1959; Sharp, 1980). This intruded into the cretaceous sedimentary units through plugs, dikes, laccoliths, and sills. The intrusive rocks appear to have solidified at shallow depths (Yates & Thompson, 1959) as a result most of the intrusive rocks are fine grained, some are aphanitic, and a few are medium grain. Using the grain size is one way to describe the intrusive igneous rock. Another is through the presence of analcite. The analcite-free rocks are rhyolite, quartz soda syenite, soda trachyte, soda latite and olivine basalt (Yates & Thompson, 1959) the analcite rocks include analcite syenite, analcite-plagioclase syenite, analcite syenogabbro, and analcite basalt (Yates & Thompson, 1959).

Regional Description

The Trans-Pecos region encapsulates the TQD. the Trans-Pecos region is a desert mountainous region. With Basin and Range features, magmatic intrusions, and volcanic activity. Currently the tectonic state is extension, but throughout history the regional tectonic activity has changed from rifting periods during the Proterozoic, to orogenic periods during the Carboniferous

Marathon Orogeny. The result of the tectonic activity has given the regional area a northwest-southeast geometry of major structural and geographical features (Page, Turner, & Bohannon, 2008). Features such as the Mesa De Anguila Monocline in the southern portion of Big Bend National Park and in the northern end the Sierra Del Carmen-Santiago Mountains Monocline (Page, Turner, & Bohannon, 2008). In the TQD there are features such as Long Draw, and Terlingua-Fresno Monocline. The Terlingua portion of the overall monocline has a slightly more west-east strike.

The most prominent geological features in the TQD are the Terlingua Uplift, Fresno-Terlingua Monocline, and Black Mesa. Other prominent features related are the Solitario Dome and the Contrabando Dome. The Fresno-Terlingua Monocline borders the west to southwest edge of the Terlingua Uplift, the northern portion of the Fresno-Terlingua Monocline, next to the Solitario is known as the Fresno Monocline (Henry & Muehlberger, 1996). The Solitario sits unconformably on top of the Terlingua Uplift, in the northwest part. The Solitario is about 37 ma (figure 5) while the Terlingua Uplift is 36-35 ma (Henry & Muehlberger, 1996). Black Mesa is found within the TQD to the northern edge of the district and 5 miles south of the Solitario (figure 4). The Black Mesa is an intrusion known as a Laccocaldera (Henry & Kunk, 1997). This rhyolitic intrusion is about 34.7 ma, the feature is associated with the late stages of the formation of the Solitario (Henry & Kunk, 1997)

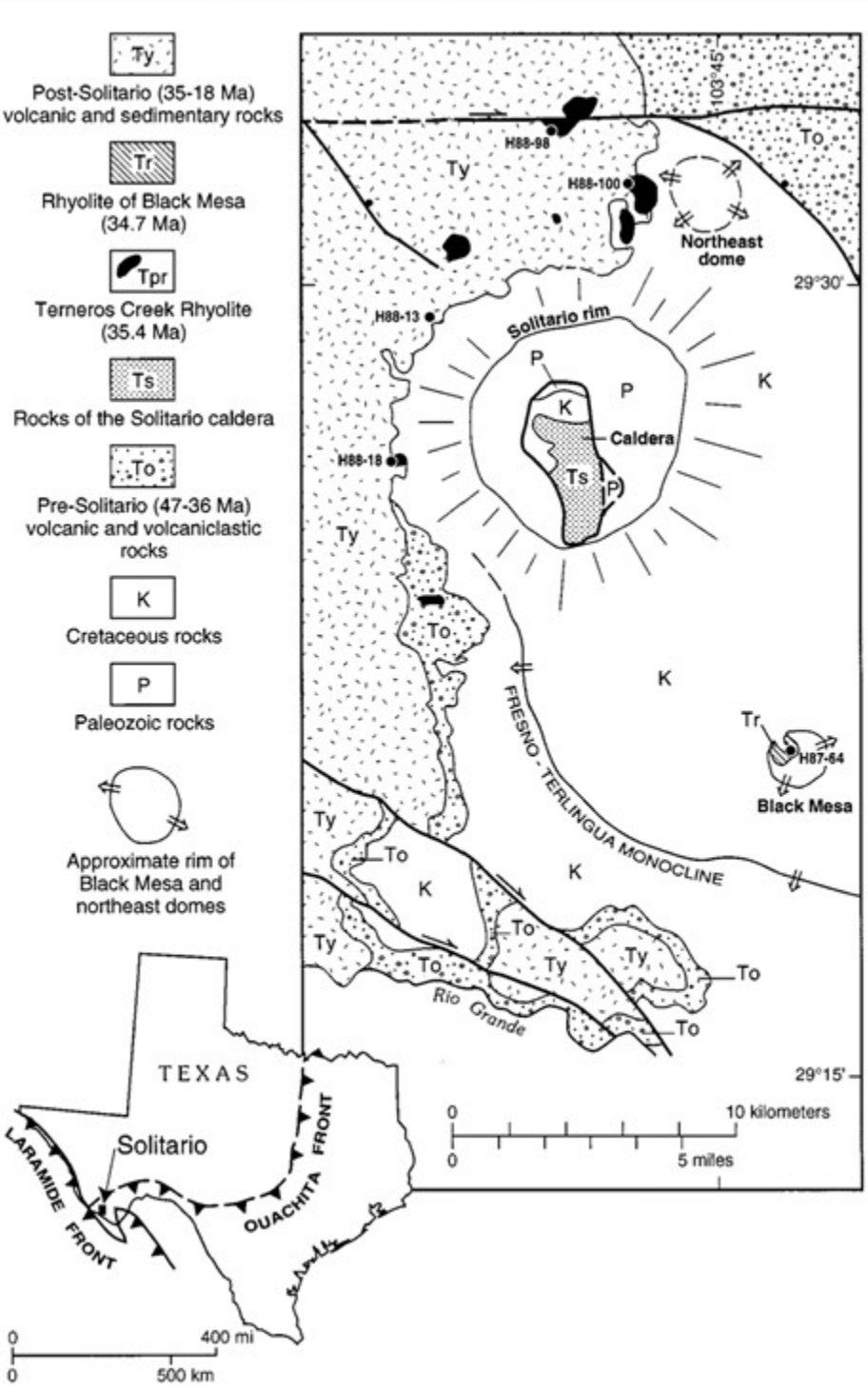

FIGURE 4: TERLINGUA UPLIFT, SHOWING THE SOLITARIO, BLACK MESA, AND TERLINGUA MONOCLINE (HENRY & KUNK, 1997)

Geological Sequence of Events

The TQD is located within the Trans-Pecos, which has undergone a series of complex tectonic events over millions of years. This series of events have created the structural geometry that controls the TQD region. Tectonic activity during the Proterozoic eon have provided several structural controls throughout the area related to the rifting and orogenic events (Page, Turner, & Bohannon, 2008). These events influenced the geology and tectonic evolution of the TQD area with northwestern trend of major structural and geographical features in the area (Muehlberger, 1980).the Grenville Orogeny is the first major tectonic event. This event is associated with the accretion of an island arc system onto the North American plate which is coeval to the Llano Terrane in central Texas (Urbanczyk, Rohr, & White, 2001). The Llano terrane, or the Llano uplift, is geologically related to the Greenville orogeny as both structures were created by the accretion of island arcs during the Proterozoic contractional tectonic activities. In central and northern Mexico Precambrian rocks are absent until hundreds of miles south of the TQD, this is caused by a system of northwest striking transform faults and northeast striking rift segments along the Appalachian-Quachita continental margin (Thomas, 1991). These faults are the control for the configuration of the Quachita-Marathon orogenic belt (Thomas, 1991). The transform faults are subparallel with the Texas lineament (Muehlberger, 1980) , a northwest trending wrench faulting zone extending from Presidio, TX.

During the Paleozoic era there were multiple cycles of supercontinent formation and fragmentation. Entering the Paleozoic era most of the land formation was part of a supercontinent, that broke up and formed a second supercontinent, Pangea during the Pennsylvanian into Permian, the Tascotal Mesa Fault zone (figure 5) is probably a component of the ancient rift margin (Dickerson, 2013). Responses to transtensional separation of Laurentia and Gondwana in the mid-Ordovician created block faulting and variable uplift and deep erosion (figure 5) for about 30 MY (Dickerson, 2013). In the Trans-Pecos region, the deformation events showing the convergent tectonic plates are tied to the Quachita-Marathon Orogeny in late Paleozoic Carboniferous period

(Thomas, 1991). In between rifting and orogenic events, this area was the site of a deep-water ocean basin (Page, Turner, & Bohannon, 2008). Around the same period, the TQD region was part of a shallow marine environment. Located at the southern edge of the North American continent, the site of marine deposits, and complex tectonic activity between north and South American plates (Page, Turner, & Bohannon, 2008). This environment left sedimentary deposits on the southern edge of the North American Plate, south of the TQD area, on the South American Plate. The oldest tectonic episode during the Paleozoic is associated with the Marathon Orogeny. This is documented in the Terlingua uplift, north of the Solitario in the central Tascotal Mesa fault zone, where late Paleozoic folding and thrusting are bounded in the north by the fault zone (Dickerson, 2013) During this event, the South American plate was thrusted onto the North American Plate in a northwestern trending thrust fault (Page, Turner, & Bohannon, 2008), and the N. American Plate was subducted under the S. American Plate.

After the Paleozoic orogenic activity, the region underwent a period of rifting. Much of the region was still submerged during the early Mesozoic Era, then the sea retreated and the region experienced uplift and erosion. From late Triassic through late Cretaceous the sea floor was spreading between North and South American plates as the Gulf of Mexico was opening (Page, Turner, & Bohannon, 2008). Contemporaneously the Chihuahua Trough and Diablo Platform were formed during this time, as well (Page, Turner, & Bohannon, 2008). The TQD area remained on the Diablo platform, which was made of Cretaceous limestones and shale deposited in a shallow open ocean (Page, Turner, & Bohannon, 2008). Late Triassic rifting and faulting along the margin between The Chihuahua Trough and Diablo Platform caused the Chihuahua Trough to subside. The Chihuahua Trough formed into an ocean basin. By late Cretaceous subsidence had ended with the filling in of the ocean basin, which shifted from a marine to a continental depositional environment (Page, Turner, & Bohannon, 2008).

As the Triassic to late Cretaceous rifting ended the Laramide Orogeny began. The Laramide Orogeny began the contractional deformation, and produce uplifts, basin, faults, and

folds in an east to northeastern compressional force (Page, Turner, & Bohannon, 2008). The Laramide orogeny is a contractional period between the Chihuahua Through and the stable Diablo platform between 80-30 MY (Muehlberger, 1980; Page, Turner, & Bohannon, 2008). In the Trans-Pecos region, Laramide deformation happens when cretaceous rockslide along a decollement zone in the underlying evaporites deposited during the previous rifting period (Henry & Price, 1985). Along the Tascotal Mesa fault zone Laramide activity is expressed in thin- and thick-skinned structures (Dickerson, 2013). As the Farallon plate subducts under the North American plate in a low-angle subduction along the western coast, this has been largely attributed to flat-slab subduction of the Farallon Plate beneath the North American Plate (Davidson, 2014). This subduction, and the corresponding contractional deformation caused several structures we have in the TQD. Structure such as the Terlingua Monocline, Fresno Monocline and Tascotal Fault (Erdlac, 1990), these three structures will be discussed in detail later. The geometry of the structures matches the same trend of tectonic activity from the Late Triassic to late Cretaceous period, which was reactivated in the opposite direction (Erdlac, 1990; Page, Turner, & Bohannon, 2008).

Rio Grande rift is currently the reginal tectonics of the area, creating a rift within the North American Plate. This is a N-S trending zone of extension, characterized by a series of linked half-grabens separated by transfer zones bounded by rift-flank uplifts (Ricketts J. , 2014). Following lithospheric shortening during the Laramide Orogeny and large-volume eruptions of volcanic rocks during the Oligocene ignimbrite flare-up (Ricketts & Karlstrom, 2016). The rift extends from central Colorado, south through New Mexico, and into west Texas. Rifting in the western United States resulted in a basin and range topographical setting. The age of rifting is up for debate; however, the consensus is rifting begins in the late Oligocene to early Miocene (Ricketts, et al., 2016). With initial stages of minor extension beginning at 36-37 Ma and the main phase beginning approximately 25 Ma (Ricketts & Karlstrom, 2016). Laramide Tectonics is the structural control for the Rio Grande Rift, after flat-slab subduction of the Farallon plate during the Laramide

Orogeny around 45 Ma, the plate eventually terminated during slab rollback, delamination, and foundering of the Farallon slab into the asthenosphere (Ricketts J. , 2014). By late Cretaceous time there was a well-established magmatic arc along the western margin of North America. In the early stages of Laramide Orogeny, the dip of the Farallon plate had shallowed, during this stage magmatism stopped along western North America and moved about 1000 Km east (Ricketts J. , 2014; Ricketts, et al., 2016). Foundering between the Farallon and North American plates exposed the hydrated lithosphere of the North American plate to the hot asthenosphere and resulted in magmatism across western North America.

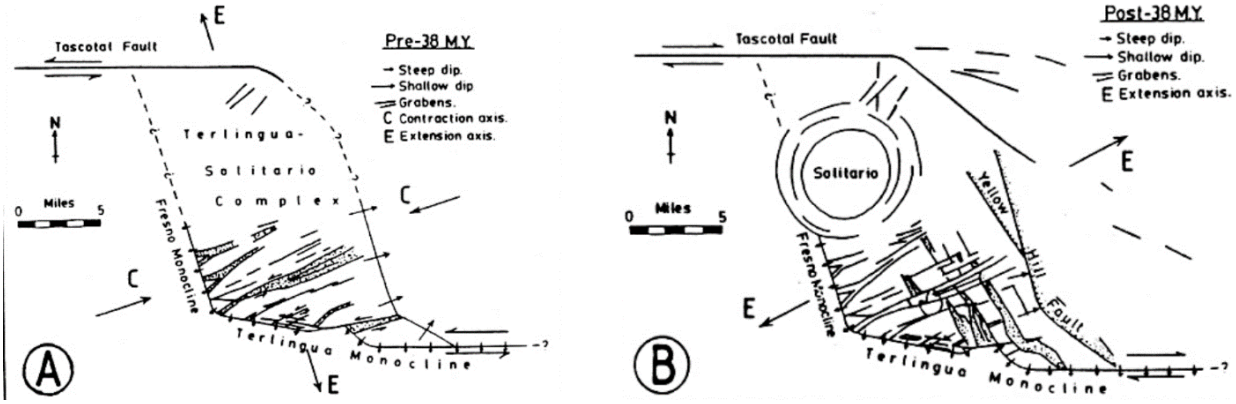

FIGURE 5: A) TERLINGUA-SOLITARIO STRUCTURAL BLOCK. RESULTED FROM TRANSPRESIONAL SINISTRAL MOVEMENT ALONG THE TASCOTAL MESA FAULT, AND INFERRED FAULTS UNDER THE TERLINGUA MONOCLINE. B) NE EXTENSION ACROSS THE REGION FROM TRANSEXTENSIONAL DEXTRAL MOVEMENT ALONG TASCOTAL MESA FAULT AND INFERRED UNDER TERLINGUA MONOCLINE STIPPLE FAULTS AND GRABENS ALONG WITH NW-TRENDING FAULTS FORMED DURING THIS TIME (ERDLAC, TECTONIC MODEL OF THE TERLINGUA UPLIFT, BIG BEND REGION, TRANS-PECOS TEXAS, 1990)

Igneous Rock Evolution

Volcanic rock in the area is upper Cretaceous to Tertiary and was thought to be a result of the shallow subduction of the Farallon Plate melt-off from the Laramide Orogeny (Page, Turner, & Bohannon, 2008). However, now the magmatism in the Trans-Pecos is tied in with the Rio Grande Rift which this area is currently experiencing. Magmatism began 47 Ma, after the end of the Laramide Orogeny (Henry & Davis, 1996) and caused much of the recent deformation in the

area. According to Sharp (1980) the Trans-Pecos area saw magmatic activity starting around 48 MY, with the deposition of tuffs, and continued up to 20 MY. Most igneous units of the Trans-Pecos region were deposited from 31 to 37 MY, with major episodes occurring in the Trans-Pecos region between 46-28 MY (figure 5) (Page, Turner, & Bohannon, 2008) . They range from lava flow to Concordant and discordant intrusions (Yates & Thompson, 1959), like shallow dikes, sills, laccoliths, and stocks (Sharp, 1980). Volcanic rock is separated into two groups based on the presence of the mineral analcite and the other using conventional nomenclature based on grain size and phenocryst composition (Sharp, 1980). Magmatic features within and around the TQD include The Solitario, north of the TQD and Contrabando Dome, located inside Big Bend Ranch State Park to the northwest. These two features are found outside the TQD. Within the TQD are the Wax Factory Laccolith and Dome on the western edge of the district, Black Mesa Dome in the north-central portion of the district and Cigar Mountain on the East side of the district. Terlingua has a varied abundance of igneous intrusions, they extend into the eastern portion of the TQD, other such intrusions are Long Draw Dome, Two-Forty-Eight Dome, and Fossil Knob Dome. The first volcanic rock in the area is the Chisos Volcanics, a group of lava flows and clastic rocks. The principal occurrence is in the Fresno mine in the west end of the district, here they unconformably overlap Boquillas (Yates & Thompson, 1959). Evidence of this unit is leftover in breccia pipes and other similar collapsed structures within the TQD led Yates (1959) to believe Chisos lava flow once extended throughout the district. The intrusive igneous rocks of the TQD are alkalic igneous rocks (Yates & Thompson, 1959; Sharp, 1980) and intruded into the Cretaceous sedimentary units through plugs, dikes, laccoliths, and sills. The intrusive rocks appear to have solidified at shallow depths (Yates & Thompson, 1959). As a result, most intrusive rocks are fine-grained, some are aphanitic, and a few are medium grain. Using the grain size is one way to describe the intrusive igneous rock. Another is through the presence of analcite. The analcite-free rocks are rhyolite, quartz soda syenite, soda trachyte, soda latite, and olivine basalt (Yates & Thompson, 1959). The

analcite rocks include analcite syenite, analcite-plagioclase syenite, analcite syenogabbro, and analcite basalt (Yates & Thompson, 1959)

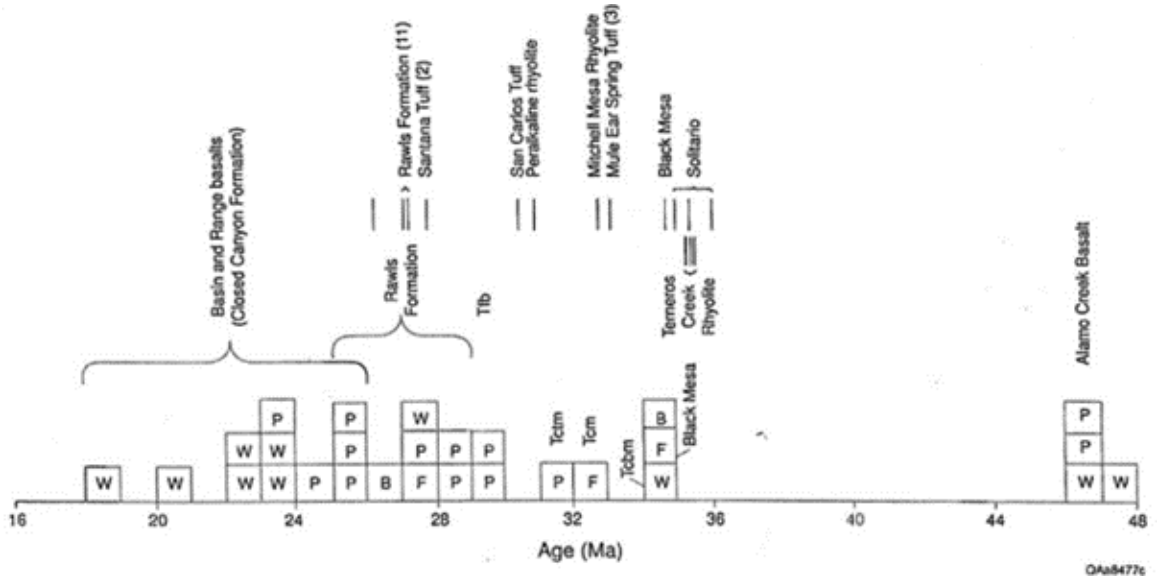

FIGURE 6: AGE OF THE VOLCANIC ROCKS OF THE SOLITARIO AND BOFECILLOS MOUNTAINS AREA. AGES ARE PLOTTED AS LINES AT THEIR VALUES; UNCERTAINTIES ARE 0.10 TO 0.13 MA. K-AR AGES ROUNDED TO NEAREST MILLION YEARS ARE PLOTTED AS BOXES; UNCERTAINTIES RANGE FROM 0.8 TO 3.1 MA. NUMBERS IN PARENTHESES REPRESENT THE NUMBER OF ANALYSES PERFORMED. W=WHOLE ROCK, P=PLAGIOCLASE, B=BIOTITE, F= SANIDINE. (HENRY & KUNK , 1996)

North of the TQD is The Solitario, a circular laccolithic dome and caldera complex that is about 14-16 km in diameter (Henry & Muehlberger, 1996), and sits atop the larger Terlingua Uplift. As the Solitario developed it first went through a process of pre-doming laccolith, sill, and dike intrusion followed by doming and concurrent intrusion then ash-flow eruptions and caldera collapse. Afterwards the Solitario underwent intercaldera sedimentation and volcanism, and last late intrusions (Henry C. D., 1996). The age of the Solitario has been placed between 36-35 MY and underwent three distinct phases (Henry & Kunk , 1996). The first phase was 36.0 Ma, where numerous rhyolitic sills intruded Cretaceous and Paleozoic rock. The second phase was a quartz-phyric dike and ash-flow tuff eruption 35.4 Ma. The third and final phase of the Solitario Dome occurred 34.9 to 35 Ma, which was an intrusion of coarsely porphyritic dikes into caldera fill. Contrabando Dome is found outside of the TQD in the Big Bend Ranch State Park. It is 2 miles in

diameter with 500- feet of relief (Yates & Thompson, 1959). The Contrabando Dome is formed from two rhyolitic sills, 20 and 40 m thick with several small dikes, sills, and irregular plugs (Henry & Davis, 1996). Henry and Davis (1996) continue to describe Contrabando Dome with many discordant intrusions that align in an east-northeast-striking fault which is probably related to doming. Much of the mercury mineralization exists within the rhyolites along this and parallel faults (Henry & Davis, 1996). Eight km south of the Solitario is the Black Mesa dome 34.7 Ma with a width of 2.5km it is the largest rhyolite plug-like body in the area (Henry & Kunk , 1996; Mosconi, 1984). The analcime-free rhyolite intruded into Santa Elena (Devils River Limestone in the Terlingua area), a breccia pipe and a tuff (Mosconi, 1984). Both Contrabando Dome and Black Mesa are flow banded with columnar jointing, however, the flow-bands are somewhat disguised by alteration in the Contrabando Dome (Henry & Davis, 1996; Mosconi, 1984) . Tuff is exposed at Black Mesa which is a light-gray, non-welded, lithic tuff to breccia with ash, rock fragments, and volcanic glass (Mosconi, 1984).

Regional Features and Structures

The Big Bend region underwent two significant deformation events, compression during the Laramide and currently undergoing extension (Yates & Thompson, 1959; Sharp, 1980). During Laramide deformation, the Cretaceous rocks were folded and produced the Terlingua Uplift, bounded on the south and southwest by the Terlingua Monocline (Sharp, 1980). Yates & Thompson (1959) divides the Big Bend region into three areas by contrasting topography. The first is the Marathon Basin; the second is the lava-covered plateaus south and west of Alpine; the third is the topographically diverse mountains and intermontane areas of the southern part of the Big Bend region. Though all the regions are connected, we are interested in the third area, the Big Bend region, which includes the Terlingua Quicksilver District.

The main features of the third division, according to Yates & Thompson (1959), are the Chisos Mountain, the Solitario, the Terlingua Uplift, and Mesa de Anguila. Other notable features

are Terlingua Monocline and Long Draw Graben. The Chisos Mountains, the Solitario, and the Mesa de Anguila are all just outside the TQD; however, they are essential to understand the area. The Chisos Mountains are the most prominent feature and are composed of mainly of volcanic and intrusive rocks piled up in the structurally lowest part of the Big Bend region (Yates & Thompson, 1959). The Solitario is a high mountainous rimmed basin carved from a dome by erosional de-roofing to expose the rocks of Paleozoic in its center (Yates & Thompson, 1959). Finally, the Terlingua Uplift extends about 13 miles south and east of the Solitario and is the dominating structure of the TQD.

Terlingua Uplift

The Solitario Dome sits on top of the Terlingua Uplift; both features are considered a single unit. Together they extend down south and east into the TQD. The Terlingua Uplift covers about half of the district. The rocks on the northeastern border dip away at angles from 10˚-20˚; while on the southwestern border, they are steeper and form the Terlingua Monocline (Yates & Thompson, 1959). After the Laramide deformation, conglomerates from the Eocene post-tectonic period were transported northward from the Tascotal Mesa fault scarp and deposited into a structural trough along the northern perimeter of the Terlingua uplift (Dickerson, 2013). Ross (1941) refers to the Terlingua Uplift as "the Terlingua Anticline." This feature has a total length of about 55 miles but nearly half is in Mexico (Ross, 1941). North of the Rio Grande, the anticline is broken up by faults; however, in Reed Plateau, it is well exposed and trends N. 50 ˚ W (Ross, 1941; Stevens & Stevens, 1989).

Further north on the Reed Plateau, the southwestern flank turns almost due west for about 8 miles, then turns N. 20˚ W. where the uplift (anticline) meets the Solitario Dome. This turn is interpreted as the result of the thrust movement (Ross, 1941). Devils River Limestone in Reed

Plateau and south of the plateau are used to measure displacement at about 2000 feet (Yates & Thompson, 1959). Between Reed Plateau and the Solitario the total displacement is about 3200 feet (Yates & Thompson, 1959). Between the Solitario and Terlingua uplift, the structural relief is about 3500 feet making the total structural relief of the Solitario and Terlingua Uplift relative to the area southwest is roughly 6700 feet (Yates & Thompson, 1959). The Terlingua Uplift and the Solitario are regarded as post-Cretaceous Laramide structures, however, contemporary views propose that The Solitario dome is now interpreted as the result of a younger intrusion compared to the primary Laramide activity. Nonetheless, one interpretation is, this intrusion is associated with a compressive regime identified as a continuation of Laramide conditions (Stevens & Stevens, 1989).

Terlingua Monocline

In the northwest corner of the TQD, the Terlingua Monocline is a zone of steep southward dipping rocks that make up the southwestern and southern flank of the Terlingua Uplift (Yates & Thompson, 1959; Erdlac, 1990). In this area, the Terlingua Monocline is made up of the Devils River Limestone (Santa Elena in Erdlac, 1990), Grayson clay, Buda limestone, and Boquillas Flags with remnants of the Chisos Volcanics (Erdlac, 1990). A conglomerate bed overlies Boquillas Flags with the Chisos Volcanic rock laying on top of the conglomerate. According to Sharpe (1980), the most productive mines are in a zone of southwest-dipping fracturing and faulting near the Terlingua Monocline and Long Draw Graben. Near the Presidio-Brewster County line, the Terlingua Monocline curves eastward (Yates & Thompson, 1959). In this area, the faults, and folds strike about 20 ˚ east-west and result in a substantial strike-slip and reverse movement (Yates & Thompson, 1959). The eastward extension of this fault zone shows only normal movement (Yates & Thompson, 1959). This fault zone is north and roughly parallel to the eastward course of the

monoline; along the zone are several intruded bodies and breccia pipes and a downfaulted synclinal area by Maggie Sink (Yates & Thompson, 1959). East toward Tres Cuevas Mountain and beyond, the Terlingua Monocline is paralleled by an anticline and syncline toward the north. At this point, the Monocline extends eastward with an average strike at S 70˚ E (Yates & Thompson, 1959). South of Mariposa Mine, the Monocline has a new strike of N 65˚ E followed by another change by Walden and Little Thirty-Eight mines, S. 50˚ E, and continues through Reed Plateau (Yates & Thompson, 1959). The southernmost fault is a reverse fault dipping at about 50 ˚ (Yates & Thompson, 1959). At the southern end of Reed Plateau, the Monocline splits, with the main branch continuing S. 60 ˚ E, and the second branch trending N. 55˚ E (Yates & Thompson, 1959). The southern extension is buried under alluvium and is therefore unknown. However, there are three low angle thrust faults in this area that parallel the Terlingua Monocline.

Breccia Pipes

Breccia pipe mineralization is a geological phenomenon distinguished by its fragmented rock structure and distinctive mineralogical composition. This investigation seeks to elucidate Breccia pipe formations' fundamental characteristics and geological implications. By delving into the existing body of knowledge and pertinent research, this section aims to provide a comprehensive overview of breccia pipe mineralization, laying the groundwork for subsequent analytical discussions and empirical inquiries. Exploring breccia pipe mineralization is essential for advancing our understanding of geological processes and their relevance to mineralization patterns.

Breccia pipe mineralization, a distinctive geological feature, is characterized by fragmented rock matrices marked by angular to sub-rounded clasts. These clasts, comprising various lithological components, are typically cemented together by mineral infillings, often contributing to forming a brecciated pipe structure. In this context, 'breccia' denotes the assemblage

of broken rock fragments, while 'pipe' refers to the conduit-like morphology frequently associated with these structures. The mineralization within these pipes commonly includes ore minerals, hydrothermal alteration minerals, and associated gangue minerals, offering insights into the geological processes that shaped the local subsurface environment. Identifying and systematically examining these features plays a pivotal role in understanding the genesis, evolution, and economic significance of breccia pipe mineralization within a given geological setting. Ollier (2007) describes Breccia-filled Pipes and defines distinguishing characteristics separating the types of breccia pipes. The author initiates the definition by explaining the different mechanisms that can produce breccia pipes: 'some are volcanic explosion breccias, some are breccia fill in collapse caves, some are formed by the intrusion of evaporate pipes followed by a later solution, some are formed by hydrothermal intrusions, and several other explanations have been proposed (Ollier, 2007).

The model describes how breccia pipes can form in a volcanic setting in volcanic breccia rocks. Volcanic rock will rise from the magma chamber through dikes that divide into individual pipes as the material rises to the surface (Ollier, 2007). The composition of the breccia pipe will vary; some will have all volcanic infill, others will have a mixture of volcanic and fragments of bedrock, while others will consist of all bedrock fragments (Ollier, 2007). Volcanic Breccia pipes are structures created with lots of energy and tend to be explosive. This environment is the case of many Kimberlite pipes; the eruptive phase deposits pyroclastic material into the pipe and onto the margins, while the post-eruptive phase is where infill of the pipe and foundering of volcanics coupled with hydrothermal fluids create mineralization, like in the Diavik NW territories in Canada (Moss, Russell, & Andrews, 2008). In the TQD, breccia pipes are adjacent to volcanic structures such as Black Mesa, Cigar Mountain, Hen Egg Mountain, The Solitario to the north, and the Contrabando dome in the NW. However, no evidence supports that the pipes are formed through volcanic brecciation. Mineralization found in the TQD is also different from mineralization in a volcanic breccia pipe.

Non-volcanic breccia pipes, in contrast to their volcanic counterparts, represent a distinctive category of geological formations characterized by fragmented rock matrices originating from processes other than direct volcanic activity. These pipes exhibit diverse origins, with mechanisms such as cave collapse, tectonic forces, or dissolution of soluble minerals playing pivotal roles in their formation. The defining feature of non-volcanic breccia pipes lies in their fragmented rock composition, where angular to sub-rounded clasts, often derived from the surrounding rock layers, are cemented together by various mineral infillings. Unlike volcanic breccia pipes, the genesis of non-volcanic varieties is not directly tied to magmatic activities, expanding the spectrum of geological processes contributing to their formation. Understanding the characteristics and origins of non-volcanic breccia pipes is essential for unraveling the geological history of a region and deciphering the intricate interplay of forces that shape the Earth's subsurface. Cave Collapse or solution and hydrothermal breccia pipes are present in the TQD. In a cave collapse, the rock goes into solution, usually by precipitation above ground permeating through or dissolving the rock with groundwater, usually in limestone. The above rock will then collapse and infill the pipe (Ollier, 2007), undergoing a lithification and mineralization process.

Hydrothermal breccia pipes, integral components of the geological landscape, emerge as distinctive formations shaped by the transformative forces of hydrothermal activity. Defined by their genesis in the dynamic interplay of heated fluids within the Earth's crust, hydrothermal breccia pipes bear unique characteristics that set them apart from non-volcanic ones. These pipes originate through the circulation of high-temperature fluids, inducing the fracturing and brecciation of pre-existing rock formations. The resulting matrix, composed of fragmented rock clasts, exhibits a diverse mineralogical composition, often featuring a juxtaposition of ore minerals and hydrothermally altered materials. The hydrothermal breccia pipes' intricacies offer valuable insights into the thermal and chemical evolution of the Earth's crust, making them pivotal subjects for geological inquiry. Understanding the characteristics and formation mechanisms of hydrothermal breccia pipes contributes to our comprehension of regional geological histories and

the exploration of mineralization patterns and associated economic resources within a given geological setting. Hydrothermal fluids are believed to impact mineralization in the TQD breccia pipes.

The Terlingua solution features can be broken down into three main types: Limestone caverns, filled caverns or cave-fill zones, and breccia pipes (Yates & Thompson, 1959). Most open caverns are in the Devils River Limestone, except a few are found in Buda Limestone. Yates & Thompson (1959) further distinguishes the open caverns into two additional categories: vertical caves, which develop mainly along fractures, and horizontal caves, which develop along the bedding plane (Yates & Thompson, 1959). The solution features in Yates and Thompson are simplified in Thompson (1950) to breccia pipes. However, both agree on the solution being the leading cause of brecciation. The dissolving agent is believed to be a hydrothermal solution, but meteoric water is a possible alternative (Thompson, 1950).

Breccia pipes emerge as pivotal features in mineral exploration, bearing substantial significance for geologists and exploration teams. These geological formations, characterized by fragmented rock matrices resulting from various geological processes, serve as valuable indicators of subsurface mineralization. The distinct mineralogical composition within breccia pipes, often featuring ore minerals and hydrothermally altered materials, offers a clear geological signature that directs exploration efforts. The irregularity and complexity of breccia pipes create favorable conditions for the concentration and deposition of economically valuable minerals. Consequently, the systematic study and identification of breccia pipes contribute indispensably to mineral exploration strategies. Understanding the role of breccia pipes in mineralization patterns not only aids in the targeted discovery of valuable resources but also enhances the overall efficacy of exploration endeavors by providing crucial insights into the geological processes shaping subsurface mineral deposits. In essence, breccia pipes are key geological indicators guiding mineral exploration toward areas of heightened economic potential.

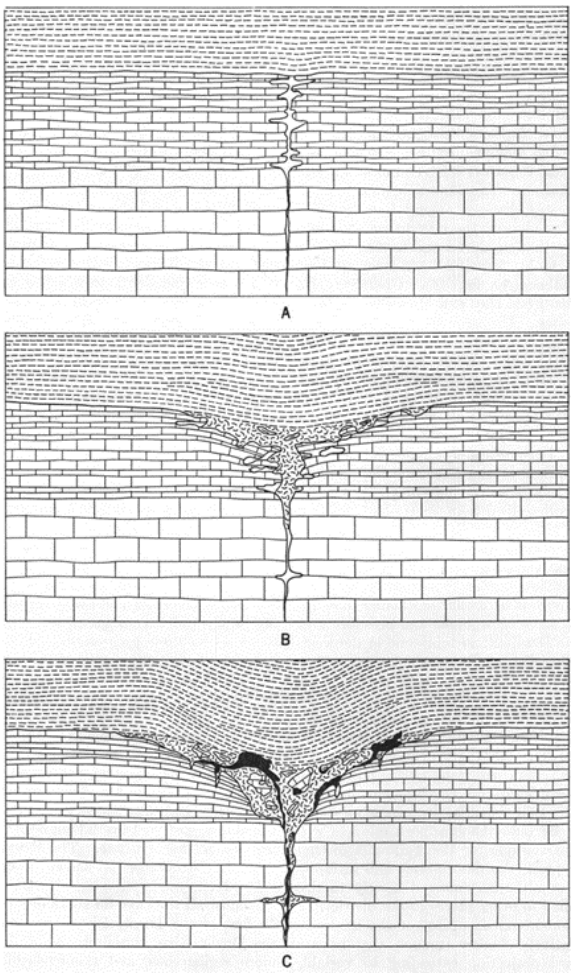

FIGURE 7: IDEALIZED SECTION SHOWING DEVELOPMENT OF BRECCIA PIPE WITH LIMESTONE DISSOLUTION, DEVELOPMENT OF LIMESTONE-CLAY DEPOSIT. A) FIRST STAGE, ENLARGING OF SOLUTION CHANNEL IN LIMESTONE, SLUMPING OF CLAY GRAYSON FORM. B) SECOND STAGE, FILLING OF SOLUTION CHANNEL BY INCREASED SLUMPING AND ADDITION OF CAVE DEBRIS, A AND B ARE CONCOMITANT. C) FINAL STAGE, ORE STAGE SHOWING CINNABAR IN CAVE FILL (YATES & THOMPSON, 1959).

Mineralization

The mineralization of breccia pipes assumes a regionally nuanced character, exemplified by distinctive patterns observed in areas such as Arizona (AZ) and Colorado (CO). In these geological landscapes, breccia pipes play a vital role as conduits for mineral-rich fluids, contributing to diverse and economically significant mineralization processes. Arizona, renowned for its geological diversity, hosts breccia pipes that exhibit mineralogical compositions reflective

of the region's complex tectonic history. These pipes may showcase concentrations of copper, gold, or other valuable minerals, providing a unique and economically valuable signature. Similarly, with its rich mining history, Colorado unveils breccia pipes that are integral to the state's mineralization tapestry. Breccia pipes in this region may host silver, lead, and zinc minerals, reflecting the geological dynamics that have shaped the Rocky Mountain terrain. Understanding the mineralization of breccia pipes in specific regions like AZ and CO informs targeted exploration strategies. It contributes to the broader comprehension of geological processes governing the distribution of valuable resources in diverse and geologically distinct areas.

In northwest Arizona, several hundered breccia pipes are strictly collapsed in origin, where the Redwall limestone went into dissolution and formed caverns, followed by the stoping of the above strata (Wenrich & Sutphin, 1988). The breccia pipes in Arizona were deposited by at least two separate mineralizing fluids: first cobalt, copper, iron, lead, nickel, and zinc, then uranium (Wenrich & Sutphin, 1988). In the Copper Basin in central Arizona, there are 25 exposed mineralized pipes, with a formation following the stock intrusion, resulting in a porphyry copper-type mineralization of sulfides and oxides (Johnston & Lowell, 1961). In Colorado's Red Mountain District, the formation of breccia pipes can be attributed to three distinct processes: an explosive release of hot gases, a more passive release of gases accompanied by the slow brecciation of country rock due to chemical and volume changes, and the emplacement of intrusive bodies in the region (Fisher & Leedy, 1973). These processes, as outlined by Fisher and Leedy (1973), contributed to the mineralization of silver, arsenic, gold, bismuth, copper, lead, antimony, and zinc (Fisher & Leedy, 1973)in the area.

Tres Marias is a Zn-Pb-(Ge) deposit mine located in the eastern boundary of the state of Chihuahua, Mx. This deposit occurs as a part of a cluster of carbonate-hosted hydrothermal orebodies (Megaw, 2001). Tres Marias is one of several Carbonate Hosted Zn-Pb deposits in northern Chihuahua within a 220 km long belt that crosses most of northern Mexico. Orebodies are found within carbonate dissolution collapse breccia pipes that occur in zones where E-W-

trending normal faults and NE-trending normal faults transcurrent and normal faults intersect major NW-trending normal faults (Megaw, 2001). Breccia fragments consist mainly of limestone, shale, and sulfide ore. Fragments range in size from millimeters to over 3 cm. The fragments are derived from Buda limestone and Del Rio Shale, which overlie the Santa Elena formation limestone (Megaw, 2001).

Within the Terlingua Quicksilver District of Texas, breccia pipes serve as conduits for the concentration of economically significant minerals, reflecting the intricate geological history of the region characterized by tectonic activity and hydrothermal processes. Noteworthy for their historical association with mercury deposits, these breccia pipes exhibit a diverse mineralogical composition, featuring prominent minerals such as cinnabar, fluorite, and barite. The careful examination of mineralization in the Terlingua Quicksilver District serves as a focal point for academic inquiry, providing valuable insights into the geological processes that govern the distribution of resources in this distinct and economically relevant geological setting.

Comparatively, the Tres Marias mine presents structural and stratigraphic parallels to the Terlingua Quicksilver District. The similar structural attributes between these two sites suggest shared geological processes, possibly influenced by comparable tectonic forces. Additionally, the congruence in stratigraphic units underscores the potential for analogous mineralization patterns. The comparative analysis of Tres Marias and the Terlingua Quicksilver District offers a valuable academic lens for understanding the broader geological context and mineralization potential in regions exhibiting comparable structural and stratigraphic characteristics.

Geology of Deposits

The chief ore mined in the Terlingua Quicksilver Deposit (TQD) was a mercury sulfide (HgS) known as cinnabar; occasional small pockets of rare minerals can also be found (Kay, 1938). Cinnabar is a hexagonal crystal with a hardness of 2-2 1/2, usually a deep red (Chesterman 1978). Finding crystals is rare; in Terlingua, the cinnabar was a chalky, red rock that required substantial

effort to break with a 3-lb sledgehammer. Cinnabar occurs as a replacement of argillaceous breccia matrix and as vein fillings in or near volcanic rocks and hot springs, where it is deposited from low-temperature (50 to 200˚C) low pressure, alkaline, aqueous solution (Sharp, 1980). The Mariposa, Waldron, and Little Thirty-Eight mines were extracting ore from deposits located in breccia tubes as a replacement of Devils River limestone and Grayson Formation. Rainbow, Chisos, and 248 Mines are located near volcanic rocks with low temperatures. Sharpe mentions that the Tertiary rocks in the Terlingua District are presumably responsible for ore formation, but the timing is uncertain (Sharp, 1980). Cinnabar was deposited following the folding of the Terlingua Monocline, the formation of Long Draw Graben, and the intrusion of igneous rocks (Sharp, 1980). Cinnabar also occurs as a crust on calcite, limestone replacement, stringers in igneous rock, and as impregnation in shale (Kay, 1938). A class system was introduced by Ross (1941) which separates the types of lodes found in the Terlingua Quicksilver district. The three quicksilver lode classes are closely related: (1) deposits localized along the Del Rio clay and the Devils River limestone contact, which are the most abundant and include nearly all the lodes west of Reed Plateau, the principal deposit of the Rainbow Mine, and the deeper workings of the Chisos Mine; (2) deposits associated with faults and other openings in strata; (3) deposits in and close to igneous rocks; the Study Butte Mine is primarily exclusively mined in this class.

Mines

Mineralization occurs in different environmental settings such as veins cutting Cretaceous sedimentary rocks and Tertiary intrusive igneous bodies or as open space fillings in a solution with brecciated pipes, and as stratigraphically controlled bodies. As mentioned above by Ross (1941), there are three types of lodes found in the TQD. Contact between Del Rio clay and Devils River limestone is typically the most abundant deposit. All the lodes west of Reed Plateau: Le Roi mine, Coltrins Camp, and unnamed localities on Reed Plateau (EM-BR-V25-23), also the principal deposits in the Rainbow mine and part of the deeper workings of the Chisos Mine are all included

in this type (Ross, 1941). Deposits associated with faults and other openings are caused by solution. Yates & Thompson (1959) separates solution features into three main types: limestone caverns, filled caverns or cave-fill zones, and breccia pipes. The caverns happen in the Devils River limestone with a few exceptions found in the Buda limestone. There are two types of open caverns (Yates & Thompson, 1959): vertical caves and horizontal caves. Vertical caves develop along fractures while horizontal caves develop along bedding. Little Thirty-eight mine is an example of vertical caves, Waldron mine is a horizontal cave, while Mariposa Mine is an example of both.

RAINBOW-CHISOS

Most of the papers read in preparation for this study place Rainbow Mine and Chisos Mine together. They are separate entities; however, geographically they are in proximity. History states the Rainbow mine entered the Chisos mine below the 800 level. The Chisos Pipe is the most famous of Terlingua breccia pipes which the Chisos Mine was exploring and extracting ore. The Chisos Pipe was the district's most significant and valuable single ore body (Yates & Thompson, 1959). The pipe does not reach the surface. It was discovered in mine workings at a depth of 550 ft and was mined and explored an additional 250 ft. The Chisos pipe forms tangential to the Chisos fault.

MARIPOSA

Description from Yates & Thompson (1959): Mariposa Mine was the second largest producing mine in the TQD. Throughout the life span the mine was producing between 20,000-30,000 flasks of quicksilver. Most of the flasks were produced in a 3,500 by 1,000 ft area, while most subsurface workings were about 3 miles of drifts, stopes, and crosscuts under California Hill. The Mariposa Mine is in Buda limestone, Grayson Formation, and Devils River limestone. Soda

latite dikes intrude Devils River limestone, and sills intrude Grayson Formation in the southwest part of the area. Faults along the northwest, southwest, and southeast bound a depressed block of Devils River limestone with a vertical displacement on the faults that do not exceed 100 ft. Fractures in the block trend northeast with a few trending northwest. East and west of California Hill, the fractures are elongated outcrops of Devils River limestone separated by narrow zones of cave-fill. The cave-fill occupies solution caverns in the Devils River limestone. At the Mariposa Mine, cave fill has been invaded by igneous rock of Tertiary age, which was later fractured, and the fractures filled with cinnabar.

STUDY BUTTE

The Study Butte Mine is almost the only mine in which deposits in intrusive rock have been extensively mined (Ross, 1941). The outcrop of the intrusive body at Study Butte is a fine-grained Quartz Syenite (Yates & Thompson, 1959).

248 MINE

248 Mine is a breccia pipe on the western side of the 248 Domes. The Dome is east of the Cigar Mountain Graben. It is about 2 miles in diameter, with a structural relief of 500 ft (Yates & Thompson, 1959). The uplift was a sill or laccolith exposing the upper Boquillas flag on top and bounded by the overlaying Terlingua clay on three sides. The 248-mine shaft explores the 248 pipe for 600 vertical-ft. The breccia consists of Boquillas Flags on the upper levels and intermixed Boquillas and Buda rock below (Yates & Thompson, 1959).

3: Methodology

Fieldwork

Selecting locations was based on previous work from (Yates & Thompson, 1959) map. Geographical coordinates were acquired by overlaying a geo-rectified version of Yates & Thompson (1959) map on Google Earth. The area of interest are possible locations of breccia pipes, contact between igneous rock and sedimentary host rock, previous mines, and dump sites.

To geo-rectify the Yates & Thompson (1959) map, a digital copy of the map was made. The digital copy was converted from the PNG file to a TIF file using Adobe Photoshop. Once this is completed, the process of georeferencing can continue by using QGIS 3.18. Using QGIS the TIF is tied into a coordinate system. Using the QGIS 3.18 software, the TIF file was loaded to a new project. Then, using the coordinates provided by Yates & Thompson, the image was georeferenced. The georeferenced map overlaid onto Google Earth makes it possible to collect coordinates for all the locations of interest. The coordinates from Google Earth can be used on a GPS watch, and a course to the location was set.

The samples were either fresh samples collected by breaking the sample off the mountain or samples collected from float nearby, and dumpsites. The sample size was referenced to our shoe size, to ensure enough material for analysis. A description of the sample was collected in the sample catalog. Also collected were the geo-location and pictures of the surrounding area. The description recorded the geology of formation name was recorded. Differentiation between country rock, breccia rock, igneous rock was also noted.

Materials Used

The sample must be prepared. In the field, a sample was collected. The criteria for collecting samples are the rock type- we are interested in brecciated rock, cinnabar, host limestone, and igneous rocks. In the field, samples about the size of our shoes were collected. Our shoes were

readily available and proved to be an adequate field sample size. Once we found a suitable sample, we labeled it and collected the geo-location and description.

To send the sample off for analysis, the sample must be prepared. To do so, we had to remove the weathered surface of the sample. In addition, we had to reduce the sample size to ship the sample. Using a 3-lb sledgehammer, the sample was prepared by chipping away until it was clear of outside weathering surfaces, a smaller and easier-to-handle size. There is no requirement regarding the size; however, to reduce shipping cost while still having a good enough sample for analysis, we decided on a palm-size sample to send in.

Sample Analysis

The samples were shipped to Actlabs. The samples will be analyzed using the lithogeochemistry "4B2- Research" and WRA +ICP "4Litho". According to the company, Actlabs:

"*Lithogeochemistry The most aggressive fusion technique employs a lithium metaborate/ tetraborate fusion. Fusion is performed by a robot at Actlabs, which provides a fast fusion of the highest quality in the industry. The resulting molten bead is rapidly digested in a weak nitric acid solution. The fusion ensures that the entire sample is dissolved. It is only with this attack that major oxides including SiO2, refractory minerals (i.e., zircon, sphene, monazite, chromite, gahnite, etc.), REE and other high field strength elements are put into solution. High sulphide-bearing rocks may require different treatment but can still be adequately analyzed. Analysis is by ICP-OES and ICP-MS. Quality of data is exceptional and can be used for the most exacting applications. Values on replicates and standards are provided at no cost, as are REE chondrite plots. Eu determinations are semiquantitative in samples having extremely high Ba concentrations (> 5 %). Code 4B2: Lithium Borate Fusion / ICP-MS Trace Element package: Codes 4B2-STD and 4B2-Research both provide research quality data. 0.5g required. Research designation: indicates lower detection limits.*"

Calculations and Statistical Analyses

In the geological exploration undertaken throughout the research, precision and insight are achieved through systematic calculations and rigorous statistical analysis. The results of the chemical analyses were scrutinized using univariant, bivariant, and multivariant analyses of the results. First, univariant analysis was completed by creating histograms of each chemical analyzed. The locations were ordered using the value of chemical enrichment. The histograms were then examined for modes or peaks, this was used to determine the number of central tendencies and the frequencies found within the data. After categorizing the histograms into modes, outliers were identified, the specific sample numbers were determined, indicating their locations, and enrichment values noted. Then a bivariant analysis was performed where the correlation coefficients were used to determine how the individual elements correlate with each other. The correlation coefficients fall between negative one and positive one, with high correlations being closer to positive one. A high-intermediate-low scale was used to separate the correlation coefficients, and these are indicated on figure 10 and Appendix 3. Finally, multivariant analysis was used to substantiate the families observed by bivariant analysis. Using Centered Log Ratio and components one through four the Centered Log Ratio transformation is used to overcome the issues associated with compositional data, such as the closure under constant sum and the high correlation between variables (Buccianti, Mateu-Figueras, & Pawlowsky-Glahn, 2006).

4: Results and Data

Chemical Analysis

Chemical analysis was performed on 55 samples collected in the Terlingua Quicksilver District. Actlabs in Acaster, Ontario in Canada. Refer to their catalog for further information and details https://actlabs.com/wp-content/uploads/2023/03/Actlabs-Schedule-of-Services-USD-2023.pdf, All samples were analyzed for 44 elements including the REEs. The full analytical results can be found in the Appendix.

Catalog

TABLE 1: SAMPLE CATALOG WITH CORRESPONDING LOCATION AND DESCRIPTION.

Mariposa Mine		Latitude	Longitude
Sample Location 1	6/8/2021	29.319264	-103.691404
MM-100	Hematite W/Limestone, calcite Fresh Limestone course crystalline calcite vein. Other sample course crystalline- minor host rock- intense brick-red hematite, Calcite Dog Tooth. Hematite W/Hg mineralization		
Sample Location 2	6/8/2021	29.319512	-103.691103
MM-101	Fresh Limestone sample- Massive Limestone (Devils River Limestone)		
MM-103	Like MM- 202. Massive Breccia- Fragments are. Limestone, minor course crystalline calcite. Angular 2-5 Cm fragments.		
MM-105	Black rock- coal or Manganese- Sooty. Some layering black has veinlets of calcite crystals. Adj to black-Redish zone of similar material found in MM-100 "Brick- red" Hematite		
Sample Location 3	6/8/2021	29.31813	-103.695658

		5	
MM-200	2 types of calcites; Dogtooth, Vein-fill. pink fine grain Limestone no layering, impregnated with 2nd calcite & veins. course crystalline. Slight amounts of Fe		
MM-201	Jarosite - Iron sulfide (impregnated with jarosite? Or Limonite). Breccia rock with Limestone pieces. Striations		
MM-202	Not silicified- bleached Limestone, Rounded breccia clast, Limestone bleached white with infill dark- light maroon matrix. Light maroon surrounding Limestone fragments. Matrix- fine grained Limonite with Limestone and Clay		
Sample Location 4	6/8/2021	29.318638	-103.687892
MM-300	Silicified- Breccia with fine grain Limestone. Small fragments about 2 Cm. minor calcite on fracture plane pinkish orange		
Rainbow Mountain Mine			
Sample location 5	6/8/2021	29.318887	-103.623044
RM-100	Dark Fine-Grained Limestone		
RM-101	Fine gray- dark grey		
RM-102	Fresh Limestone. Fine grained massive Limestone, Minor calcite fractures.		
RM-103	Dark grey powder/ yellow fragments of limonite. With shale fragments.		
RM-104	Dirt from dump site like RM-101		
RM-105	Turritella fossil in fine grain grey to reddish-brown Limestone		
Sample location 6	6/8/2021	29.317963	-103.621371
RM-106A	Breccia Rock with calcite veins, Limestone fragments. Limestone is fine graine nearly white		
RM-106B	Bleached Limestone???		
RM-107	Mega Grain size, vein calcite, minor Limestone		
Sample from Centennial Museum			
CM-100	M59.4.1 Cinnabar from Lonestar Mine, Terlingua		
CM-101	M36.32.17 Cinnabar Terlingua		
Black Mesa Field Day 1			

Bm-100	Flaggy LIMESTONE, shale + LIMESTONE. Large crystalline calcite fracture infill. No infill between flaggy layers.	29.349949	-103.727025
Bm-101a	Float- breccia rock- clastic pieces 2-5 cm possible bleached LIMESTONE. Some zoning within the clast. Matrix light maroon	29.350343	-103.727973
Bm-101b	Float- breccia rock- clastic pieces 5-10 cm possible bleached LIMESTONE, with smallest pieces being 1 mm. bleached matrix infill from clast, zoning in matrix.	29.350343	-103.727973
Bm-102	Float- breccia rock clastic pieces 5-10 cm down to 1 mm, possibly LIMESTONE. Brick-red matrix	29.350119	-103.730605
Pd-100	prospect mine site- calcite zoning with 5 zones: zone 1 possible cinnabar zone- bright red, thine zone. zone 2 rhombohedral calcite crystals, small about 4- 5mm. Zone 3 larger rhombohedral calcite almost 1 cm dark gray. zone 4 white rhombohedral calcite about 8-9mm. gradational zone5 from light grey to dark calcite.	29.312083	-103.711391
Nelsons Loop: Breccia Pipe 1 Field day2			
Bp1-200	possible breccia rock that has been bleached- calcite. infill between 1 mm clast. Could also be bleached. Limestone with calcite infill in fractures.	29.32532	-103.748949
Bp1-201	loosely consolidated breccia rock. clast of bleached LIMESTONE. Brachiopod fossil found within sample.	29.325044	-103.749342
Bp1-202	Possible Aguja Formation: sandy/Limestone, with thin bed lamination, and calcite crystals.	29.325122	-103.749822
Nl1	Breccia rock clast ~ 3cm calcite crystals vein/matrix		
Nl2	Breccia rock Devils River Limestone clast, muddy/limy matrix		
Nlp1	Sample in same bag		
Nlp2	Sample in same bag		
Black Mesa/ Lonestar mine field day 3			
Bm-300	Porphyritic rhyolite with spars phenocryst about 5 mm and transparent to white	29.340067	-103.720669
Bm-301	Altered DRLIMESTONE- some pyrite. Massive LIMESTONE	29.340046	-103.720678
Bm-302	Float -Breccia rock, possible Limestone clast between mm- 5cm. Banding inward toward center. Matrix gradational- bleaching from clast leach out into matrix	29.353859	-103.746431
Bm-303	Breccia rock, more matrix than clast- deep maroon. Clast between 2-10 cm possibly altered LIMESTONE	29.35499	-103.726455

Bm-304	Breccia rock, matrix rhyolitic w/ anhedral sphalerite	29.35857	-103.736477
Bm-305	Breccia rock, Devils River Limestone clast ~2-3 cm.	29.358586	-103.73643
Bm-306	Breccia rock???	29.358586	-103.73643
Bm-307	Dump/prospect- breccia rock mostly matrix maroon. Clast about 1-5mm	29.358829	-103.735924
Bm-308			
Bm-309A	Large calcite crystals w/ cinnabar banding.	29.327796	-103.724193
Bm-309B	Large calcite crystals w/ cinnabar banding.	29.327796	-103.724193
Lonestar Mine Samples			
Ls-100	Possibly Devil River Limestone with calcified fossils. Leached white with calcite crystals in fractures	29.323846	-103.721236
Ls-101	Clay/LIMESTONE- Limestone chalky white with thin layering and fossil fragments	29.323846	-103.721236
Ls-102	from calcite vein in LIMESTONE. Zoning from large to small rhombohedral calcite crystals	29.316377	-103.71734
Ls-103	Limestone seems to have undergone hydrothermal. alteration, fracture infill with calcite	29.316377	-103.71734
Ls-104		29.316377	-103.71734
Ls-105	Calcite zoning- pink zone large 5mm calcite crystals. White layer med-fine grain calcite crystals. Darker zone with rhombohedral calcite crystals. Gray zone no crystal chalky	29.316377	-103.71734
Ls-106	altered Limestone calcite banded crystals	29.317413	-103.71857
Ls-107		29.317413	-103.71857
Nelsons Loop: Breccia pipe 2/ Cigar Mountain day 4			
Bp2-400	Chalky white partially bleached LIMESTONE. Sandy/Clay LIMESTONE . Calcite in fractures	29.325783	-103.743809
Bp2-401	Limestone, possibly Devil River LIMESTONE. Thin fractures with fine grained calcite infill	29.325915	-103.743851
Bp2-402	Breccia rock- partially bleached Limestone clast		
Bp2-403	Fresh Devil River Limestone	29.325557	-103.743993
Bp2-404	Fresh Devil River Limestone	29.32633	-103.743334
Bp2-405	Highly fractured bleached Limestone. Calcite crystal infill of fractures	29.326649	-103.743493
Cm-400	Volcanic rock Rhyolite/diorite	29.327619	-103.575431

Map

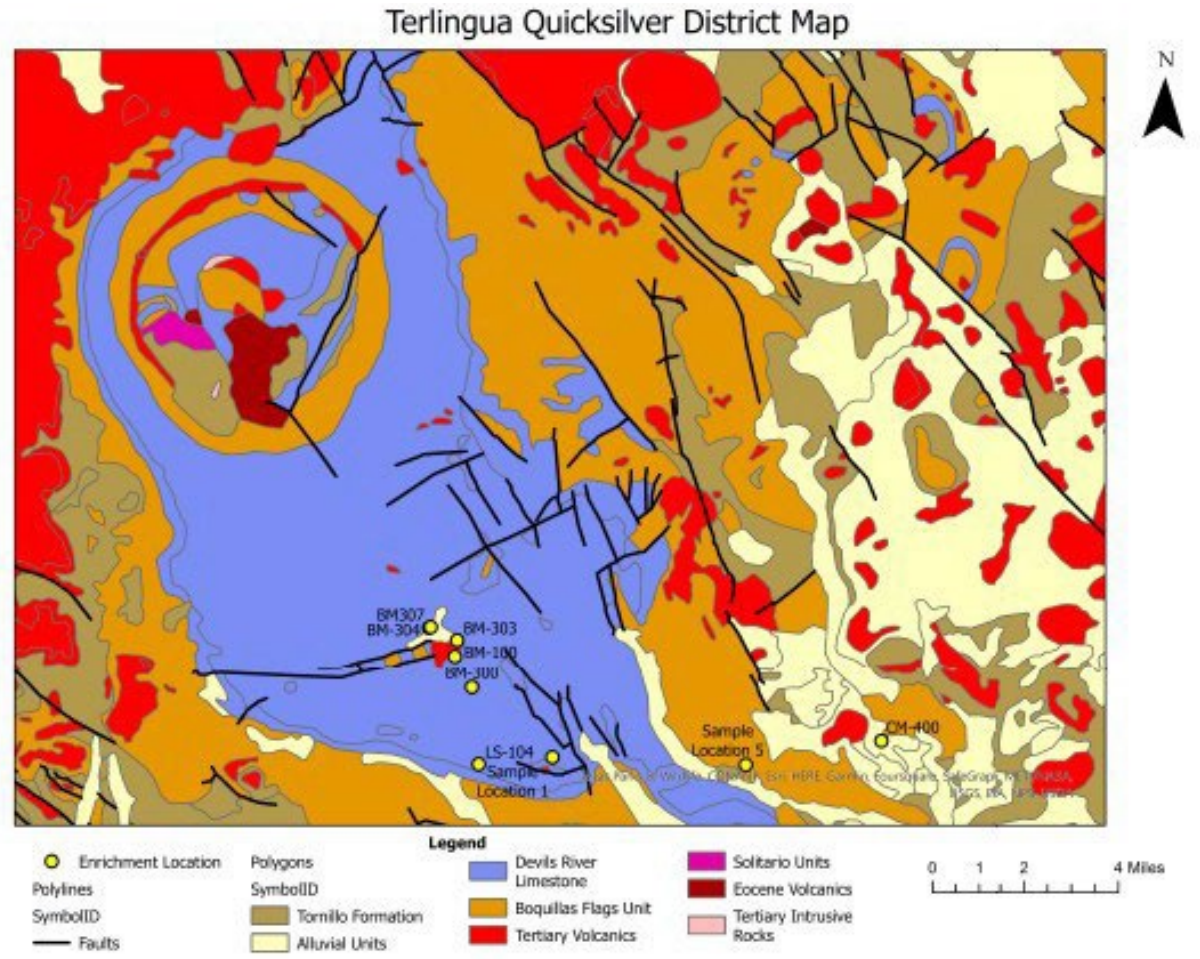

FIGURE 8: USING THE GEOLOGICAL MAPS FROM YATES AND THOPSON (1959) THIS MAP IS AN OVERVIEW MAP OF THE TQD SHOWING SAMPLE LOCATIONS WITH THE MOST ENRICHMENT. SAMPLE LOCATION ONE CONSISTS OF MULTIPLE SAMPLES, BUT THE SAMPLE SHOWING MOST ENRICHMENT IS MM-100 IN THE GROUP OF SAMPLES. SAMPLE CATALOGUE WILL HAVE THE FULL LIST OF SAMPLES IN THIS SAMPLE LOCATION. SAMPLE LOCATION 5 HAS MULTIPLE SAMPLES, BUT THE SAMPLES OF INTEREST ARE: RM-105, RM-100, RM-101, RM-103, MM-105, AND RM-104. SAMPLES COLLECTED IN THE NW CORNER NAMED BM-###, WERE COLLECTED FROM BLACK MESA. WHILE FARTHER SOUTH, SAMPLE LS-104 WAS COLLECTED FROM THE LONE STAR MINE. IN THE FAR EAST BY THE TERLINGUA AIRPORT IS SAMPLE CM-400, THIS SAMPLE WAS COLLECTED FROM THE FOOT OF THE CIGAR MOUNTAIN

Enrichment List

TABLE 2: LIST OF ELEMENTS AND CITE OF ENRICHMENT, THE ENRICHMENT SITES ARE THE OUTLIERS OF THE HISTOGRAMS

- Vanadium:
  - Average: 55.55
  - Min/Max: 2.5/680
  - Enriched Samples: BM-304: 680, RM-100: 241, BM-308: 161, BM-303: 153, BM-307: 141, BM-100: 114, RM-104: 100, CM-400: 96, Bp1-202: 90,
- Chromium:
  - Average: 28.73
  - Min/Max: 10/260
  - Enriched Samples: RM-100: 260, Bm-101b: 100, BM-100: 80, BM-303: 80, BM-305: 80, BM-101a: 70, BM-302: 70
- Cobalt:
  - Average: 6.07
  - Min/Max: .5/188
  - Enriched Samples: MM-105: 188, RM-100: 35, CM-400: 20, MM-201: 19
- Zinc:
  - Average: 49.58
  - Min/Max: 15/250
  - Enriched Samples: MM-105: 250, BM-304: 200,
- Gallium:
  - Average: 3.86
  - Min/Max: .5/19
  - Enriched Samples: CM-400: 19, RM-100: 18, RM-101: 17, RM-103: 15, RM-104: 15, BM-308: 10
- Germanium:
  - Average: 1.08
  - Min/Max: .2/14.6
  - Enriched Samples: BM-304: 14.6, BM-308: 5.4, BM-307: 5.3
- Arsenic:
  - Average: 103.35
  - Min/Max: 2.5/2000
  - Enriched Samples: BM-300: 2000, BM-308: 1620, BM-307: 877, BM-304: 572
- Rubidium:
  - Average: 12.18
  - Min/Max: .5/143
  - Enriched Samples: RM-100: 143, RM-101: 118, RM-103: 84, RM-104: 71, CM-400: 45, MM-201: 30
- Strontium:
  - Average: 460.25
  - Min/Max: 20/1580
  - Enriched Samples: MM-100:1580, CM-400: 1200, RM-107: 1120, MM-200: 996, LS-101: 919, BM-300: 852, MM-105: 843, MM-101: 827, RM-100: 782, Bp2-405: 725, RM-104: 641

- Yttrium:
    - Average: 6.71
    - Min/Max: .2/34.5
    - Enriched Samples: RM-105: 34.5, BM-303: 31.8, CM-400: 28.9, RM-101: 21.8, RM-100: 20.4, RM-103: 20.1
- Zirconium:
    - Average: 54.74
    - Min/Max: .5/688
    - Enriched Samples: BM-303: 688, CM-400: 302, RM-103: 176, RM-101: 152, RM-100: 149, Rm-105: 139, RM-104: 138
- Niobium:
    - Average: 7.39
    - Min/Max: .1/210
    - Enriched Samples: BM-303: 210, CM-400: 56.6
- Molybdenum:
    - Average: 7.76
    - Min/Max: 2/91:
    - Enriched Samples: BM-307: 91, BM-303: 47, Bp2-404: 34 BM-304: 28, BM-308: 21, BM-305: 15, Bp1-201: 14, MM-105: 13
- Tin:
    - Average: 1.32
    - Min/Max: .5/15
    - Enriched Samples: BM-303: 15, Bp1-202: 4, BM-302: 4
- Antimony:
    - Average: 7.65
    - Min/Max: .1/159
    - Enriched Sample: BM-300: 159, BM-307: 78.1, MM-100: 29.7, MM-202: 21.2
- Cesium:
    - Average: 2.92
    - Min/Max: .1/97.4
    - Enriched Samples: RM-100: 97.4, RM-101: 15.1, RM-103: 10.7
- Barium:
    - Average: 853.72
    - Min/Max: 1.5/13700
    - Enriched Samples: MM-100: 13700, MM-105: 9260, BM-303: 4630, MM-300: 4160, MM-200: 4120, MM-103: 3230, BM-300: 1520, BM-307: 1080
- Lanthanum:
    - Average: 10.56
    - Min/Max: .1/86.1
    - Enriched Samples: BM-100: 86.1, CM-400: 53.9, RM-100: 35.3, RM-101: 33
- Cerium:
    - Average: 19.7
    - Min/Max: .3/139
    - Enriched Samples: BM-100: 139, CM-400: 111, RM-100: 66.5, RM-101: 66.1, RM-105: 64.1, RM-103: 63.9, RM-104: 53.7, BM-101A: 43.6
- Praseodymium:
    - Average: 2.30

- Min/Max: 0/13.4
- Enriched Samples: BM-100: 13.4, CM-400: 12.5, RM-100: 8.69, RM-105: 8.68, RM-101:8, RM-103: 7.59

- Neodymium:
  - Average: 8.79
  - Min/Max: .1/53.6
  - Enriched Samples: CM-400 53.6, BM-100: 47.3, RM-105: 37.6, RM-100: 35.9, RM-101: 29.8, RM-103: 27.7, RM-104: 23.8, MM-201: 16.2
- Samarium:
  - Average: 1.62
  - Min/Max: 0/9.9
  - Enriched Samples: CM-400: 9.9, RM-105: 9.3, RM-100: 7.5, RM-101: 6, BM-100: 5.5, RM-103: 5.32, RM-104: 4.53BM-303: 4.12
- Europium:
  - Average: .34
  - Min/Max: 0/ 3.08
  - Enriched Samples: CM-400: 3.08, RM-100: 2, RM-105: 1.87, RM-101: 1.07
- Gadolinium:
  - Average: 1.25
  - Min/Max: .02/8.35
  - Enriched Samples: RM-105: 8.35, CM-400: 7.99, RM-100: 5.77, RM-101: 4.39, BM-303: 4.18, RM-103: 3.78, RM-104: 3.11, BM-100: 3.03, MM-201: 2.58, Bp2-404: 2.55
- Terbium:
  - Average: .20
  - Min/Max: .01/1.40
  - Enriched Samples: RM-105: 1.4, CM-400: 1.10, BM-303: 0.9, RM-100: 0.8, RM-101:0.7, RM-103: 0.6, RM-104: 0.5, MM-201: 0.4, Bp2-404: 0.4,
- Dysprosium:
  - Average: 1.18
  - Min/Max: .01/7.45
  - Enriched Samples: RM-105: 7.45, CM-400: 6.24, BM-303: 5.91, RM-101: 4.42, RM-100: 4.31, RM-103: 3.86, RM-104: 3.18, MM-201: 2.41 Bp2-404: 2.40
- Holmium:
  - Average: .23
  - Min/Max: .01/1.27
  - Enriched Samples: Rm-105: 1.27, BM-303: 1.24, CM-400: 1.04, RM-101: 0.8, RM-103: 0.8, RM-100: 0.8, RM-104: 0.6, MM-201: 0.5, Bp2-404: 0.4
- Erbium:
  - Average: .65
  - Min/Max: .01/3.67
  - Enriched Samples: BM-303: 3.67, RM-105: 3.25, CM-400: 2.79, RM-101: 2.41, RM-103: 2.28, RM-100: 1.93, RM-104: 1.86, MM-201: 1.30, Bp2-404: 1.20, MM-200: 1.12

- Thulium:
  - Average: .10
  - Min/Max: 0/.61

    - Enriched Samples: BM-303: .61, RM-105: 0.4, CM-400: .35, RM-101: .35, Rm-103: .34,
- Ytterbium:
    - Average: .63
    - Min/Max: .01/4.33
    - Enriched Samples: BM-303: 4.33, RM-105: 2.47, RM-101: 2.37, RM-103: 2.25, CM-400: 2.25, RM-104: 1.9, RM-100: 1.7, MM-201: 1.2, MM-200: 1.1, Bp2-404: 1.1
- Lutetium:
    - Average: .09
    - Min/Max:0/.61
    - Enriched Samples: BM-303: .68, RM-105: 0.4, RM-101: .35, CM-400: .34, RM-103: .34, RM-104: 0.3, RM-100: 0.23, MM-201: 0.2, MM-202: 0.2, MM-200: 0.2, MM-103: 0.2
- Hafnium:
    - Average: 1.32
    - Min/Max: .05/16.8
    - Enriched Samples: BM-303: 16.80, CM-400: 6.5, RM-103: 4.3, RM-101:3.7, RM-100: 3.5, RM-104: 3.4, BM-102: 3.4, RM-105: 2.9, MM-200: 2.8, Bp2-404: 2.3
- Tantalum:
    - Average: .60
    - Min/Max: 0/17.60
    - Enriched Samples: BM-303: 17.60, CM-400: 3.7, BM-102: 1.02,
- Tungsten:
    - Average: 10.56
    - Min/Max: .2/337
    - Enriched Samples: MM-105: 337, BM-307: 71.2, BM-304: 24.7, BM-308: 21.2
- Thallium:
    - Average: 1.27
    - Min/Max: .025/21.6
    - Enriched Samples: BM-307: 21.6, MM-105: 8.55, BM-308: 5.7, BM-304: 5.25, RM-104: 5.13, BM-305: 3.4, RM-104: 5.1, BM-305: 3.4, BM-300: 3.22, Bp1-201: 2.3
- Lead:
    - Average: 8.16
    - Min/Max: 2.5/97
    - Enriched Samples: MM-105: 97, BM-303: 55, BM-101A: 34, BM-101B: 22, BM-300: 18
- Thorium:
    - Average: 2.42
    - Min/Max: .03/12.2
    - Enrichment Samples: RM-103: 12.2, RM-101: 11.4, RM-100: 10.7, RM-104: 10.1, BM-303: 8.3, MM-200, 7.7, BM-100: 6.3, CM-400: 6.01, MM-201: 5.9, RM-105: 5.6, MM-103: 5.3, MM-202: 5

- Uranium:
    - Average: 3.71
    - Min/Max: .12/23.9

- Enriched Samples: BM-304: 23.9, BM-307: 19, BM-300: 11.4, BM-303: 9.7, MM-200: 8.37, RM-104: 7.4, BM-308: 7.2, BM-306: 7

- Mercury:
  - Average: 12,819.26
  - Min/Max: 2.5/100,000
  - Enriched Samples: RM-104: 100,000 PD-100: 100,000, RM-103: 92,300, LS-104: 86,800, BM-309: 65800, MM-300:38700, LS-105: 38100, LS-103: 35700, BM-307: 27200

Univariant Analysis

TABLE 3 BIMODAL HISTOGRAMS, AND THE NUMBER OF OUTLIERS (ALONG WITH THE SAMPLE LOCATION.)

Bimodal 1 outlier	Bimodal 2 outliers	Bimodal 3 outliers	Bimodal 4 outliers	Bimodal 5 outliers
Thallium BM-307: 21.6	Zinc MM-105: 250 BM-304: 200		Gallium CM-400: 19 RM-100: 18 RM-101: 17 RM-103: 15	Mercury PD-100: 100,000 RM-104: 100,000 RM-103: 92,300 LS-104: 86,800 BM-309:65,800
Germanium BM-304: 14.6	Thorium RM-103: 12.2 RM-101: 11.4		Yttrium RM-105: 34.5 BM-303: 31.8 CM-400: 28.9 RM-101: 21.8	
Ytterbium BM-303: 4.33				
Thulium BM-303: .61				

TABLE 4 UNIMODAL HISTOGRAMS AND THE NUMBER OF OUTLIERS (ALONG WITH THEIR SAMPLE LOCATION.)

Unimodal 1 outlier	Unimodal 2 outliers	Unimodal 3 outliers	Unimodal 4 outliers	Unimodal 5 outliers	Unimodal 6 outliers:	Unimodal 7 outliers:
Vanadium BM-304: 680	Barium MM-100: 13700 MM-105: 9260	Neodymium CM-400 53.6 BM-100: 47.3 RM-100: 37.6	Arsenic BM-300: 2000 BM-308: 1620 BM-307: 877 BM-304: 572		Holmium RM-105: 1.27 BM-303: 1.24 CM-400: 1.04 RM-100: 0.8 RM-101: 0.8 RM-103: 0.8	Erbium BM-303: 3.67 RM-105:3.25 CM-400 RM-101: 2.41 RM-103: 2.28 RM-100: 1.93 RM-104: 1.86
Tungsten MM-105: 337						
Chromium RM-100: 260	Zirconium BM-303: 688 CM-400: 302					
Cobalt MM-105: 188		Europium CM-400: 3.08 RM-100: 2 RM-105: 1.87				
Cesium RM-100: 97.4	Niobium BM-303: 210 CM-400: 56.6		Rubidium RM-100: 143 RM-101:118 RM-103:84 RM-104: 71			
Tantalum BM-303: 17.60						
Hafnium: BM-303: 16.80	Antimony BM-300: 159 BM-307: 78.1	Gadolinium RM-105: 8.35 CM-400: 7.99 RM-100: 5.77				
Praseodymium BM-100: 13.4						
Samarium CM-400: 9.9	Cerium BM-100: 139 CM-400: 111		Lanthanum BM-100: 86.1 CM-400: 53.9 RM-100: 35.3 RM-101: 33			
Lutetium : BM-303: .68		Dysprosium RM-105: 7.45 CM-400: 6.24 BM-303: 5.91				
Tin BM-303: 15	Molybdenum BM-307: 91 BM-303: 47					
	Lead					

	MM-105: 97 BM-303: 55					
	<u>Uranium</u>					
	BM-304: 23.9 BM-307: 19					
	<u>Terbium</u>					
	CM-400: 1.10 RM-105: 1.4					

TABLE 5 REES AND THE HIGHEST LEVEL OF ENRICHMENT BY LOCATION.

REE	RM	Bp2	MM	CM	BM
Y Yttrium:	RM-100: 20.4, RM-101: 21.8, RM-103: 20.1, RM-105: 34.5			CM-400: 28.9,	BM-303: 31.8
La Lanthanum:	RM-100: 35.3, RM-101: 33			CM-400: 53.9,	BM-100: 86.1
Ce Cesium:	RM-100: 97.4, RM-101: 15.1, RM-103: 10.7				
Pr Praseodymium:	RM-100: 8.69, RM-101:8, RM-103: 7.59 RM-105: 8.68			CM-400: 12.5	BM-100: 13.4
Nd Neodymium:	RM-100: 35.9, RM-101: 29.8, RM-103: 27.7, RM-104: 23.8, RM-105: 37.6		MM-201: 16.2	CM-400 53.6	BM-100: 47.3
Pm					
Sm Samarium:	RM-100: 7.5, RM-101: 6, RM-103: 5.32, RM-104: 4.53 RM-105: 9.3,			CM-400: 9.9	BM-100: 5.5, BM-303: 4.12
Eu Europium:	RM-100: 2, RM-101: 1.07 RM-105: 1.87,			CM-400: 3.08	
Gd Gadolinium:	RM-100: 5.77, RM-101: 4.39, RM-103: 3.78, RM-104: 3.11, RM-105: 8.35	Bp2-404: 2.55	MM-201: 2.58	CM-400: 7.99	BM-100: 3.03 BM-303: 4.18
Tb Terbium:	RM-100: 0.8, RM-101:0.7, RM-103: 0.6, RM-104: 0.5, RM-105: 1.4,	Bp2-404: 0.4	MM-201: 0.4	CM-400: 1.10	BM-303: 0.9
Dy Dysprosium:	RM-100: 4.31, RM-101: 4.42, RM-103: 3.86, RM-104: 3.18 RM-105: 7.45,	Bp2-404: 2.40	MM-201: 2.41	CM-400: 6.24	BM-303: 5.91

Ho Holmium:	RM-100: 0.8 RM-101: 0.8, RM-103: 0.8, RM-104: 0.6 RM-105: 1.27	Bp2-404: 0.4	MM-201: 0.5	CM-400: 1.04	BM-303: 1.24
Er Erbium:	RM-100: 1.93, RM-101: 2.41, RM-103: 2.28, RM-104: 1.86 RM-105: 3.25,	Bp2-404: 1.20	MM-201: 1.30, MM- 200: 1.12	CM-400: 2.79	BM-303: 3.67
Tm Thulium:	RM-101: .35, RM-103: .34 RM-105: 0.4,			CM-400: .35	BM-303: .61
Yb Ytterbium:	RM-100: 1.7, RM-101: 2.37, RM-103: 2.25, RM-104: 1.9, RM-105: 2.47	Bp2-404: 1.1	MM-200: 1.1 MM-201: 1.2	CM-400: 2.25, CM- 400: 2.25	BM-303: 4.33
Lu Lutetium:	RM-100: 0.23 RM-101: .35, RM-103: .34, RM-104: 0.3, RM-105: 0.4,		MM-201: 0.2, MM-202: 0.2, MM-200: 0.2, MM-103: 0.2	CM-400: .34	BM-303: .68

TABLE 6 CULMINATION OF ALL THE HISTOGRAMS IN APPENDIX. THIS TABLE COMPILES THE LOCATIONS OF OUTLIERS AND THE ELEMENTS IN WHICH THEY ARE MOST ENRICHED. THE DATA IS COMPILED BY THE SAMPLE LOCATION WITH THE MOST ENRICHMENT OF ELEMENTS AT THE TOP TO THE SAMPLE LOCATION WITH THE LEAST ENRICHED AT THE BOTTOM.

Sample Name	Enriched in:
Cm-400	Er, Ho, Dy, Gd, Eu, Sm, Nd, Pr, Ce, La, Y, Tb, Nb, Zr, Ga
BM-303	Lu, Dy, Yb, Tm, Er, Ho, Y, Pb, Ta, Hf, Zr, Nb, Mo, Sn
RM-105	Dy, Er, Tb, Gd, Eu, Sm, Y, Ho, Nd
RM-100	Ho, Gd, Eu, Sm, Cs, Rb, Ga, Cr
RM-103	Ho, Er, Rb, Ga, Th, Hg
RM-101	Er, Ho, Y, Rb, Ga, Th
BM-307	U, Tl, Sb, As, Mo
BM-304	U, As, Ge, Zn, V
MM-105	Pb, W, Ba, Zn, Co
BM-100	Pr, Ce, La, Nd
RM-104	Ho, Hg, Rb
MM-100	Ba, Sr
BM-300	Sb, As
BM-308	As, Ge
PD-100	Hg
LS-104	Hg

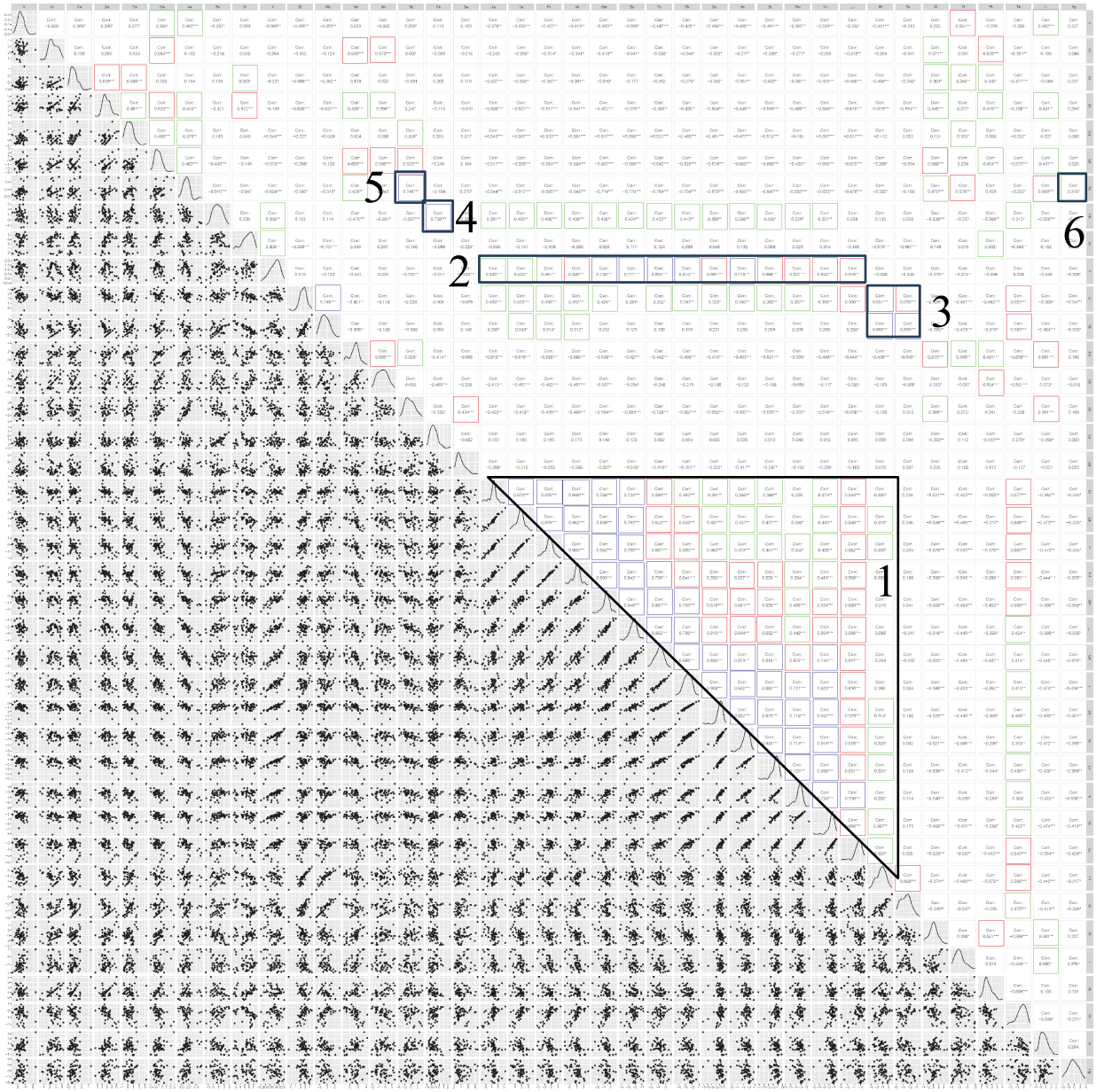

FIGURE 9 BIVARIANT ANALYSIS OF THE DATA, THE CORRELATION COEFFICIENT. THE BLUE BOXES IDENTIFY THE HIGH CORRELATION VALUES HIGHER THAN 0.7, RED BOXES IDENTIFY THE INTERMEDIATE VALUES BETWEEN 0.5- 0.7, AND THE GREEN BOXES IDENTIFY THE LOW CORRELATION COEFFICIENTS VALUES BETWEEN 0.3-0.5. FAMILIES ARE INDICATED WITH CORRESPONDING NUMBER.

5: Discussion

Univariant

Table 4 shows the number of outliers present in unimodal histograms. Unimodal with one outlier had the greatest number of outliers, as seen in table 4, with ten Elements having a single outlier. The sample area with the designation BM- from the Black Mesa has the most outliers, five, while RM-, and MM- have two, and CM- with one. BM-304 had the highest enrichment of vanadium with 680 ppm. Unimodal with two outliers has 9 elements with outliers: Barium being the highest with 13,700 ppm, and 9260 ppm both samples were collected at the Mariposa Mine site. The samples collected from Black Mesa had the most occurrence of outliers with 6 samples, zirconium has the highest enrichment value from Black Mesa at 688 ppm. The unimodal histograms with three outliers are enriched in Nd, Eu, Gd, and Dy. In this group the sample collected at CM-400 shows enrichment of all four REEs. The samples collected at RM-100, 101, and 105 locations are enriched in all four REEs as well. The BM-100, and 303 samples are enriched in Nd, and Dy. The unimodal histograms with 4 outliers show Black Mesa are enriched with As, and La. Black Mesa has the most occurrences of As enrichment with all 4 outliers collected at Black Mesa. The sample location BM-300 has a concentration value of 2000 ppm, followed by BM-308 at 1620 ppm. These two sample locations are the most enriched in As. The sample locations Rainbow mine, shown with the distinction RM-###, is enriched in Rb. With the sample location RM-100 being the highest concentration value at 143 ppm, followed by RM-101 at 118 ppm. Lanthanum is found at Black Mesa, BM-100 at 86.1 ppm; Cigar Mountain, CM-400 with 53.9 ppm; and Rainbow Mine, RM-100: 35.3 ppm, and RM-101: 33 ppm. The unimodal histograms with six and seven outliers are enriched in one REE each. The six-outlier histogram is enriched with Ho most of the enrichment happens in the Rainbow Mine, with RM-105 being the highest at 1.27 ppm followed but RM-100,101, and 103 all with 0.8 ppms. Black Mesa and Cigar

Mountain have outliers of Ho with BM-303 at 1.24 ppm, and CM-400 at 1.04 ppm. There are no unimodal histograms with 5 outliers.

Looking at Bimodal histograms, table 3 shows that bimodal histograms are enriched with one, two, four and five outliers. First looking at the bimodal histogram with one outlier Black Mesa is enriched with four elements. Thallium is enriched by 21.6 ppm at sample location BM-307, germanium is at 14.6 ppm at BM-304, ytterbium is at 4.33 ppm at BM-303, and thulium is at .61 ppm at BM-303. The bimodal histogram with two outliers is enriched with zinc at sample location MM-105, enriched by 250 ppm, and BM-304 with 200 ppm. Rainbow Mine is enriched in thorium at location RM-103 with 12.2 ppm, and RM-101 with 11.4 ppm. The next bimodal histogram with three outliers shows no enrichment. Bimodal histograms with four outliers show enrichment at Rainbow Mine, Blac Mesa, and Cigar Mountain. Those sample locations are enriched with gallium and ytterbium. The most enriched location for gallium is CM-400 at 19 ppm followed by RM-100, 101, and 103 ranging from 18 ppm to 15 ppms. Yttrium concentration shows at sample location RM-105 with 34.5 ppm, BM-303 with 31.8 ppm, CM-400 with 28.9 ppm, and RM-101 at 21.8 ppm. There is only one bimodal histogram with 5 outliers, mercury. PD-100, and RM-104 are enriched in mercury at 100,000 ppms, Rm-103 is enriched with 92,300 ppms, LS-104 has an enrichment of 86,600, while BM-309 I at 65,800 ppm.

Focusing on REE enrichment, Table 5 shows Rainbow mine is enriched in REEs. Rainbow Mine is enriched in 15 REEs: Y, La, Ce, Pr, Nd, Sm, Eu, Gd, Tb, Dy, Ho, Er, Tm, Yb, and Lu. There are 63 instances where the samples collected at Rainbow Mine show enrichment of REEs. The samples with the most occurrences of REE enrichment come from sample location RM-100, RM-101, RM-103, and RM-105 with a few at RM-104. Cigar Mountain is the second location with the most REE enrichments Y, La, Pr, Nd, Sm, Eu, Gd, Tb, Dy, Ho, Er, Tm, Yb, and Lu show enrichment. Black Mesa shows the same occurrences of enrichment as Cigar Mountain. However, Eu is not enriched in Black Mesa. Mariposa Mine (MM-###) and Breccia Pipe two (Bp2-###) also show enrichment is some REEs, but not as much as Rainbow Mine and Black Mesa. Mariposa

Mine in enriched with more REEs with Nd, Gd, Tb, Dy, Ho, Er, Yb, Lu showing enrichment values are sample locations MM-200, 201 with Lu also found at MM-202 and 103. Brecia Pipe two has the least occurrences of REE enrichment, only Gd, Tb, Dy, Ho, Er, Yb show enrichment at sample location Bp2-404.

Table 6 shows the sample locations with the highest occurrences of enrichment, separating REE from other elements. CM-400 has the highest number of occurrences. Cigar Mountain is enriched with fifteen elements, twelve of which are REEs. Black Mesa with sample location BM-303 has the second greatest number of occurrences with fourteen elements, seven of which are REEs. Black Mesa shows up on the list five more times with sample location BM-307, and 304 at occurrences of enrichment; BM-100 with four, BM-300 and 308 at two.

Bivariant

Figure 10 are the results of the correlation coefficients of the bivariant analysis. The chart is enhanced with high-intermediate-low by colors. The blue represents a high correlation above 0.7, while the red represents an intermediate correlation, and the green is the lowest correlation between 0.3- 0.5. When looking at the correlation coefficient chart there is noticeably a large family of coefficients and several smaller families of coefficients. The large family of coefficients is between the REEs. It starts at La on the vertical axis, which has a high correlation with Ce, Pr, Nd, Sm, and Eu, of which the correlation between La and Ce and La and Pr are 0.970. working diagonally to the bottom right corner, the family of coefficients ends at Tm with a high correlation with Yb and Lu. This large family of coefficients has an intermediate and low zone of correlations. The group ends at around the one-to-one correlation with Hf. The other smaller families are above the larger triangular-shaped family of the REEs. The first small family is between Rb on the vertical axis, and Cs with a 0.730 coefficient plus As and Sb with a 0.748 coefficient. Another family is with Y and Sm a 0.736 coefficient Y and Eu 0.777, Y and Gd 0.854, Y and Tb 0.814, Y

and Dy 0.661, and Y and Ho 0.778. The third family is between Zr and Hf 0.851, Nb and Hf 0.868, Nb and Ta 0.835. There is an outlier with Zr and Nb with a correlation of 0.746.

The following families are identified from bivariant analysis. They will subsequently be explored, tested, and verified in multivariant analysis.

1. Intercorrelation within REEs: LREE stronger blue, HREE intermediate values (red)
2. Inclusion of Y with LREE
3. Zr-Hf-Nb-Ta
4. Rb-Cs
5. As-Sb
6. Hg (As)

Family 1: Intercorrelation within REEs: LREE stronger blue, HREE intermediate values (red): the large triangle section in the lower central area (figure 10) with the matrix diagonal being the hypotenuse of the triangle. Generally, colors diminish, blue to red to green, away from the hypotenuse. Family 2: row 10 down from the top illustrated by a long line of red and blue boxes. Family 3: red and blue boxes located immediately to the lower-right of Y row of #2. Family 6: Hg is the last column on the right and has only a slight positive correlation (0.316) with As. It is noted that Hg has a moderate negative correlation with families 1 and 2 containing REE. Family 7 (not on list): it is noted that Zn-Ga-Ge is not a prominent family.

Multivariant

Centered log ratio multivariant analysis was carried out on the data (Buccianti, Mateu-Figueras, & Pawlowsky-Glahn, 2006). The first four components account for 77.79% of the variance in the data. Figures 11, 12, and 13, show the following components plotted against each other; respectively: 1 to 2, 2 to 3, and 3 to 4. Chemical families are readily substantiated by bivariant correlation coefficients and are listed previously. Components are defined by simultaneous equations giving relative weights to the chemical constituents. Those families are

circled and labeled on these three multivariant diagrams where identifiable. The more populated families 1 and 2 contain so many overprints that they are not readable. The multivariant analysis thus serves to substantiate the choices made for the bivariant families.

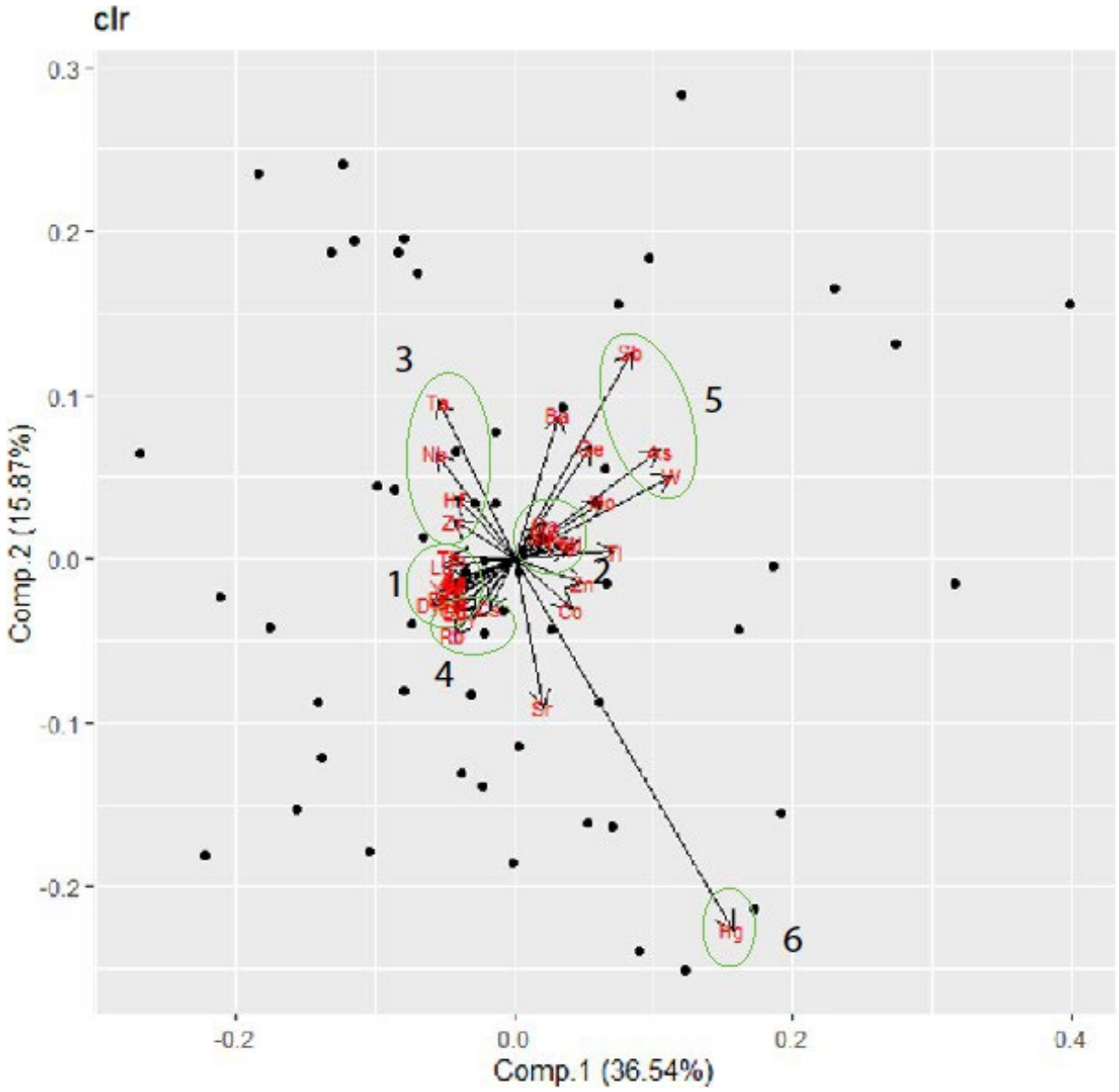

FIGURE 10 CENTERED LOG RATIO OF COMPONENTS 1 AND 2

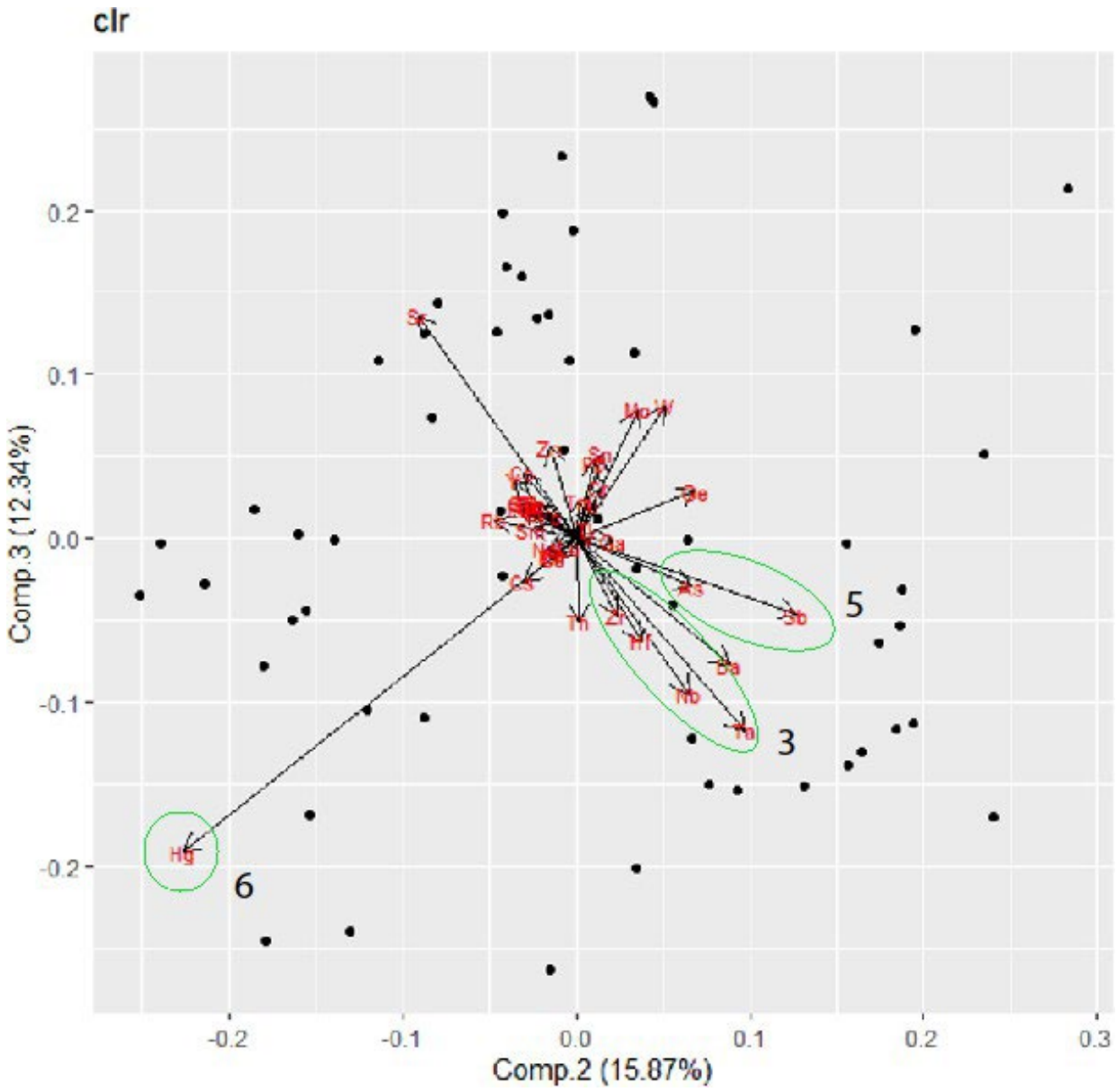

FIGURE 11 CENTERED LOG RATIO OF COMPONENTS 2 AND 3

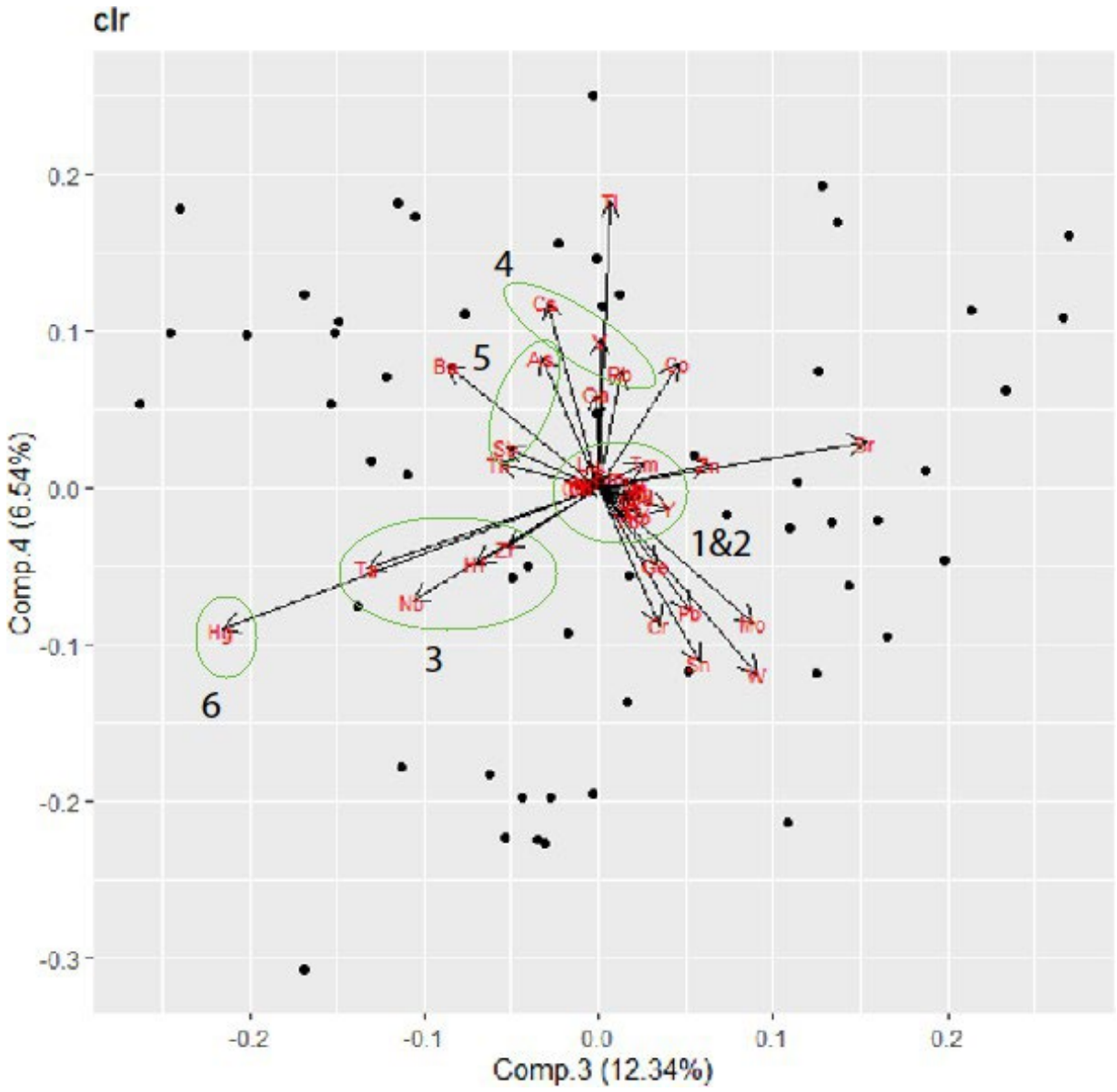

Figure 12 Centered Log ratio of Components 3 and4

Speculation on the Genisis

The genesis of the deposit was not a particular objective of this work, however, enough has been learned to be able to make some reasonable statements concerning the origins of the deposits. Intrusive consisting of analcite ($NaAlSi_2O_6 \cdot H_2O$) as a primary constituent in felsic, sodic, rocks are widespread and unusual. Several enriched areas are centered on such intrusive. Epithermal solutions motivated by these intrusive and maybe containing a magmatic component appear responsible for the enriched CM that is documented. These same solutions moved outwards to mineralize the fractures and breccia pipes.

6: Conclusion

Three types of lodes are found in TQD, the contact between Devils River Limestone and Grayson formations Del Rio Clay, deposits associated with faults, and Deposits close to igneous intrusions. Mercury mineralization is found E-NE in Fifty-five samples have been collected and analyzed for forty-four different chemicals. Univariant, bivariant, and multivariant analyses have been applied to these data. Geochemical families identified are 1) REEs, 2) Y with LREE, 3) Zr-Hf-Nb-Ta, 4) Rb-Cs, 5) As-Sb, 6) Hg (As). The special distributions have been placed on a map, which shows the locations of three significant hydrothermal systems that have been enriched in CM and REEs, which are Black Mesa, Rainbow-Chisos mine, and Cigar Mountain. Centered log ratio multivariant analysis was carried out on the data (Buccianti, Mateu-Figueras, & Pawlowsky-Glahn, 2006) and the first four components account for 78% of the variance in the data. Chemical families are substantiated by bivariant correlation coefficients. Future exploration should be directed at the sites mentioned above and located on the map. The genesis of the deposit is believed to be caused by epithermal solutions, associated with analcite bearing sodic felsic rocks.

REFERENCES

Buccianti, A., Mateu-Figueras, G., & Pawlowsky-Glahn, V. (2006). *Compositional Data Analysis in the Geosciences: From Theory to Practice.* The geological Society, London.

Davidson, M. E. (2014). *Zircon Geochronology of Volcanic Rocks from the Trans-Pacos Orogenic Belt, Western Texas: Timing the Cessation of Laramie Folding, Uplift, and Post Flat-Slab Ignimbrite Flare-Ups* . Ms Thesis University of Houston, Houston pp 1-152.

Dickerson, P. W. (2013). Tascotal Mesa Transfer Zone- An Element of the Border Corridor Transform System, Rio Grande Rift of West Texas and Adjacent Mexico. *The Geological Society of America Special Paper 494*, 475-500.

Erdlac, R. J. (1990). A Laramide-age Push-up Block: The Structures and Formation of the Terlingua-Solitario Structural block, Big Bend Region, Texas. *Geological Society of America Bulletin*, 1065-1076.

Erdlac, R. J. (1990). Tectonic Model of the Terlingua Uplift, Big Bend Region, Trans-Pecos Texas. *Bulletin of South Texas Geological Society, 31*(1), 9-17.

Fisher, F. S., & Leedy, W. P. (1973). *Geochemical Characteristics of Mineralized Breccia Pipes in the Red Mountain District, San Juan Mountains, Colorado.* Washington: US Geological Survey Bulletin 1381.

Henry , C. D., & Price, J. G. (1985). *Summary of The Tectonic Development of Trans-Pecos Texas.* Bureau of Economic Geology Report, Austin.

Henry, C. D. (1996). Igneous Geology of the Solitarion. In C. D. Henry , & W. R. Muehlberger, *Geology of the Solitario Dome, Trans-Pecos Texas: Paleozoic, Mesozoic, and Cenozoic Sedimentation, Tectonism, and Magmatism.* Bureau of Economic Geology, Austin pp 57-80.

Henry, C. D., & Davis, L. L. (1996). Tertiary Volcanic, Volcaniclastic, and Intrusive Rocks Adjacent to the Solitario. In C. D. Henry, & W. R. Muehlberger, *Geology of the Solitario Dome, Trans-Pacos Texas: Paleozoic, Mesozoic, and Cenozoic Sedimentation, Tectonism, and Magmatism.* Bureau of Economic Geology Report, Austin pp. 81-105.

Henry, C. D., & Kunk , M. J. (1996). Geochronology of the Solitario and Adjacent Volcanic Rock. In C. D. Henry, & W. R. Muehlberger, *Geology of the Solitario Dome, Trans Pacos Texas: Paleozoic, Mesozoic, and Cenozoic Sedimentation, Tectonism, and Magmatism.* Bureau of Economic Geology, Austin pp 109-119.

Henry, C. D., & Kunk, M. J. (1997). Igneous evolution of a complex laccolith-caldera, the Solitario, Trans-Pecos Texas: Implications for calderas and subjacent plutons. *Geological Society of America Bulletin, 109*(8), pp. 1036-1054.

Henry, C. D., & Muehlberger, W. R. (1996). *Geology of the Solitario Dome, Trans-Pecos TEXAS:Paleozoic, Mesozoic, and Cenozoic Sedimentation, Tectonism, and Magmatism.* Bureau of Economic Geology Report, Austin pp 1- 158.

Johnston, W. P., & Lowell, D. J. (1961). Geology and Origin of Mineralized Breccia Pipes in Copper Basin, Arizona. *Economic Geology*, 916-940.

Kay, W. W. (1938). *Merccury in the Terlingua District of Texas.* Rolla: Missouri University of Science & Technology.

Lehman, T. M. (1985). *Stratigraphy, Sedimentology, and Paleontologu of Upper Cretaceous (Campanian-Maastrichtian) Sedimentary Rocks in Trans-Pacos Texas.* Austin: Ph. D Thesis The University of Texas at Austin.

Megaw, P. K. (2001). *Tres Marias Zinc/Germanium Project.* Chihuahua State: War Eagle Mining Company INC. Private Report.

Mosconi, L. S. (1984). *Tectonic History of The Black Mesa - Lowes Valley Area Brewster County, Texas.* Ms. Thesis Graduate school of Stephen F. Austin, Austin.

Moss, S., Russell, J. K., & Andrews, G. D. (2008, June 20). Progressive infilling of a Kimberlite Pipe at Diavik, Northwest Territories, Canada: INsights from volcaninc facies architecture, textures and granulometry. *Journal of Volcanology and Geothermal Research, 174*(1-3), 103-116.

Muehlberger, W. R. (1980). Texas Linament Revised. In P. W. Dickerson , J. M. Hoffer, & J. F. Callender, *New Mexico Geological Society Fall Field Conference Trans Pecos Region (southeastern New Mexico and West Texas) Guidebook 31* (pp. 113-121). Soccoro : New Mexico Geological Society.

Ollier, C. D. (2007). Breccia-Filled Pipes: Distinguishing Between Volcanic and Non-volcanic. *Supplementi di Geografia Fisica e Dinamica Quateraria*, 63-76.

Ostendorf, J., Henjes-Kunst, F., Schneider, J., Melcher, F., & Gutzmer, J. (2017). Genesis of the Carbonate-Hosted Tres Marias Zn-Pb-(Ge) Deposit, Mexico: Constraints from Rb-Sr Sphalerite GeoChrongology and Pb Isotopes. *Society of Economic Geologist, Inc.* , 1075-1087.

Page, W. R., Turner, K. J., & Bohannon, R. G. (2008). Tectonic History of Big Bend National Park. In J. E. Grey, & W. R. Page, *Geological, Geochemical, and Geophysical Studies by the U.S. Geological Survey in Big Bend National Park, Texas* (pp. 3-13). U.S. Geological Survey Circular 1327.

Ricketts, J. (2014). *Structural Evolution of The Rio Grande Rift: Synchronous Exhumation of Rift Flanks From 20-10 MA, Embryonic Core Complexes, and Fluid-Enhanced Quaternary Extension.*

Ricketts, J. W., & Karlstrom, K. E. (2016). Processes Controlling the Development of the Rio Grande Rift at Long time scales. In B. A. Frey, K. E. Karlstrom, S. G. Lucas, S. Williams , K. Zeigler, V. McLemore, & D. S. Ulmer-Scoole, *Guidebook 67 - Geology of the Belen Area* (pp. 195-202).

Ricketts, J. W., Karlstrom, K. E., Kelley, S. A., Schmandt, B., Donahue, M. S., & Wijk, J. v. (2016, March 01). Synchronous opening of the Rio Grande rift along its entire length at 25-10 Ma supported by apatite (U-TH)/He and fission-track thermochronology and evalution of possible driving mechanisms. *Geological Society of America Bulletin*, 397-424. Retrieved from GeoScienceWorld: https://pubs.geoscienceworld.org/gsa/gsabulletin/article/128/3-4/397/126171/Synchronous-opening-of-the-Rio-Grande-rift-along

Ross, C. P. (1941). The Quicksilver Deposits of the Terlingua Region, Texas. *Society of Economic Geology, 36*, 115-142.

Saini-Eidukat, B., Leoben, M., & Goettlicher, J. (2016). Chemical Environment of Unusually Ge- and Pb-Rich Willemite, Tres Marias Mine, Mexico. *Minerals*, 6-20.

Sharp, R. D. (1980). *Development of the Mercury Mining Industry, Trans-Pacos Texas.* Austin: Bureau of Economic Geology.

Stevens, J. B., & Stevens, M. S. (1989). Stratigraphy and Major Structural-Tectonic Events Along and Near the Rio Grande, Trans-Pecos Texas and Adjacent Chihuahua and Coahuila, Mexico. In P. W. Dickerson, M. S. Stevens, & J. B. Stevens, *South Texas Geological Society Field Trip Guidebook: Geology of the Big Bend, and Trans-Pecos, Texas* (pp. 73-116). South Texas Geological Society, San Antonio.

Thomas, W. A. (1991, March 1). The Appalachian-Ouachita rifted margin of southeastern North America. *Geologica Society of America Bulletin*, pp. 415-431.

Thompson, G. A. (1950). *structural Geology of the Terlingua Quicksilver District, Texas.* United States Gological Survey Open-File Report.

Urbanczyk, K., Rohr, D., & White, J. C. (2001). Geology of West texas. In *Aquifers of West Texas* (pp. 17-25). Department of Earth and Physcal Sciences, Sul Ross State University, Alpine.

Wenrich, K. J., & Sutphin, H. B. (1988). Recognition of Breccia Pipes in Norther Arizona. *Arizona Bureau of Geology and Mineral Technology, 18*(1), 1-5.

Yates, R. G., & Thompson, G. A. (1959). *Geology and Quicksilver Deposits of the Terlingua District Texas.* Washington : U.S. Department of the Interior.

Appendix 1

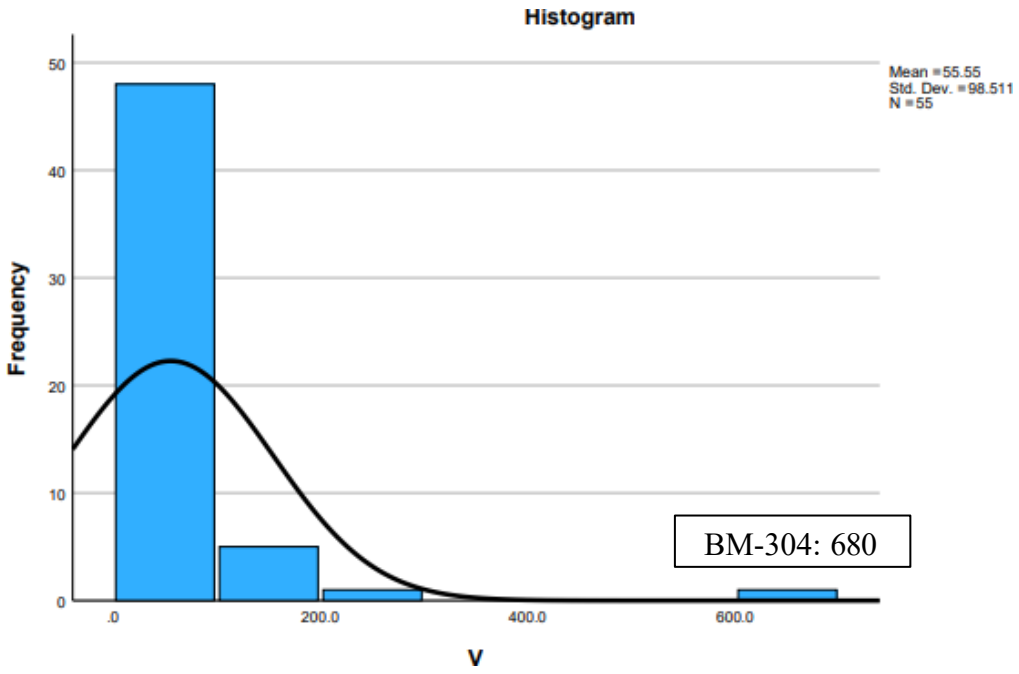
Histogram
Mean = 55.55
Std. Dev. = 98.511
N = 55
Frequency
50
40
30
20
10
0
.0
200.0
400.0
600.0
V
BM-304: 680

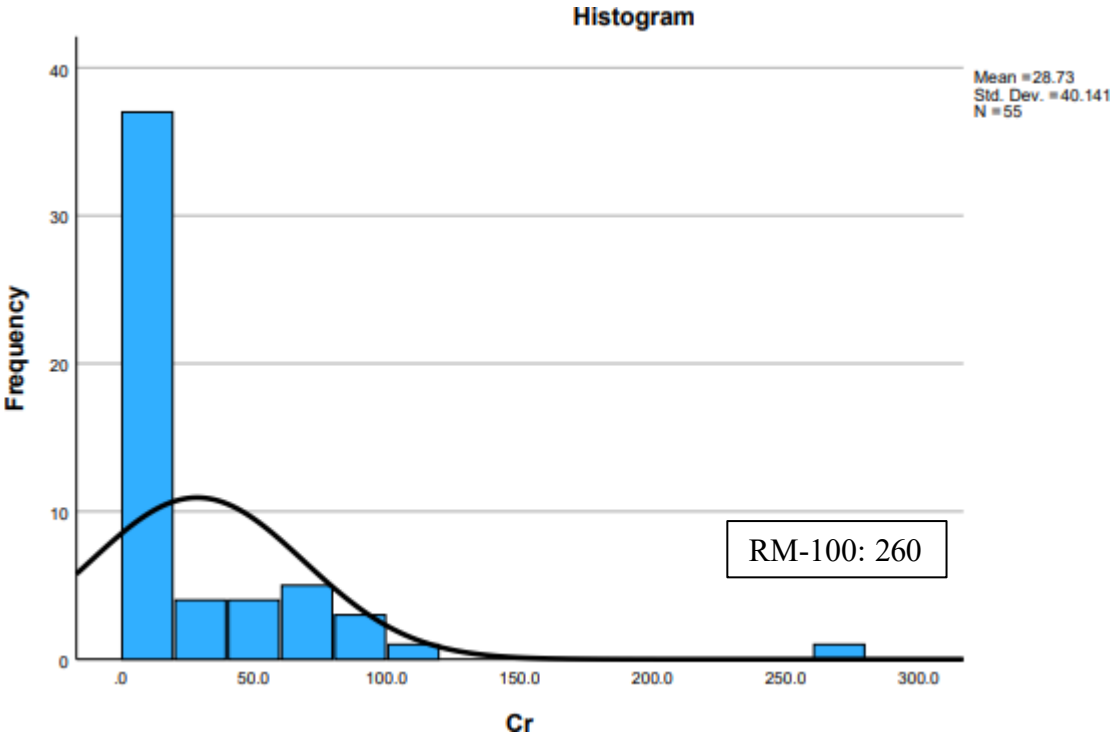
Histogram
Mean = 28.73
Std. Dev. = 40.141
N = 55
Frequency
40
30
20
10
0
.0
50.0
100.0
150.0
200.0
250.0
300.0
Cr
RM-100: 260

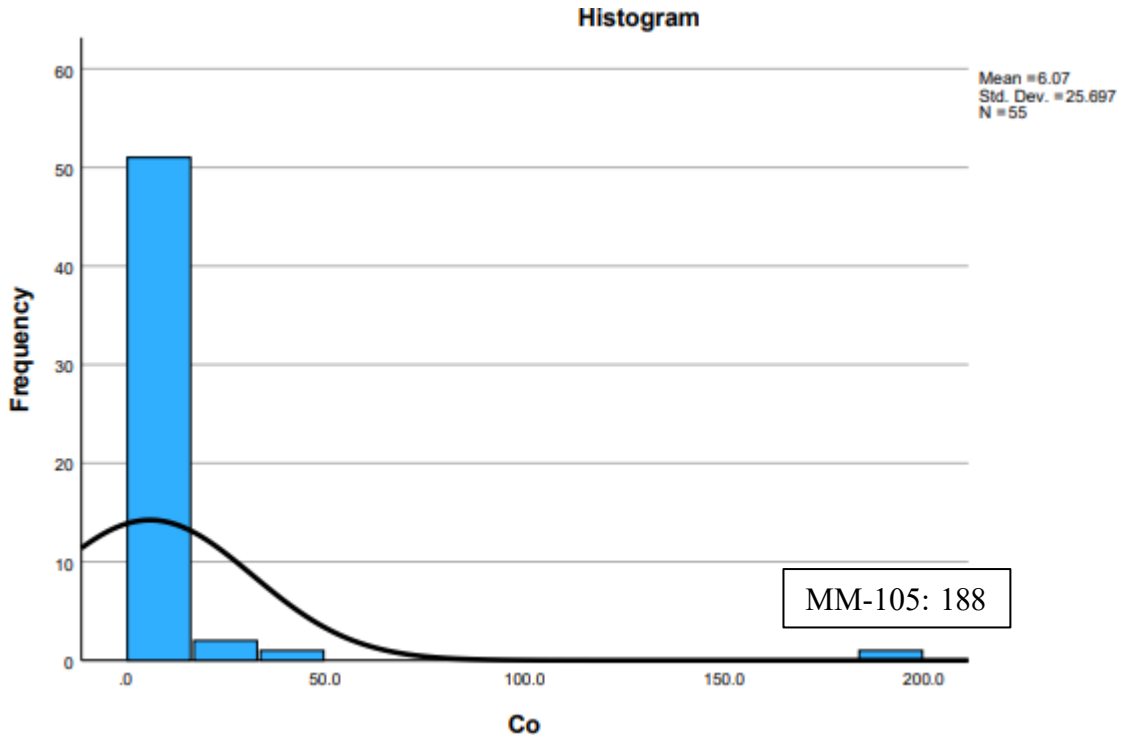
Histogram
Mean =6.07
Std. Dev. =25.697
N =55
Frequency
Co
MM-105: 188

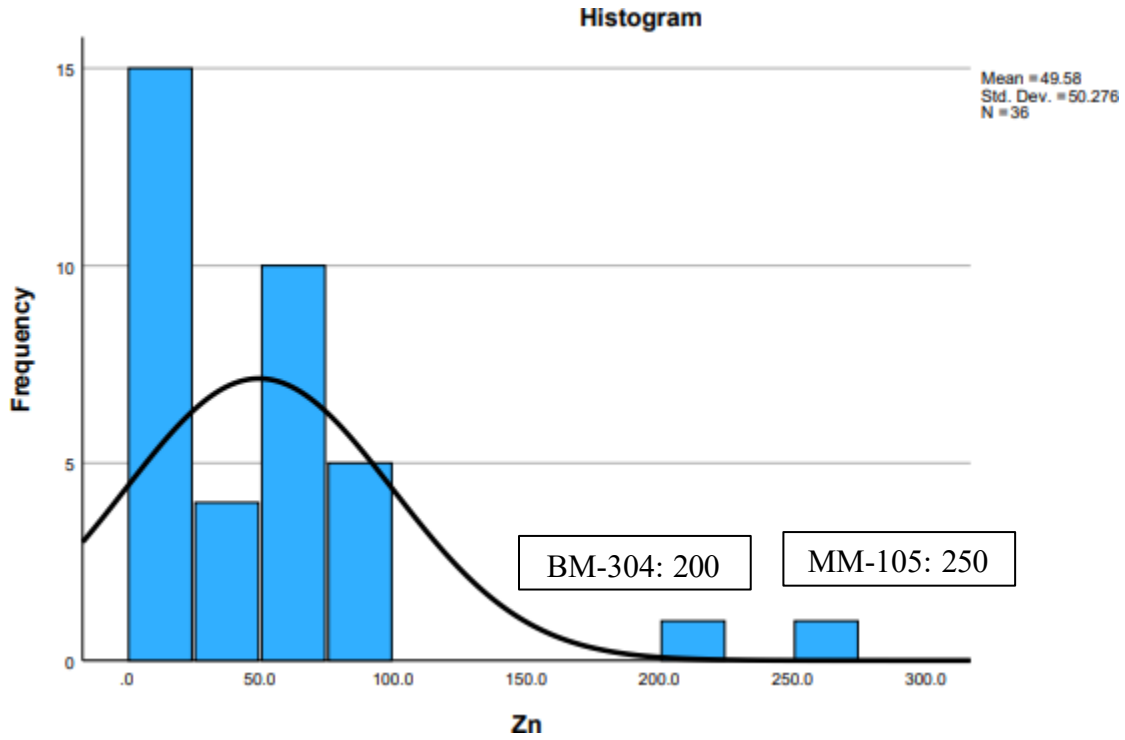
Histogram
Mean =49.58
Std. Dev. =50.276
N =36
Frequency
Zn
BM-304: 200
MM-105: 250

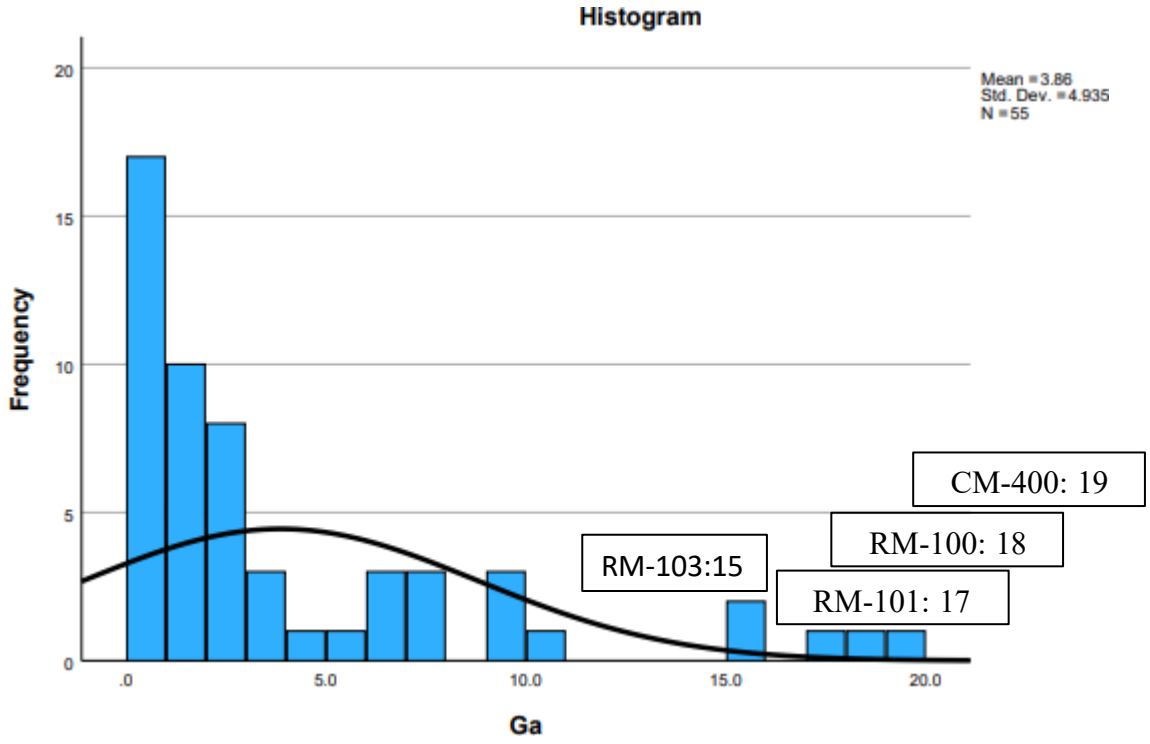
Histogram
Mean = 3.86
Std. Dev. = 4.935
N = 55
Frequency
Ga
CM-400: 19
RM-100: 18
RM-103:15
RM-101: 17

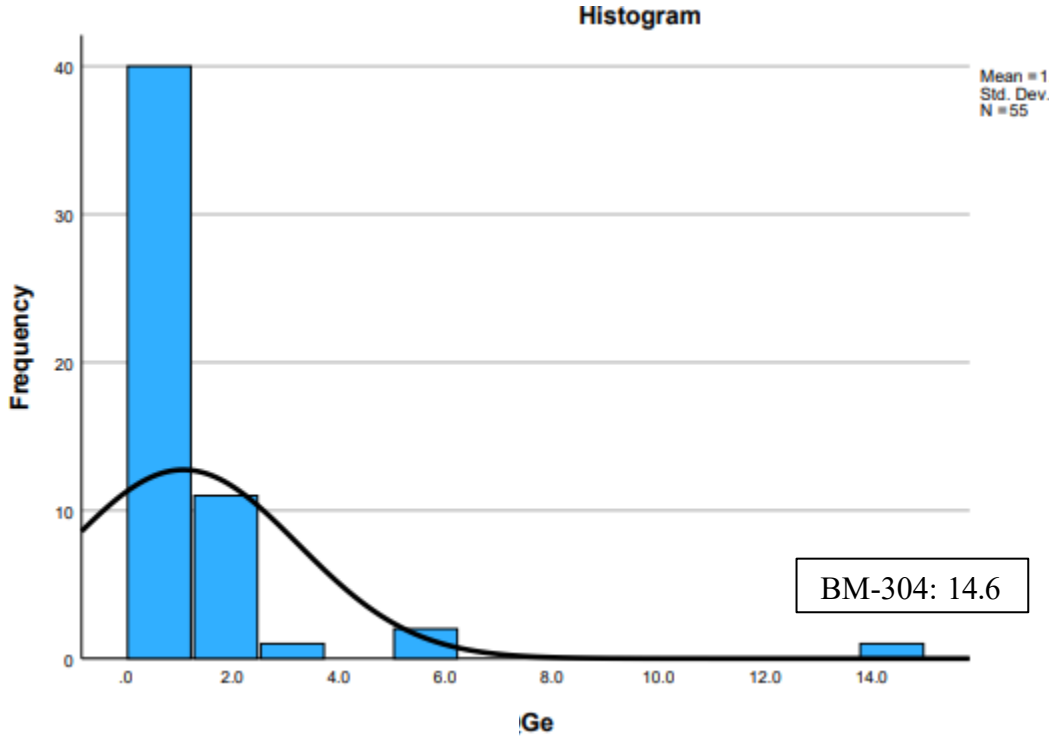
Histogram
Mean = 1.08
Std. Dev. = 2.152
N = 55
Frequency
Ge
BM-304: 14.6

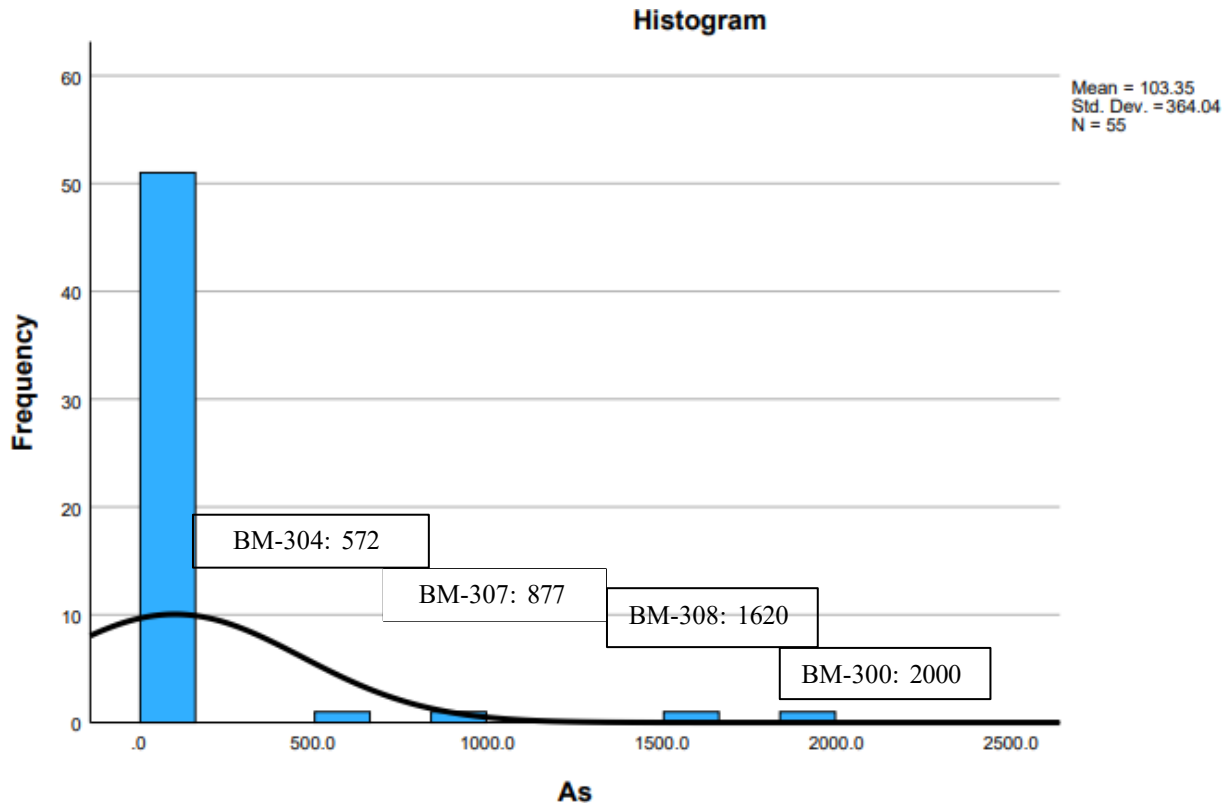
Histogram
Mean = 103.35
Std. Dev. = 364.04
N = 55
Frequency
60
50
40
30
20
10
0
BM-304: 572
BM-307: 877
BM-308: 1620
BM-300: 2000
.0
500.0
1000.0
1500.0
2000.0
2500.0
As

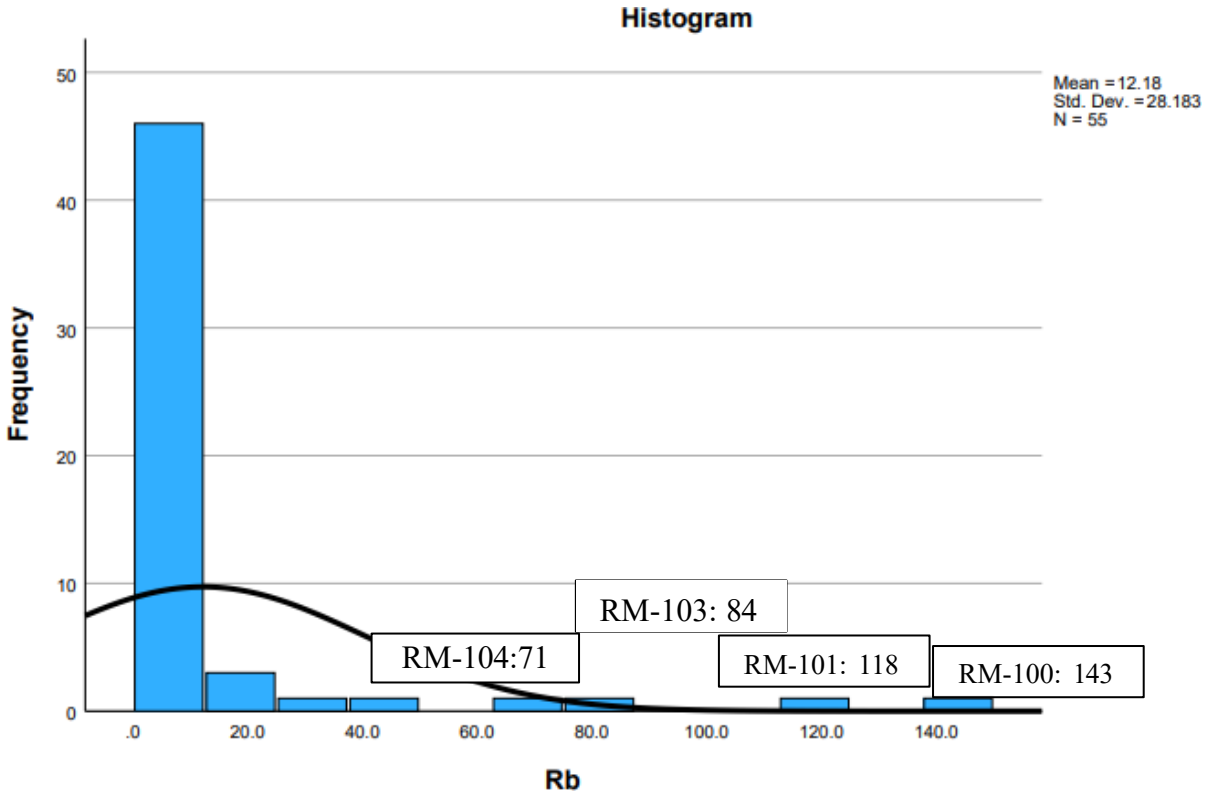
Histogram
Mean = 12.18
Std. Dev. = 28.183
N = 55
Frequency
50
40
30
20
10
0
RM-103: 84
RM-104:71
RM-101: 118
RM-100: 143
.0
20.0
40.0
60.0
80.0
100.0
120.0
140.0
Rb

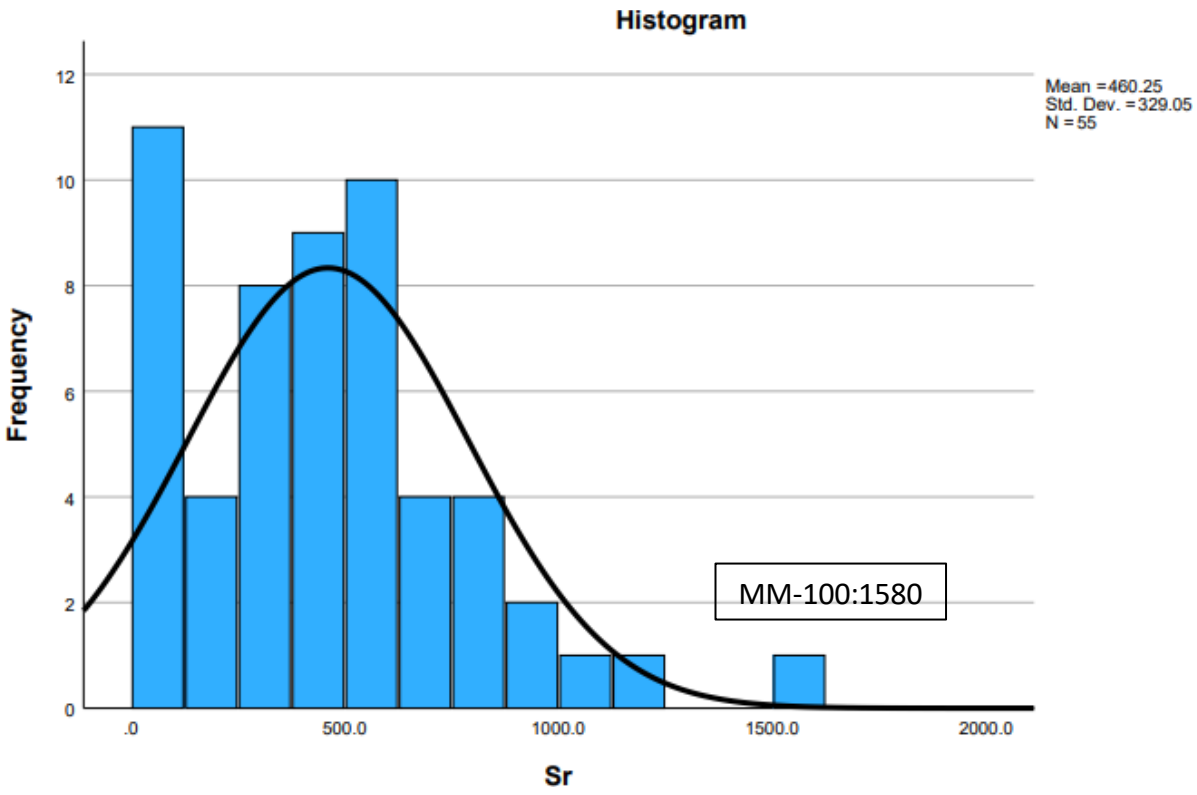
Histogram
Mean =460.25
Std. Dev. =329.05
N =55
Frequency
Sr
MM-100:1580

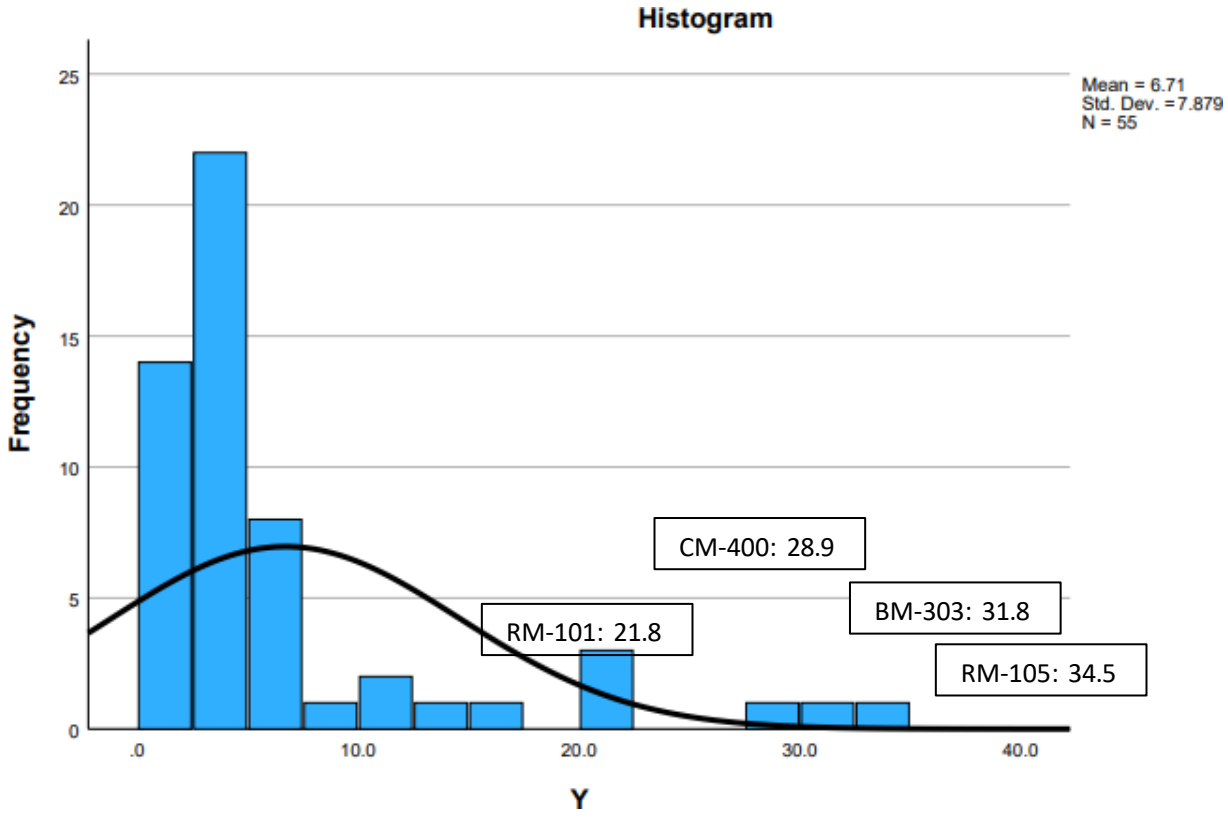
Histogram
Mean = 6.71
Std. Dev. =7.879
N = 55
Frequency
Y
CM-400: 28.9
BM-303: 31.8
RM-101: 21.8
RM-105: 34.5

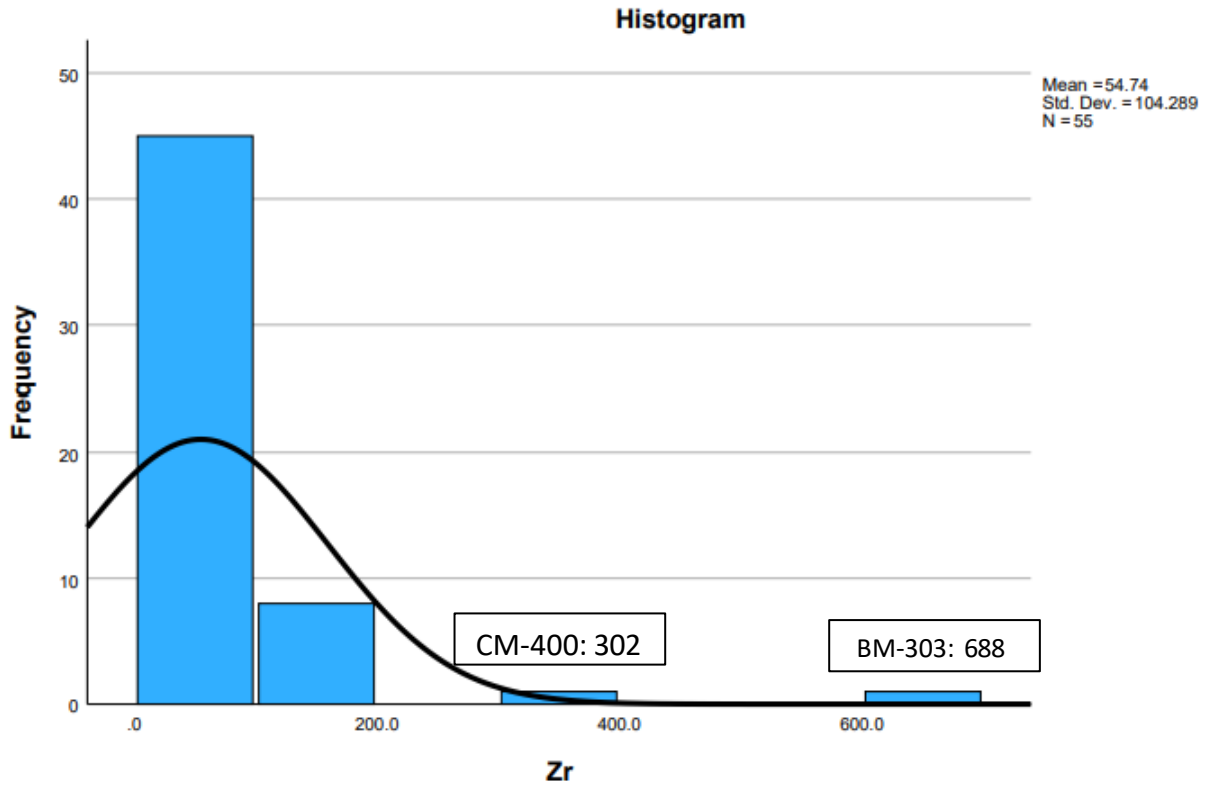
Histogram
Mean =54.74
Std. Dev. =104.289
N =55
Frequency
50
40
30
20
10
0
.0
200.0
400.0
600.0
Zr
CM-400: 302
BM-303: 688

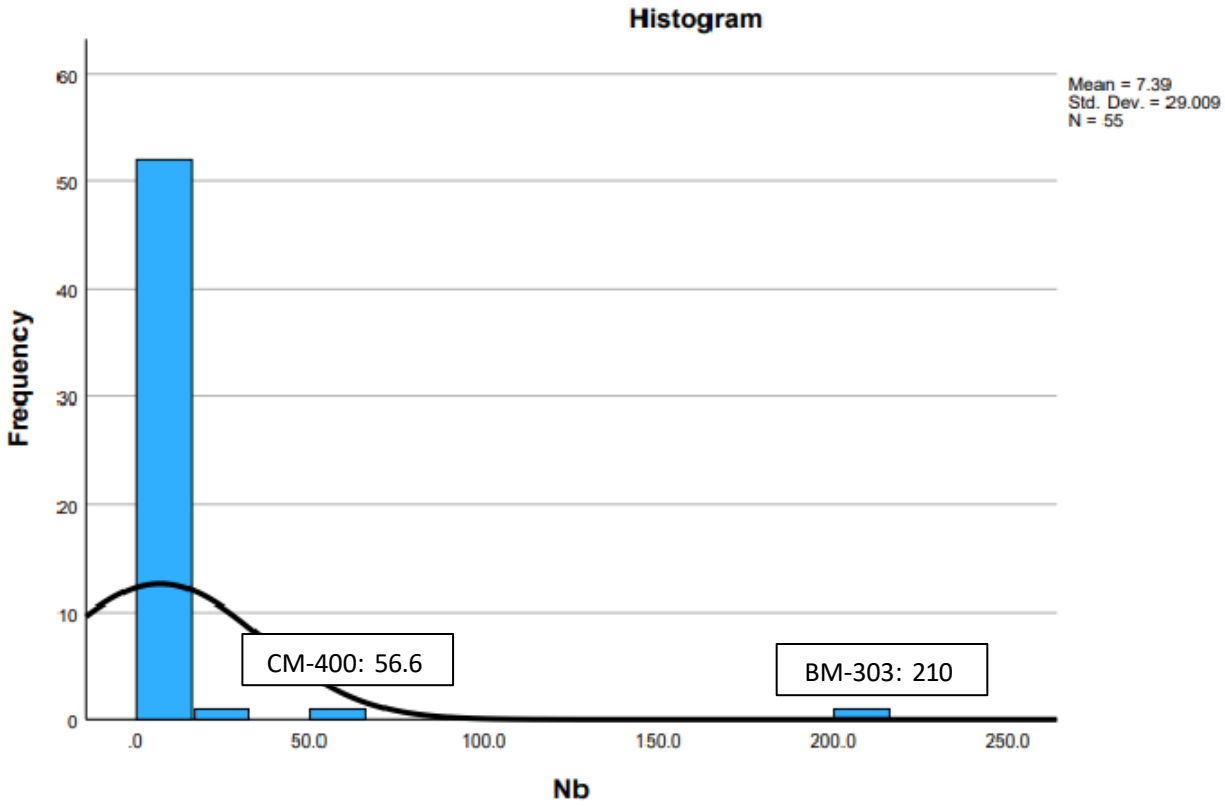
Histogram
Mean = 7.39
Std. Dev. = 29.009
N = 55
Frequency
60
50
40
30
20
10
0
.0
50.0
100.0
150.0
200.0
250.0
Nb
CM-400: 56.6
BM-303: 210

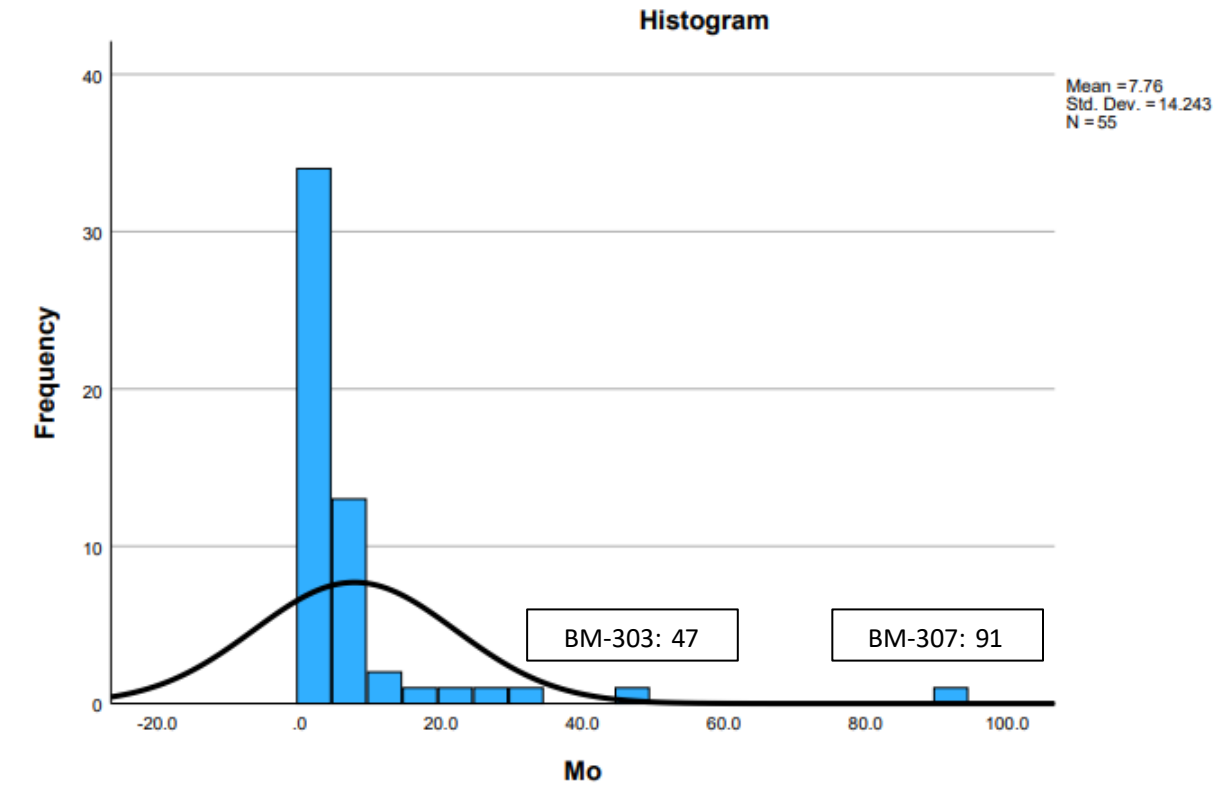
Histogram
Mean =7.76
Std. Dev. =14.243
N =55
Frequency
40
30
20
10
0
-20.0
.0
20.0
40.0
60.0
80.0
100.0
Mo
BM-303: 47
BM-307: 91

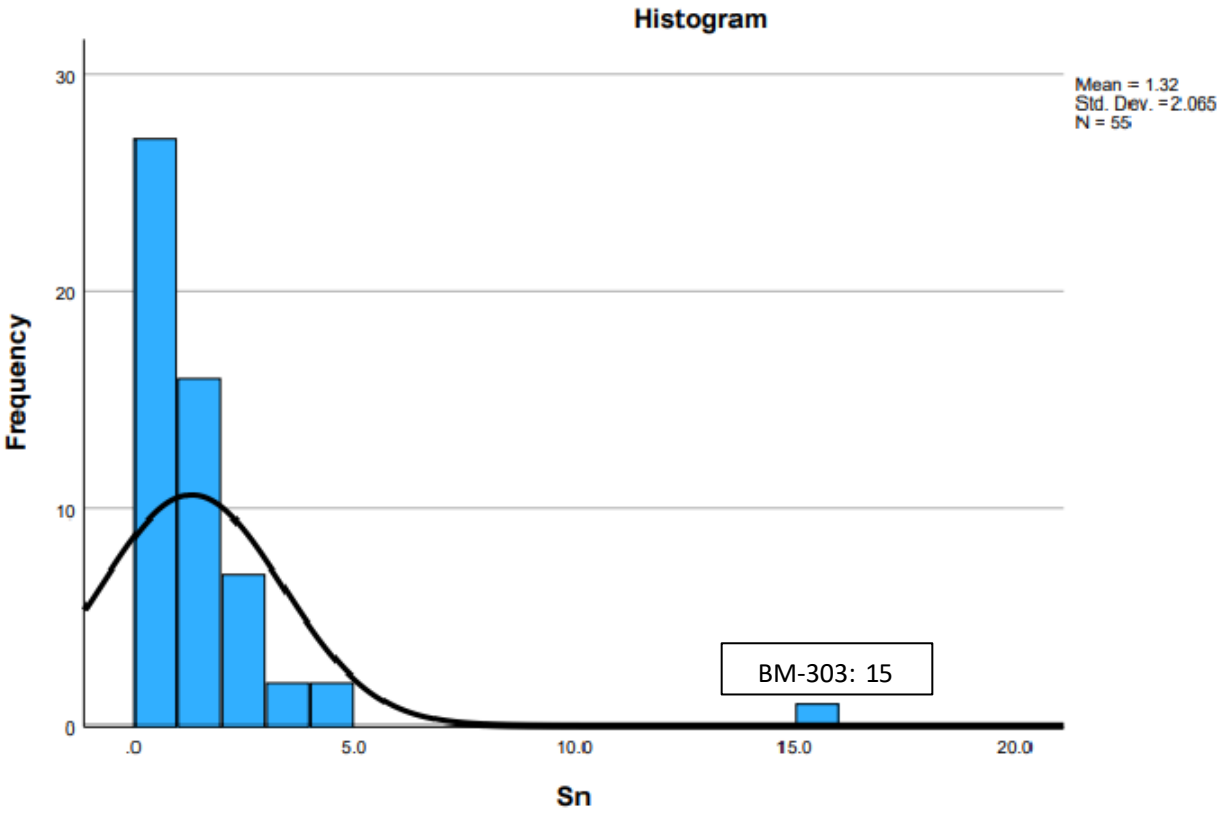
Histogram
Mean = 1.32
Std. Dev. =2.065
N = 55
Frequency
30
20
10
0
.0
5.0
10.0
15.0
20.0
Sn
BM-303: 15

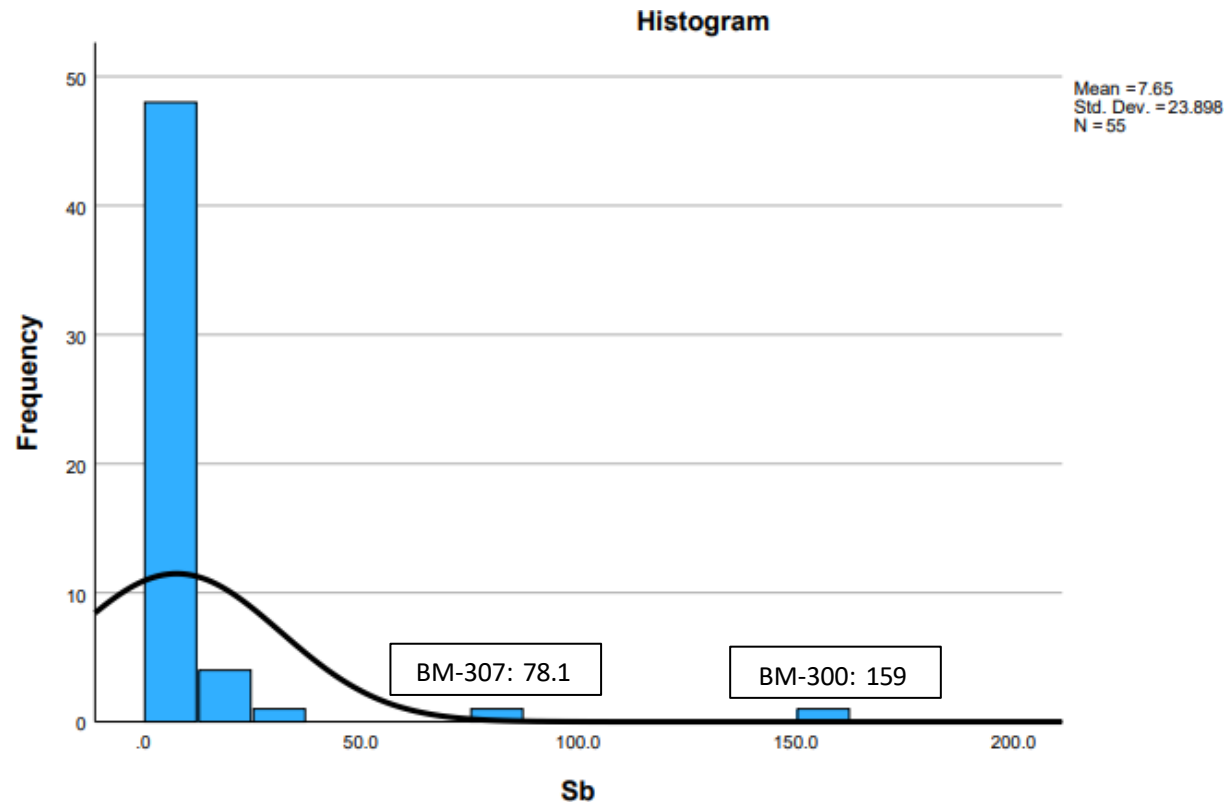
Histogram
Mean =7.65
Std. Dev. =23.898
N =55
Frequency
Sb
BM-307: 78.1
BM-300: 159
0
10
20
30
40
50
.0
50.0
100.0
150.0
200.0

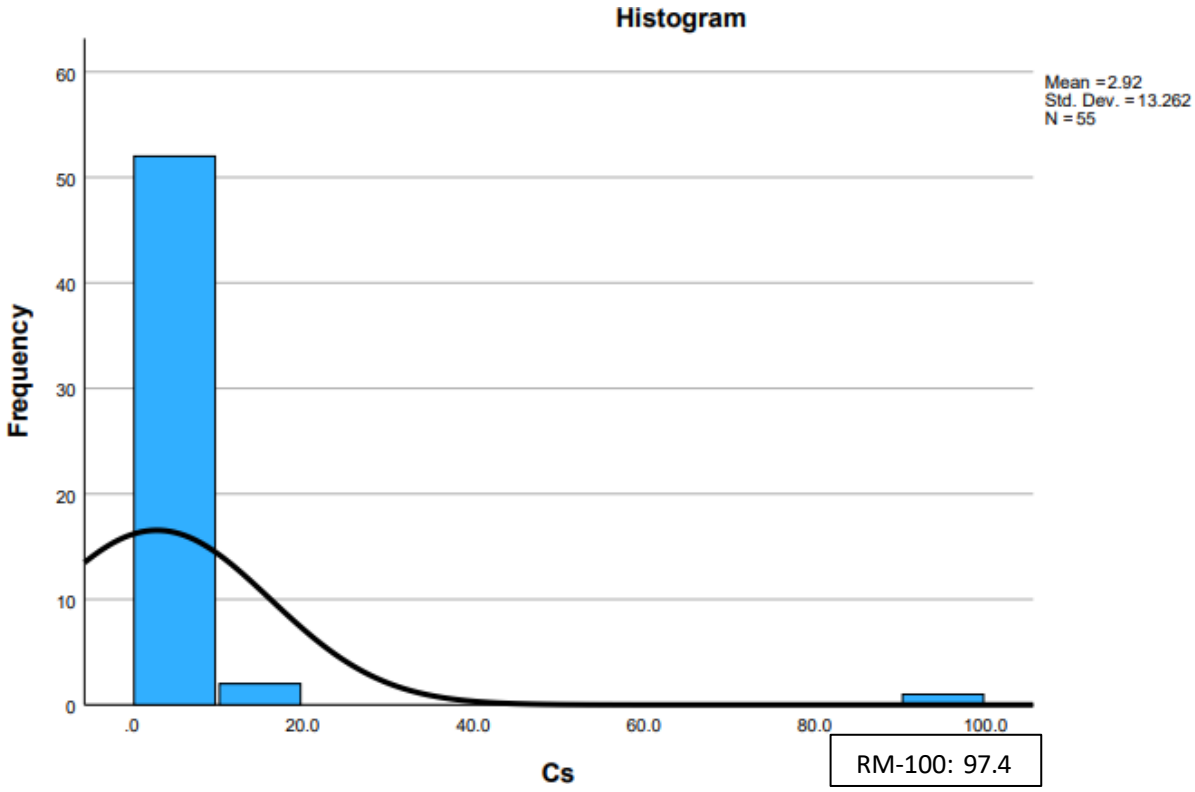
Histogram
Mean =2.92
Std. Dev. =13.262
N =55
Frequency
Cs
RM-100: 97.4
0
10
20
30
40
50
60
.0
20.0
40.0
60.0
80.0
100.0

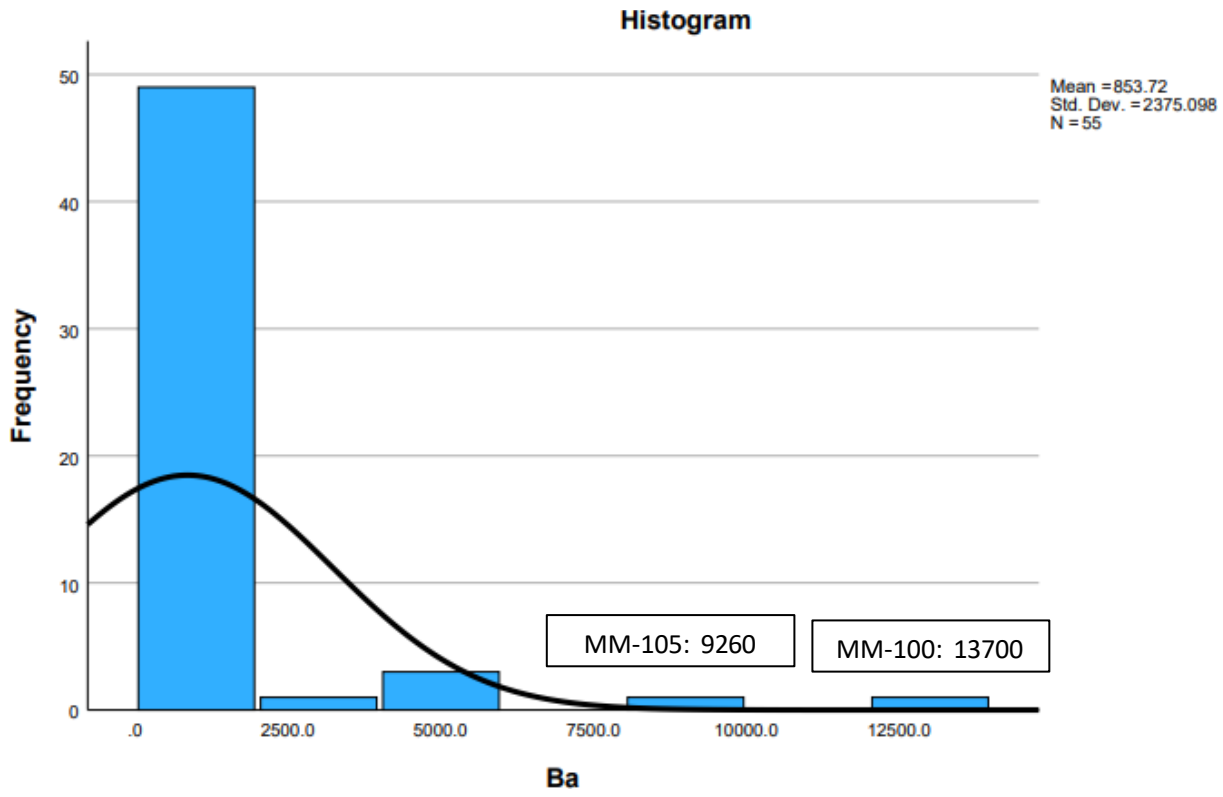
Histogram
Mean = 853.72
Std. Dev. = 2375.098
N = 55
Frequency
50
40
30
20
10
0
.0
2500.0
5000.0
7500.0
10000.0
12500.0
Ba
MM-105: 9260
MM-100: 13700

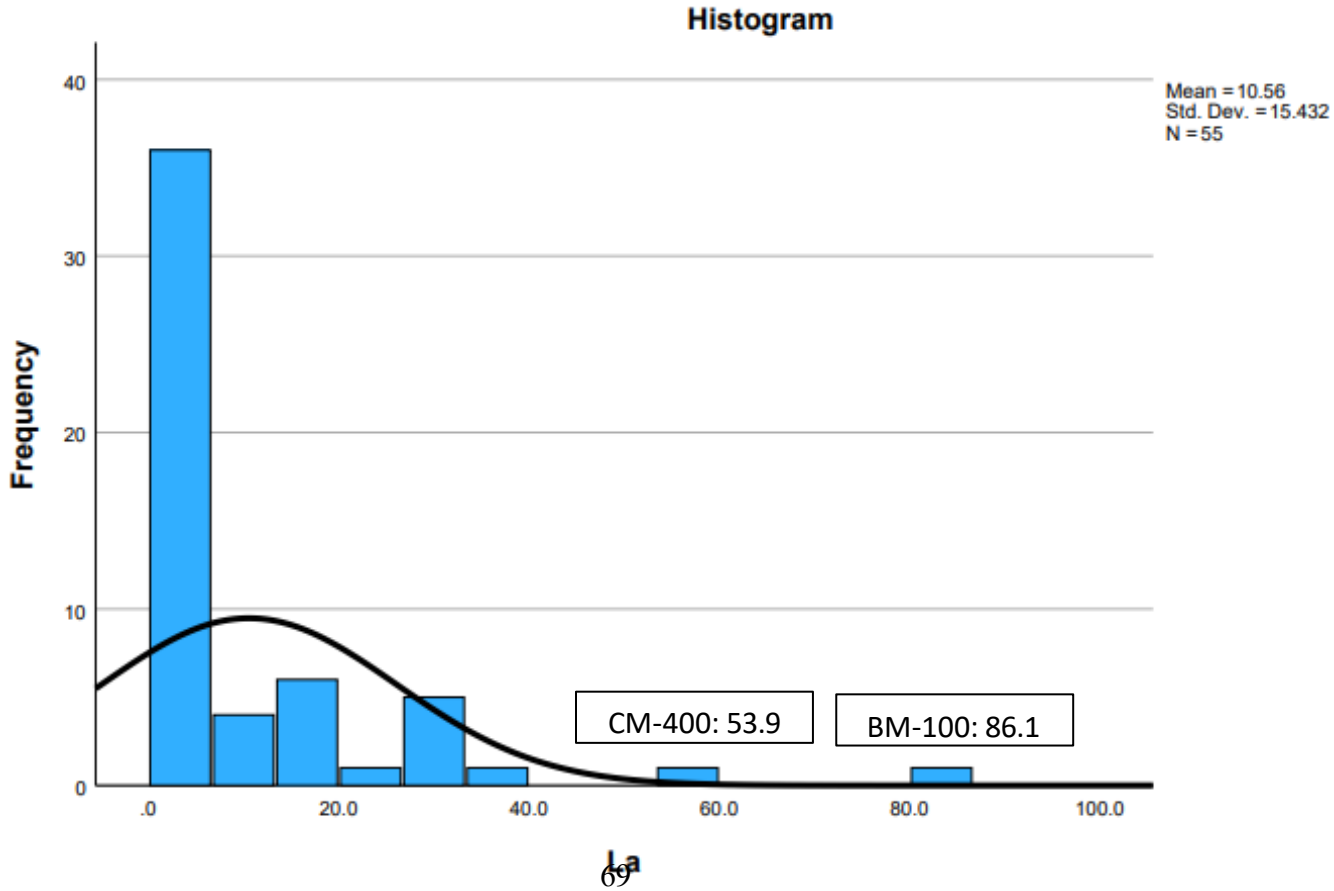
Histogram
Mean = 10.56
Std. Dev. = 15.432
N = 55
Frequency
40
30
20
10
0
.0
20.0
40.0
60.0
80.0
100.0
La
CM-400: 53.9
BM-100: 86.1

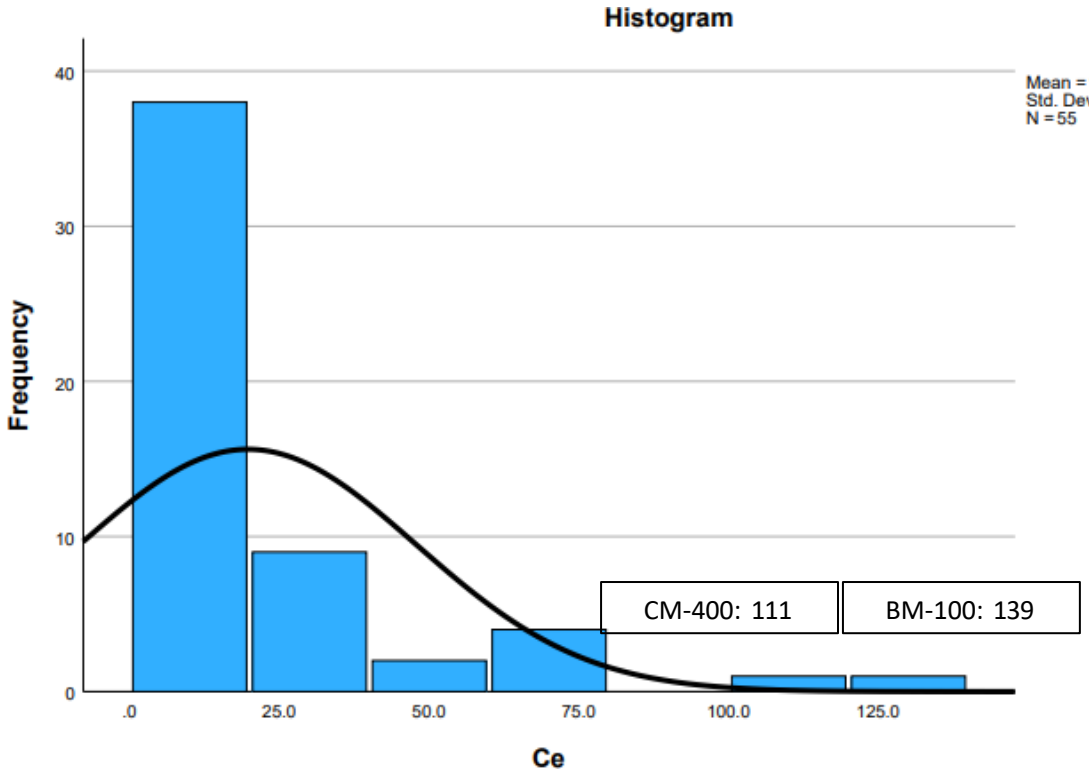
Histogram
Mean = 19.73
Std. Dev. = 28.094
N = 55
Frequency
40
30
20
10
0
.0
25.0
50.0
75.0
100.0
125.0
Ce
CM-400: 111
BM-100: 139

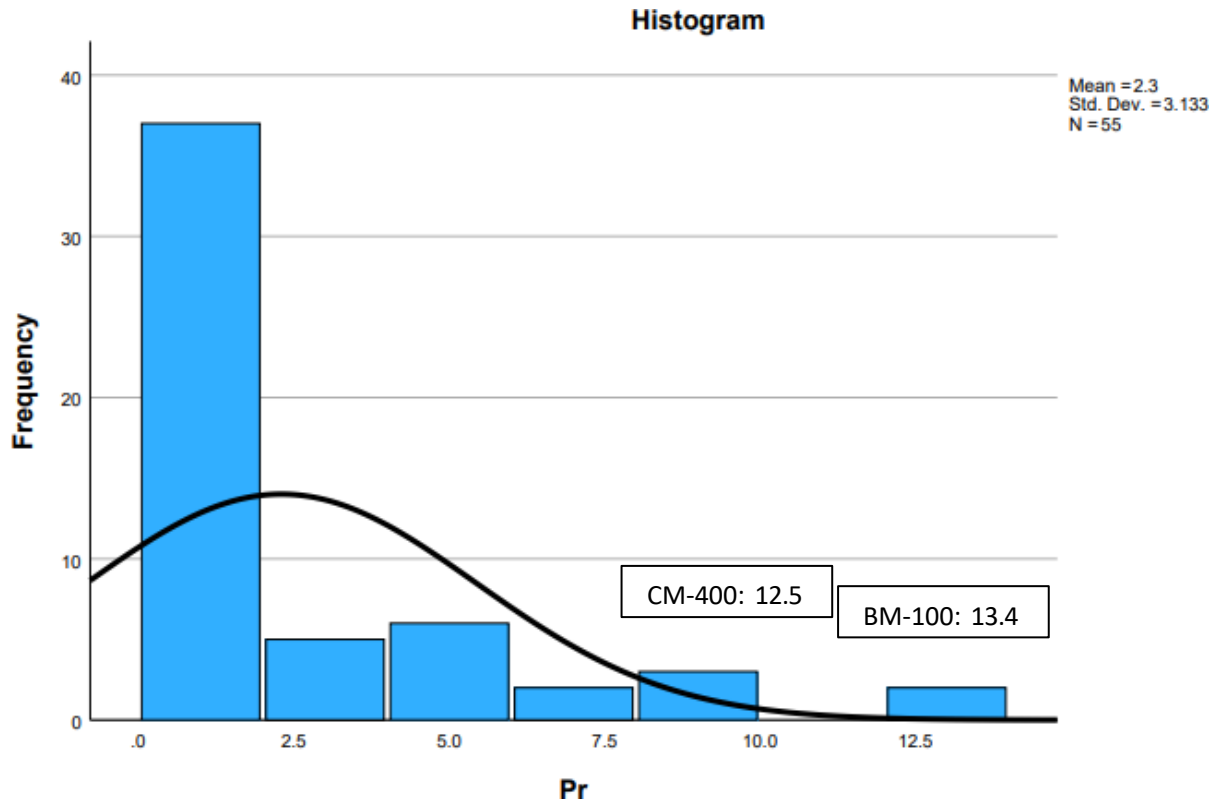
Histogram
Mean = 2.3
Std. Dev. = 3.133
N = 55
Frequency
40
30
20
10
0
.0
2.5
5.0
7.5
10.0
12.5
Pr
CM-400: 12.5
BM-100: 13.4

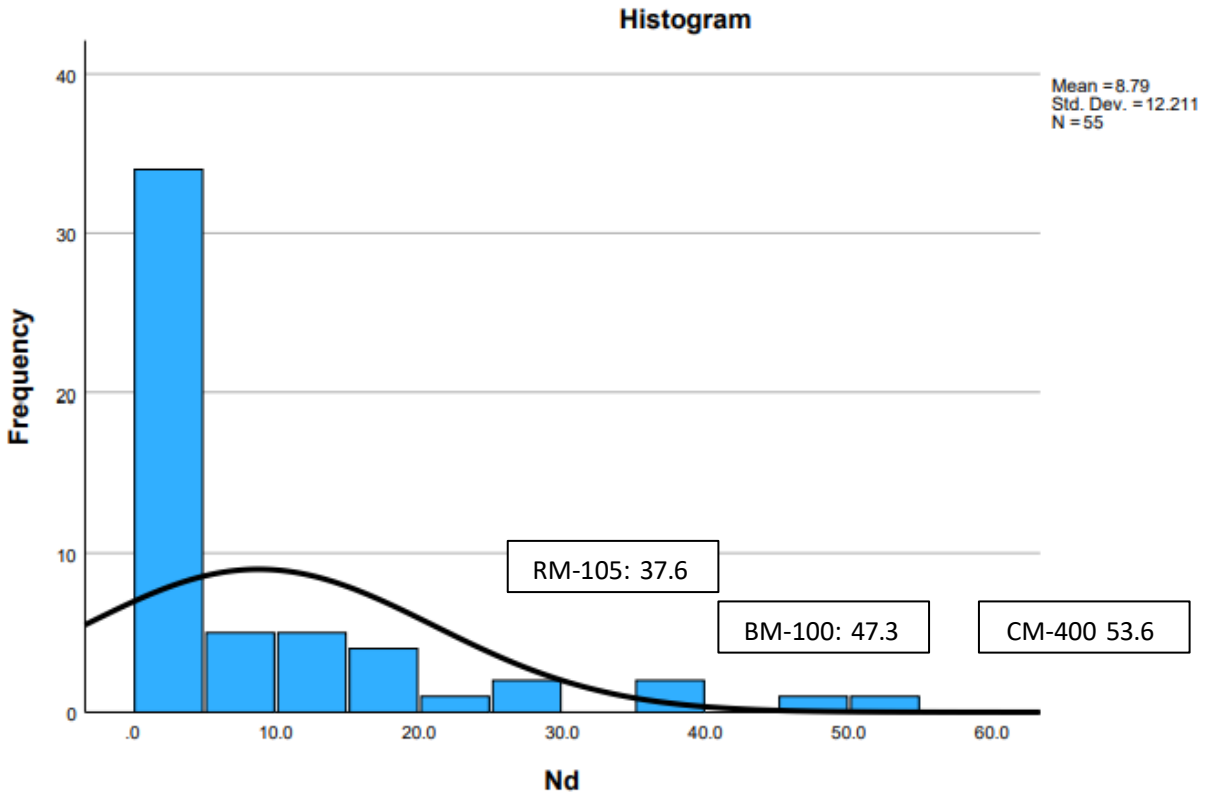
Histogram
Mean = 8.79
Std. Dev. = 12.211
N = 55
Frequency
40
30
20
10
0
.0
10.0
20.0
30.0
40.0
50.0
60.0
Nd
RM-105: 37.6
BM-100: 47.3
CM-400 53.6

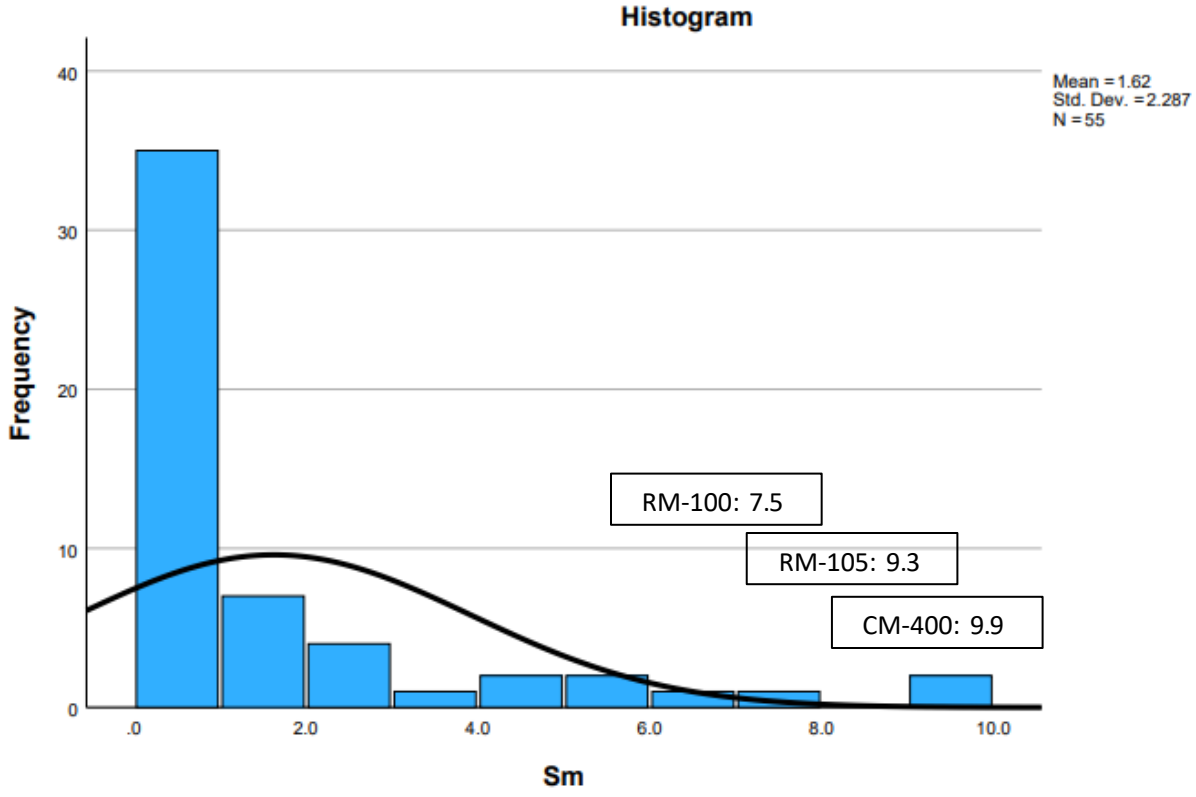
Histogram
Mean = 1.62
Std. Dev. = 2.287
N = 55
Frequency
40
30
20
10
0
.0
2.0
4.0
6.0
8.0
10.0
Sm
RM-100: 7.5
RM-105: 9.3
CM-400: 9.9

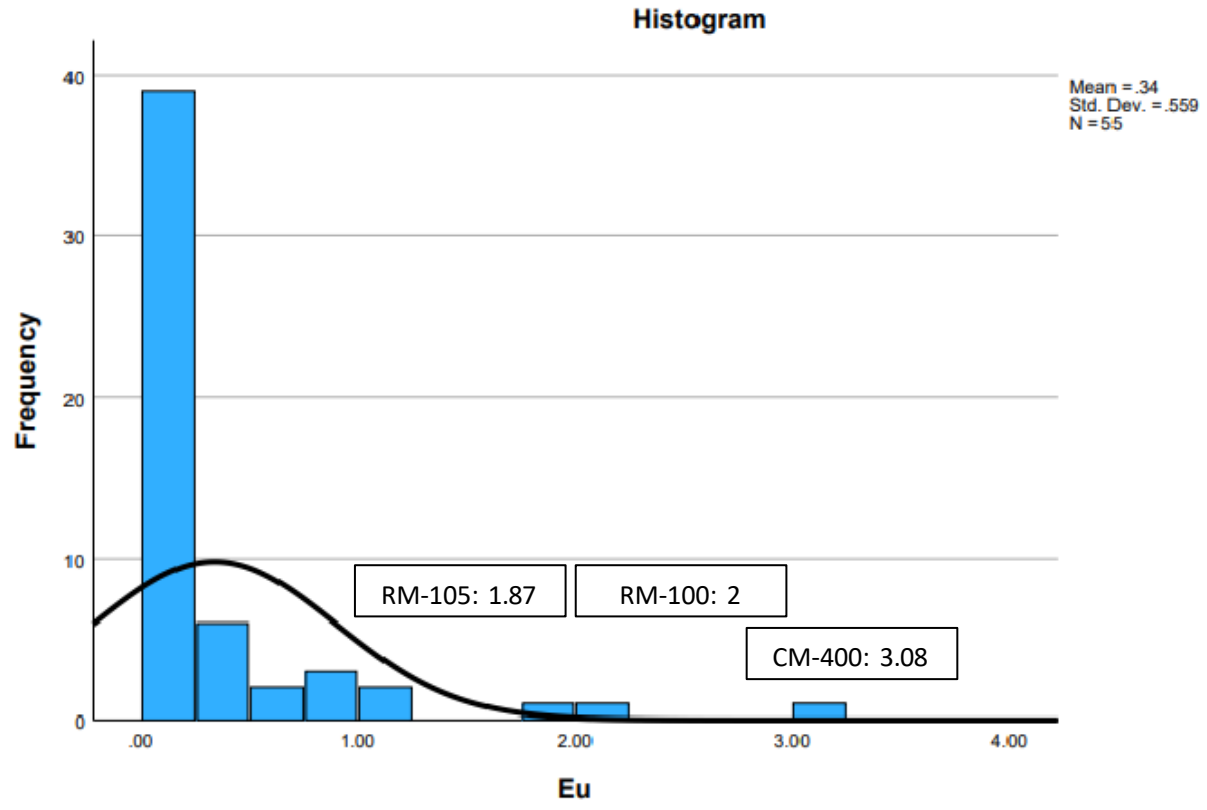
Histogram
Mean = .34
Std. Dev. = .559
N = 55
Frequency
40
30
20
10
0
.00
1.00
2.00
3.00
4.00
Eu
RM-105: 1.87
RM-100: 2
CM-400: 3.08

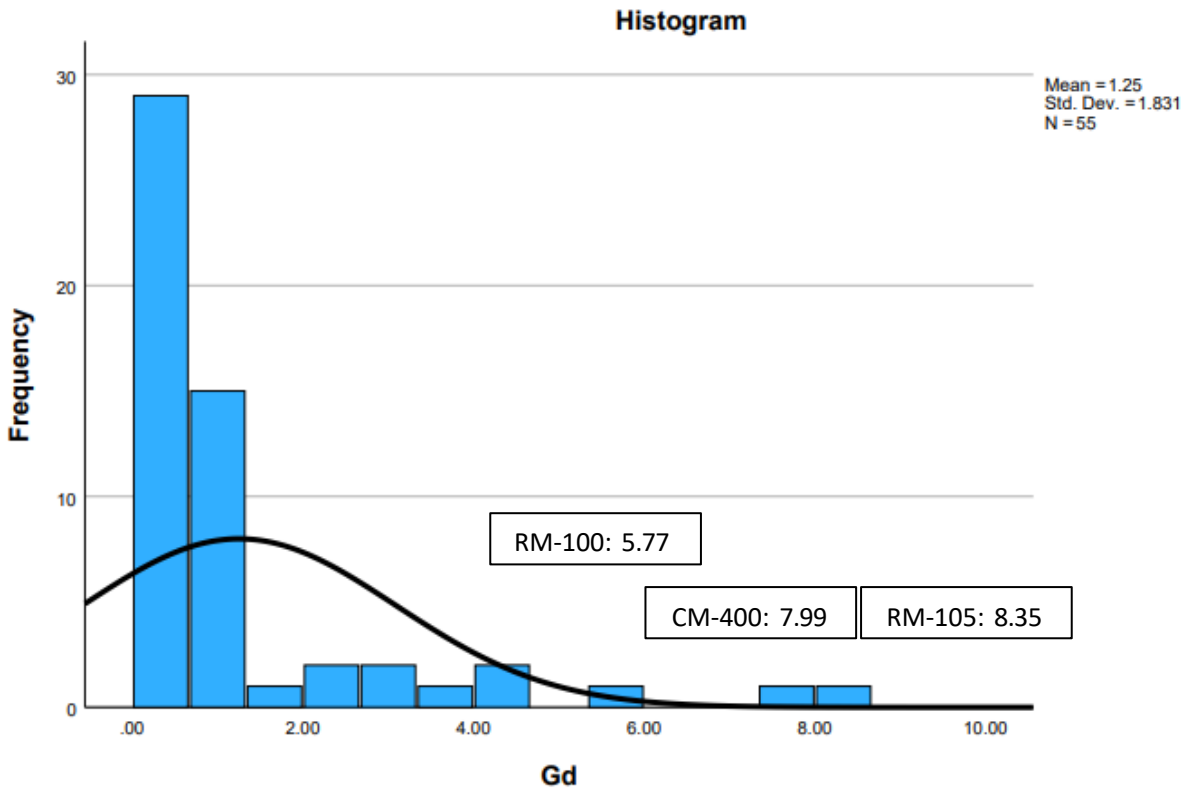
Histogram
Mean = 1.25
Std. Dev. = 1.831
N = 55
Frequency
30
20
10
0
.00
2.00
4.00
6.00
8.00
10.00
Gd
RM-100: 5.77
CM-400: 7.99
RM-105: 8.35

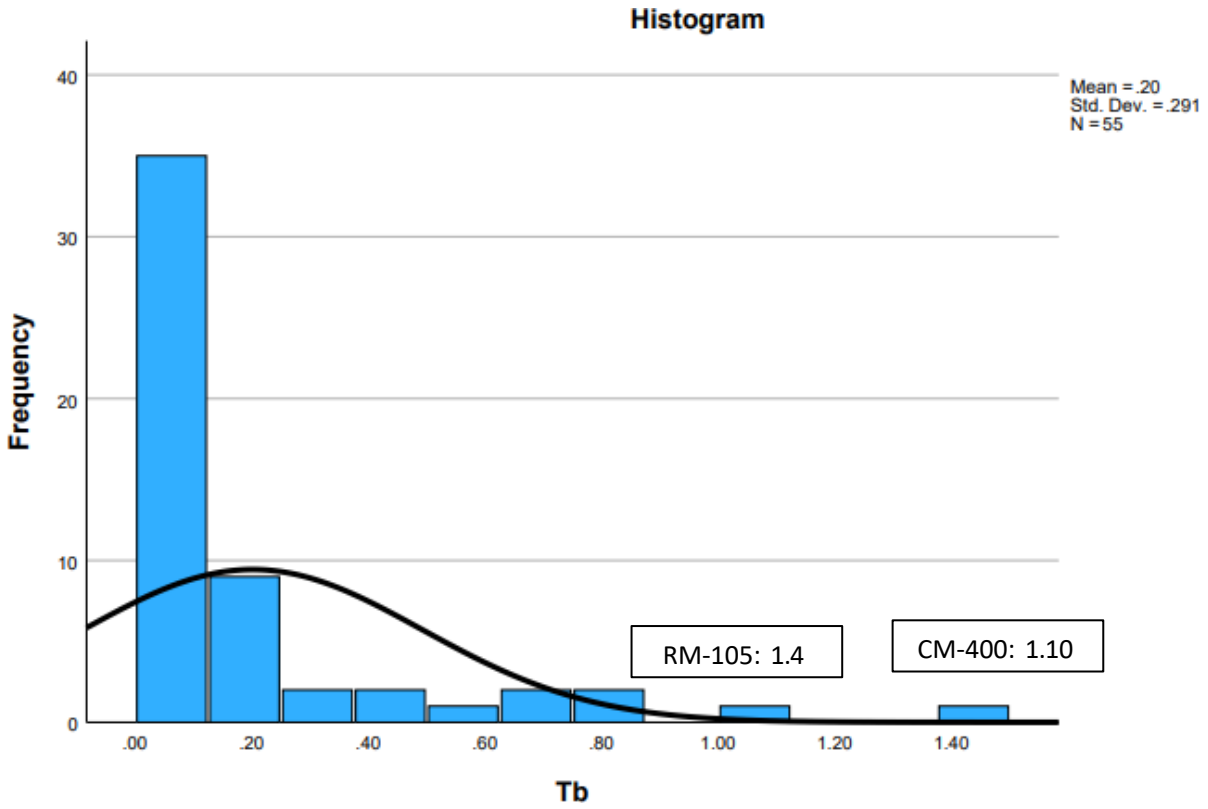
Histogram
Mean = .20
Std. Dev. = .291
N = 55
Frequency
40
30
20
10
0
.00
.20
.40
.60
.80
1.00
1.20
1.40
Tb
RM-105: 1.4
CM-400: 1.10

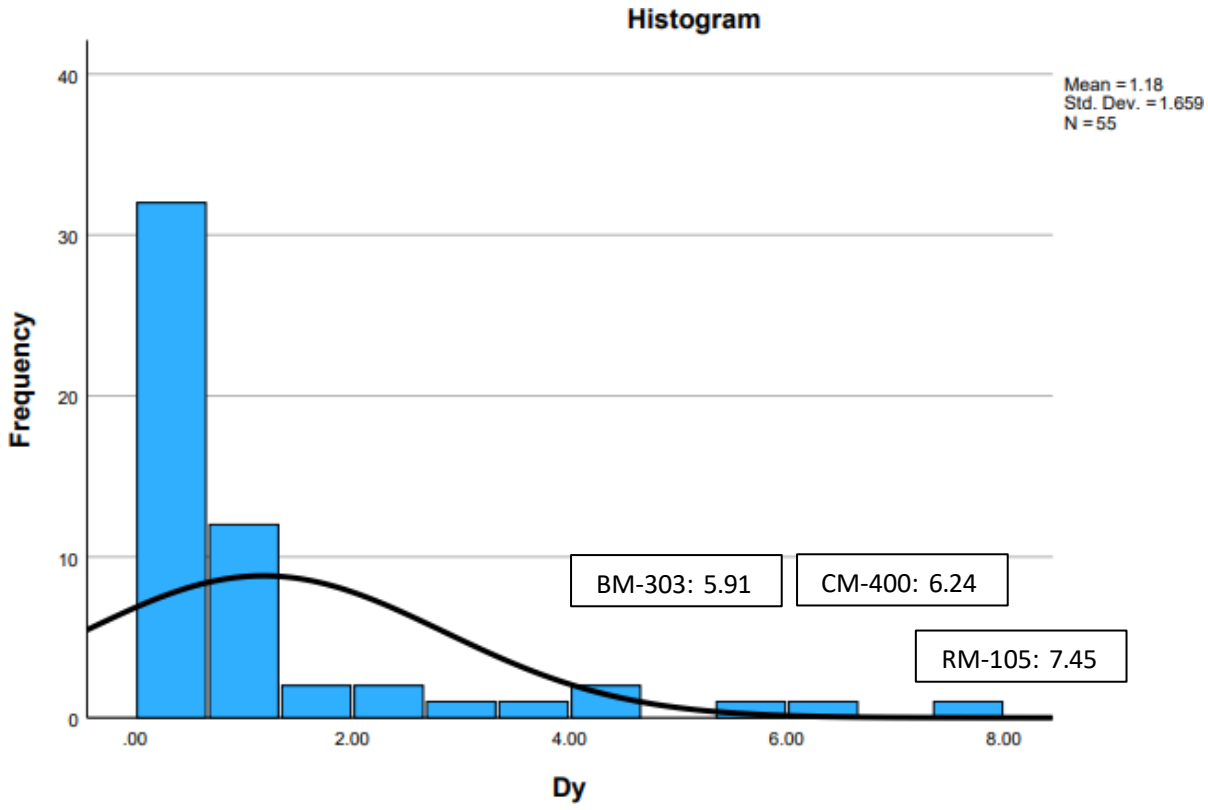
Histogram
Mean = 1.18
Std. Dev. = 1.659
N = 55
Frequency
40
30
20
10
0
.00
2.00
4.00
6.00
8.00
Dy
BM-303: 5.91
CM-400: 6.24
RM-105: 7.45

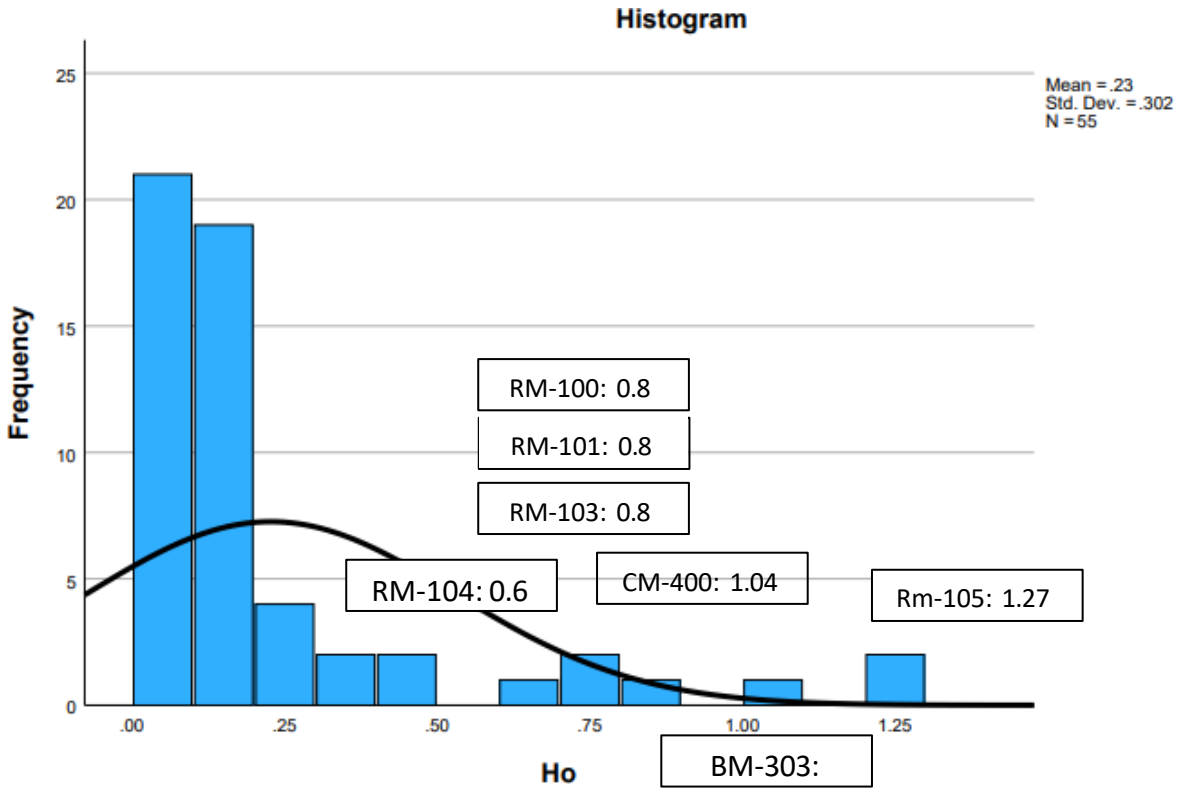
Histogram
Mean = .23
Std. Dev. = .302
N = 55
Frequency
25
20
15
10
5
0
.00
.25
.50
.75
1.00
1.25
Ho
RM-100: 0.8
RM-101: 0.8
RM-103: 0.8
RM-104: 0.6
CM-400: 1.04
Rm-105: 1.27
BM-303:

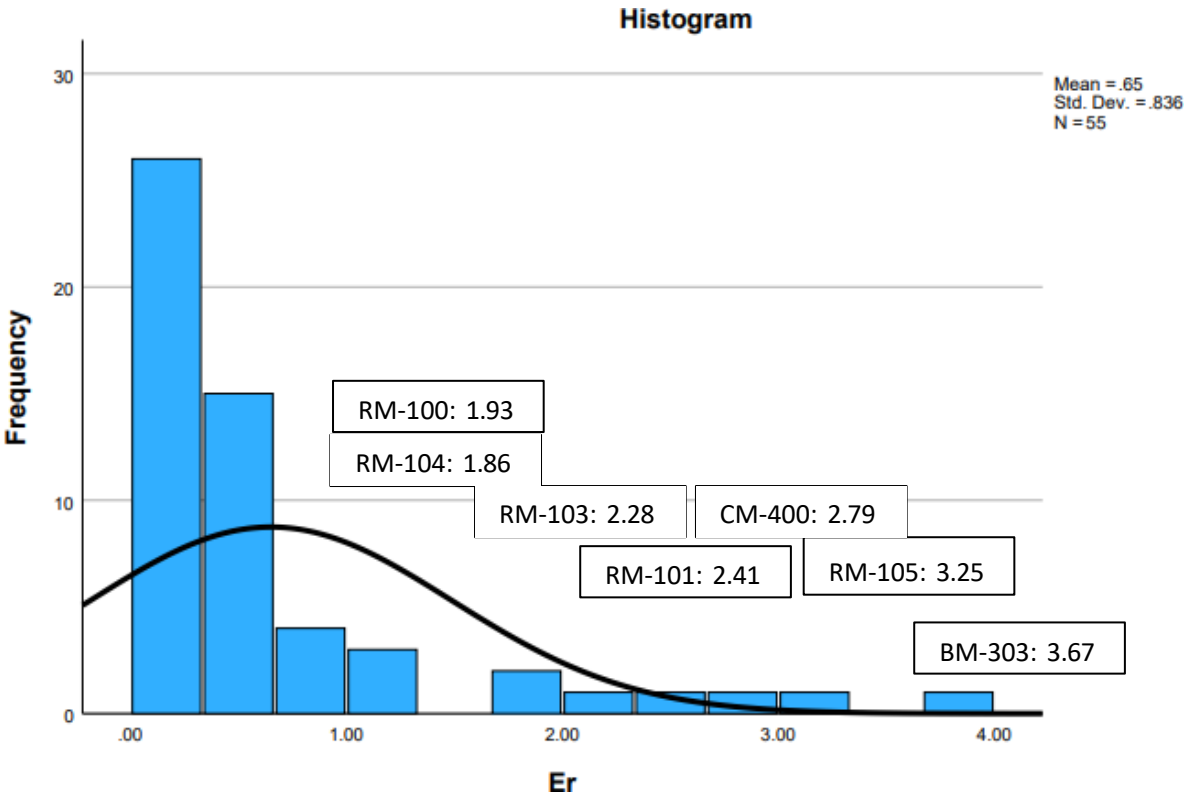
Histogram
Mean = .65
Std. Dev. = .836
N = 55
Frequency
30
20
10
0
.00
1.00
2.00
3.00
4.00
Er
RM-100: 1.93
RM-104: 1.86
RM-103: 2.28
CM-400: 2.79
RM-101: 2.41
RM-105: 3.25
BM-303: 3.67

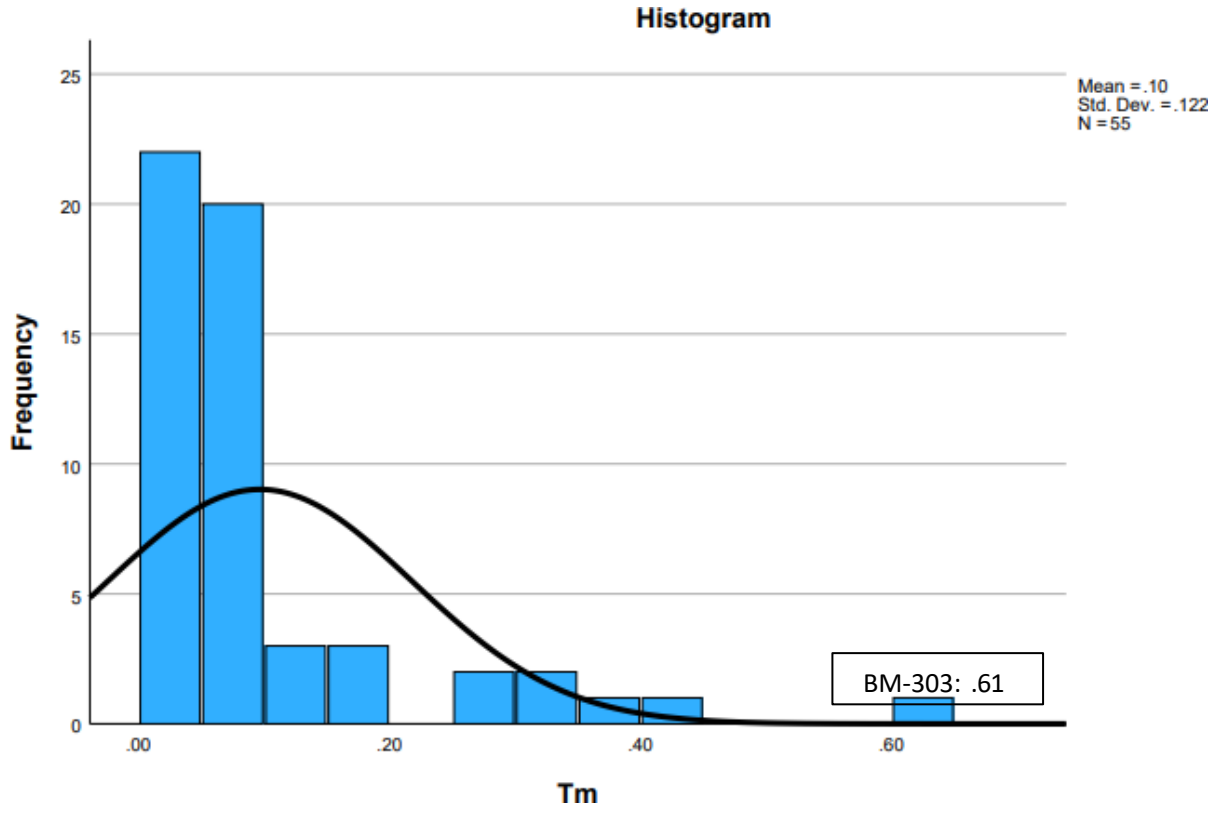
Histogram
Mean = .10
Std. Dev. = .122
N = 55
Frequency
25
20
15
10
5
0
.00
.20
.40
.60
Tm
BM-303: .61

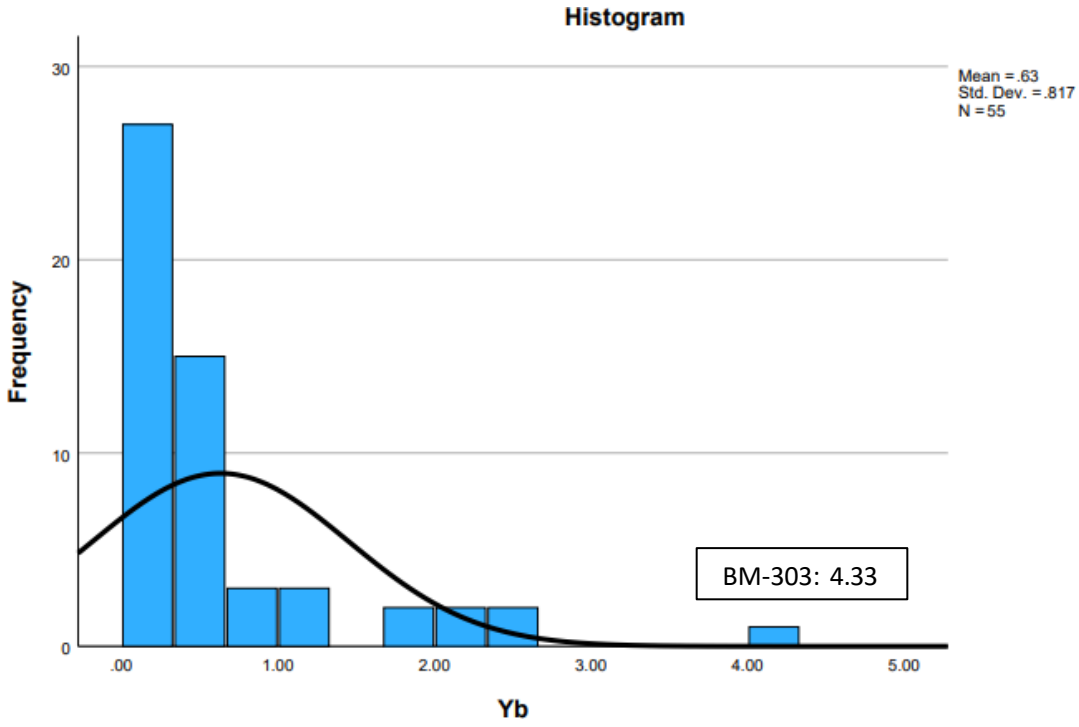
Histogram
Mean = .63
Std. Dev. = .817
N = 55
Frequency
30
20
10
0
.00
1.00
2.00
3.00
4.00
5.00
Yb
BM-303: 4.33

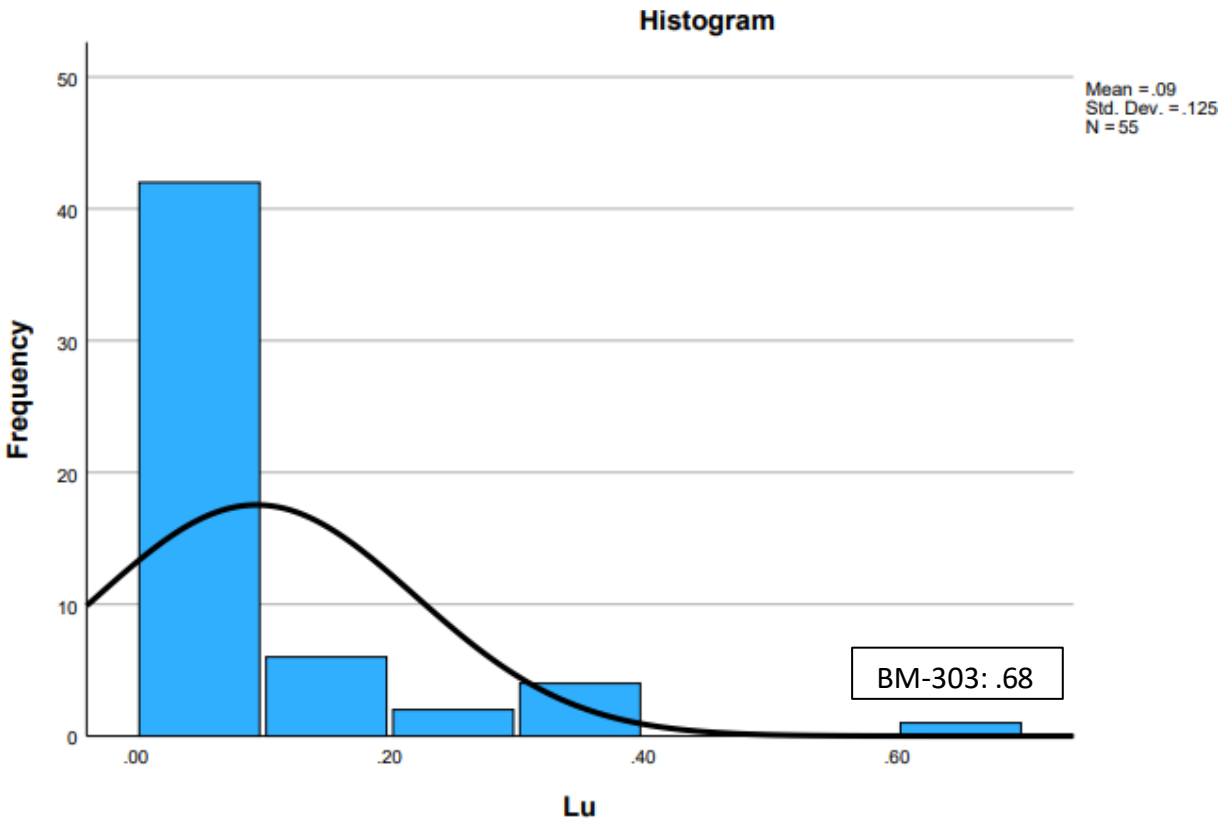
Histogram
Mean = .09
Std. Dev. = .125
N = 55
Frequency
50
40
30
20
10
0
.00
.20
.40
.60
Lu
BM-303: .68

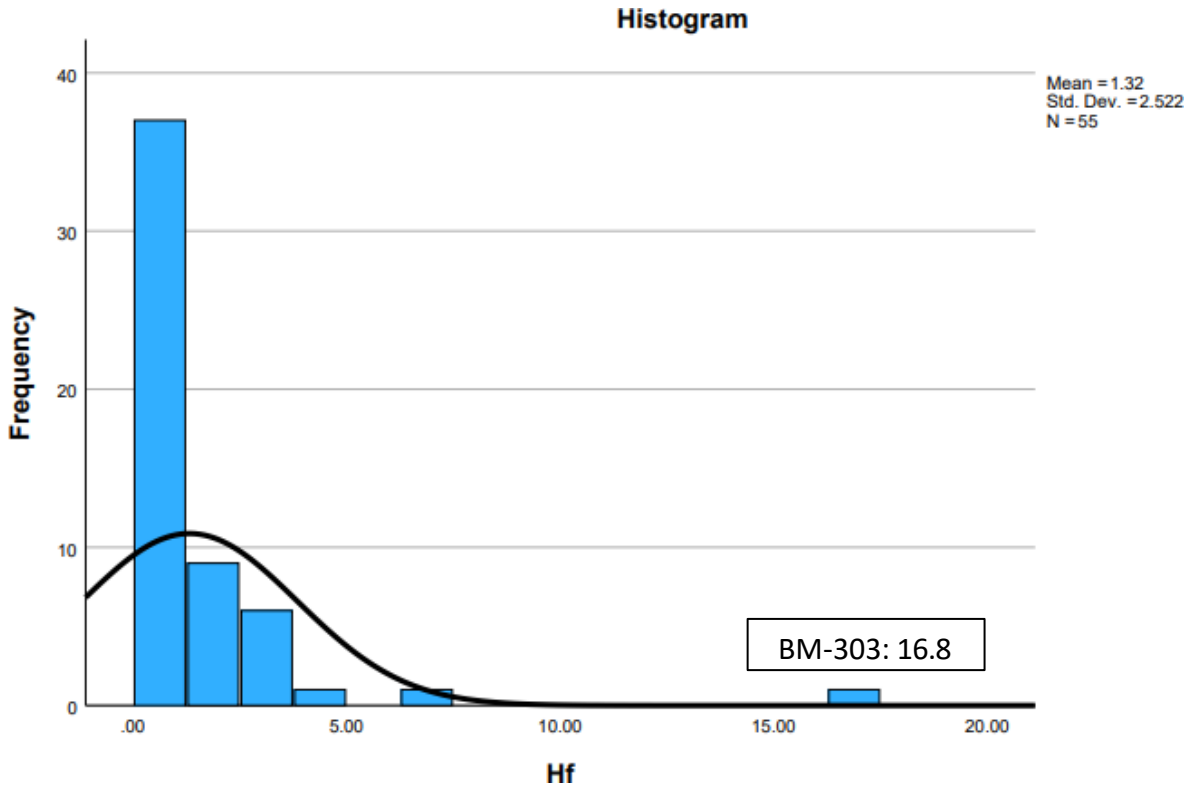
Histogram
Mean = 1.32
Std. Dev. = 2.522
N = 55
Frequency
40
30
20
10
0
.00
5.00
10.00
15.00
20.00
Hf
BM-303: 16.8

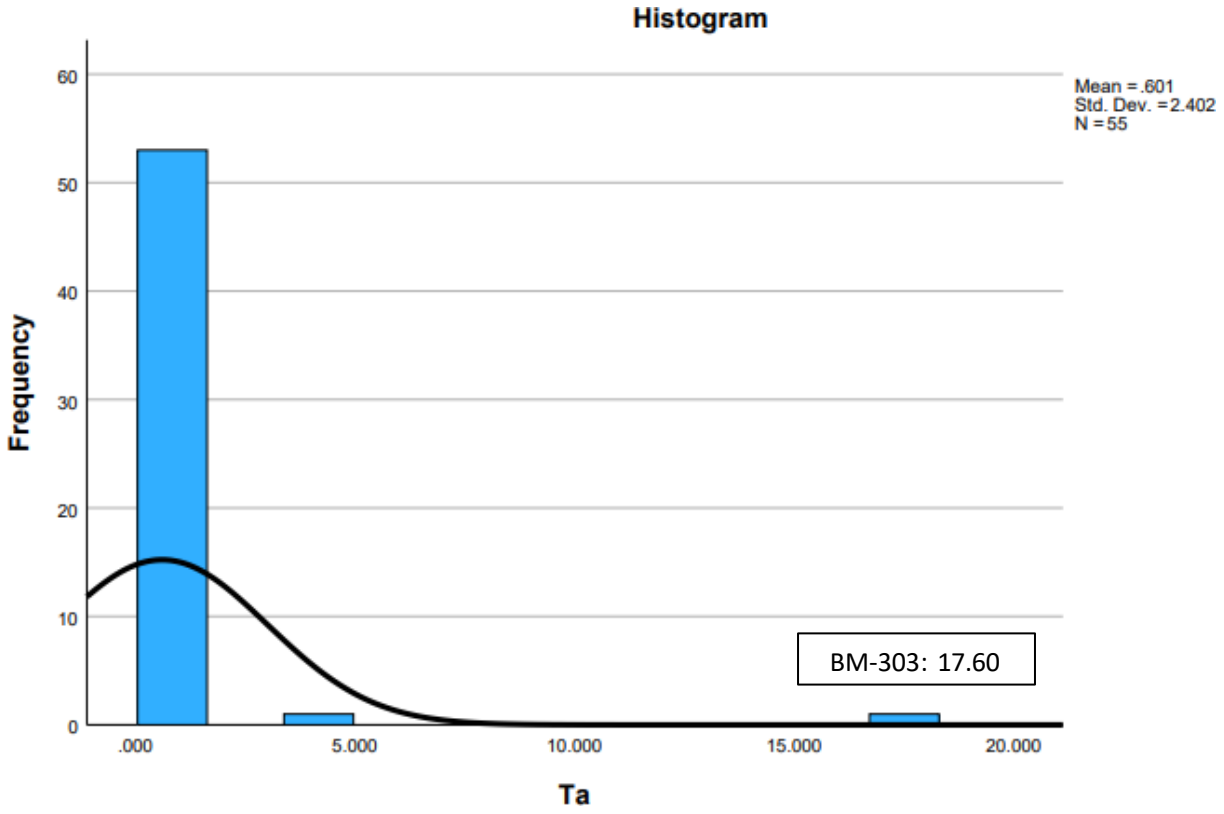
Histogram
Mean = .601
Std. Dev. = 2.402
N = 55
Frequency
60
50
40
30
20
10
0
.000
5.000
10.000
15.000
20.000
Ta
BM-303: 17.60

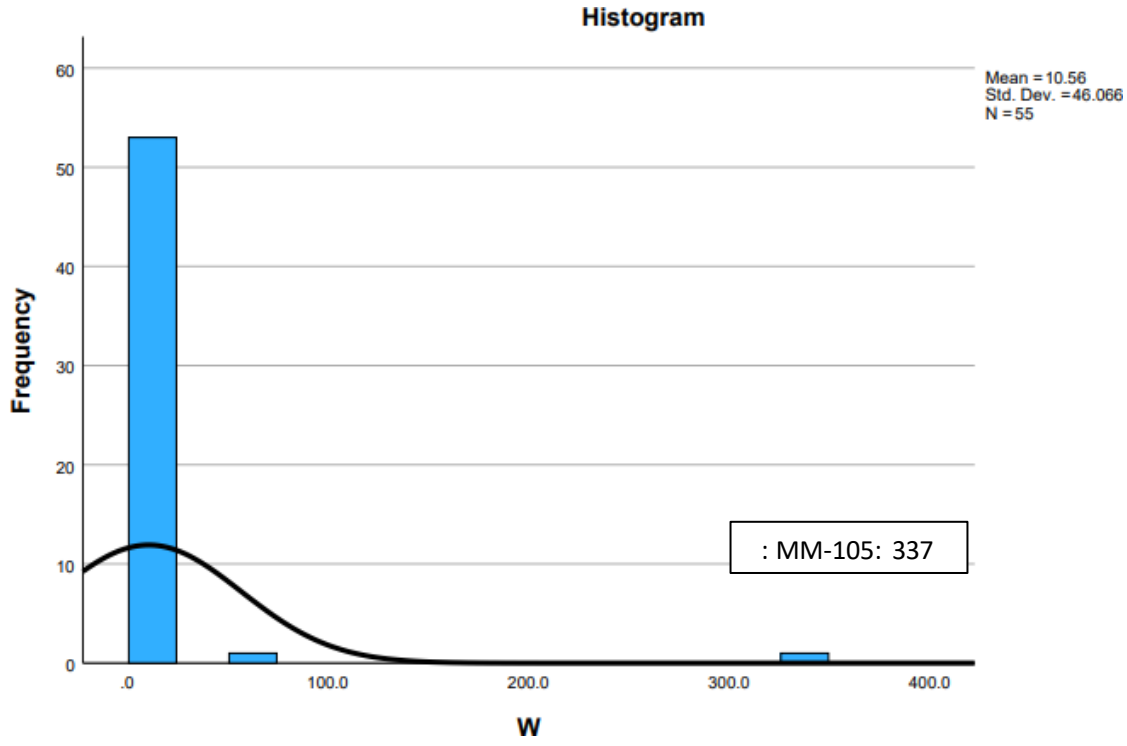
Histogram
Mean = 10.56
Std. Dev. = 46.066
N = 55
Frequency
60
50
40
30
20
10
0
.0
100.0
200.0
300.0
400.0
W
: MM-105: 337

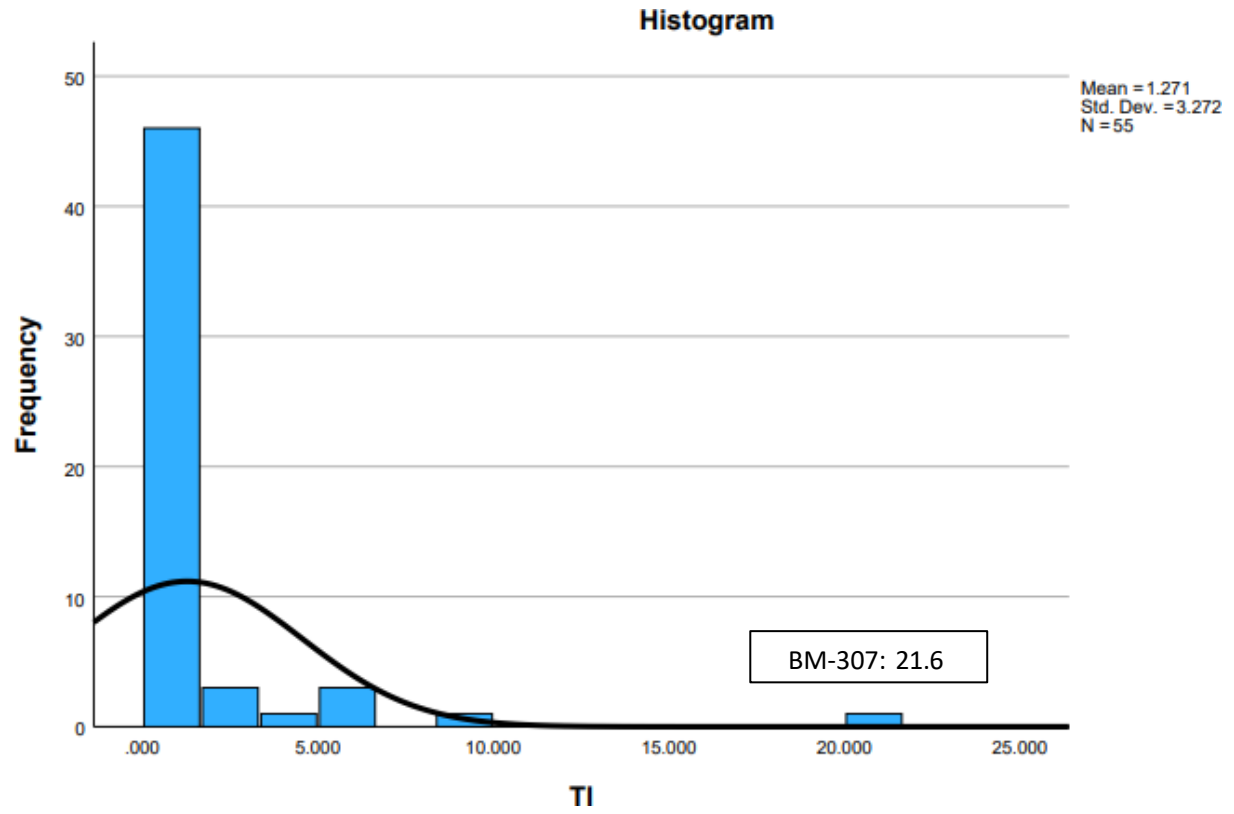
Histogram
Mean = 1.271
Std. Dev. = 3.272
N = 55
Frequency
50
40
30
20
10
0
.000
5.000
10.000
15.000
20.000
25.000
Tl
BM-307: 21.6

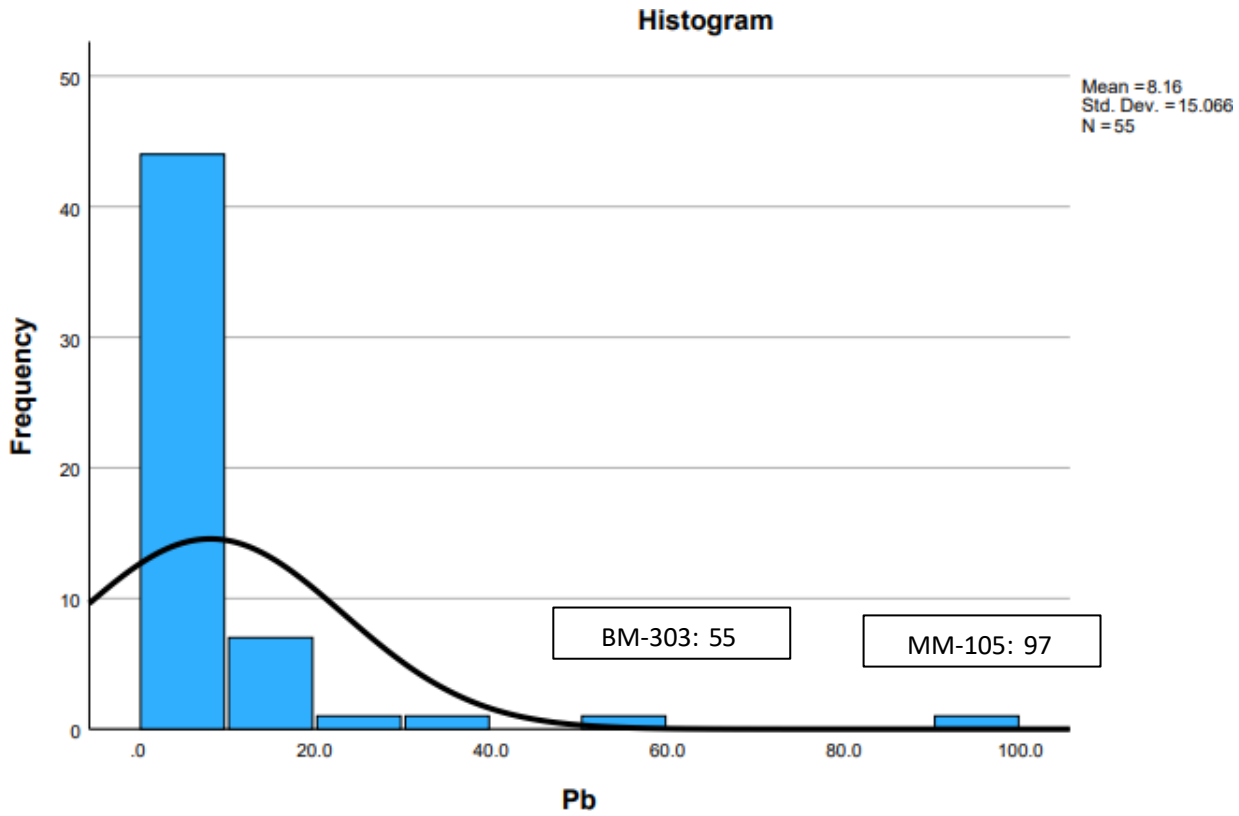
Histogram
Mean = 8.16
Std. Dev. = 15.066
N = 55
Frequency
50
40
30
20
10
0
.0
20.0
40.0
60.0
80.0
100.0
Pb
BM-303: 55
MM-105: 97

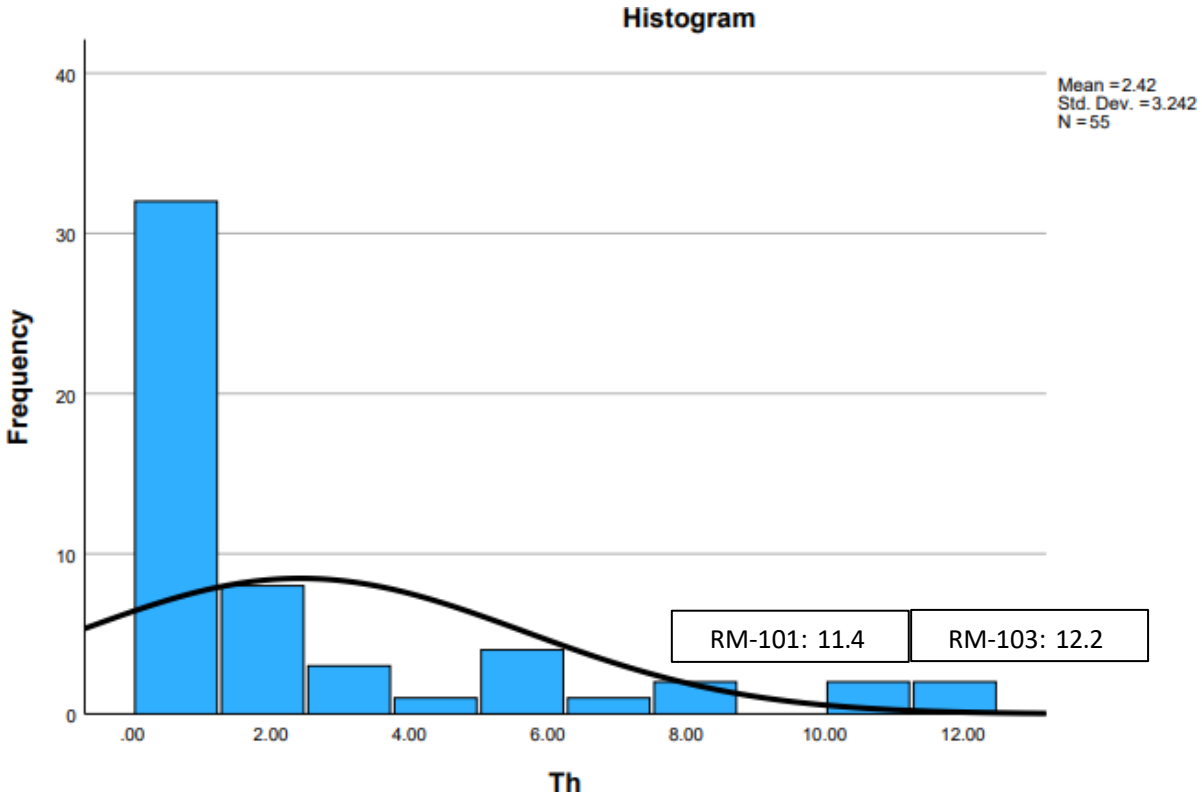
Histogram
Mean =2.42
Std. Dev. =3.242
N =55
Frequency
40
30
20
10
0
.00
2.00
4.00
6.00
8.00
10.00
12.00
Th
RM-101: 11.4
RM-103: 12.2

,

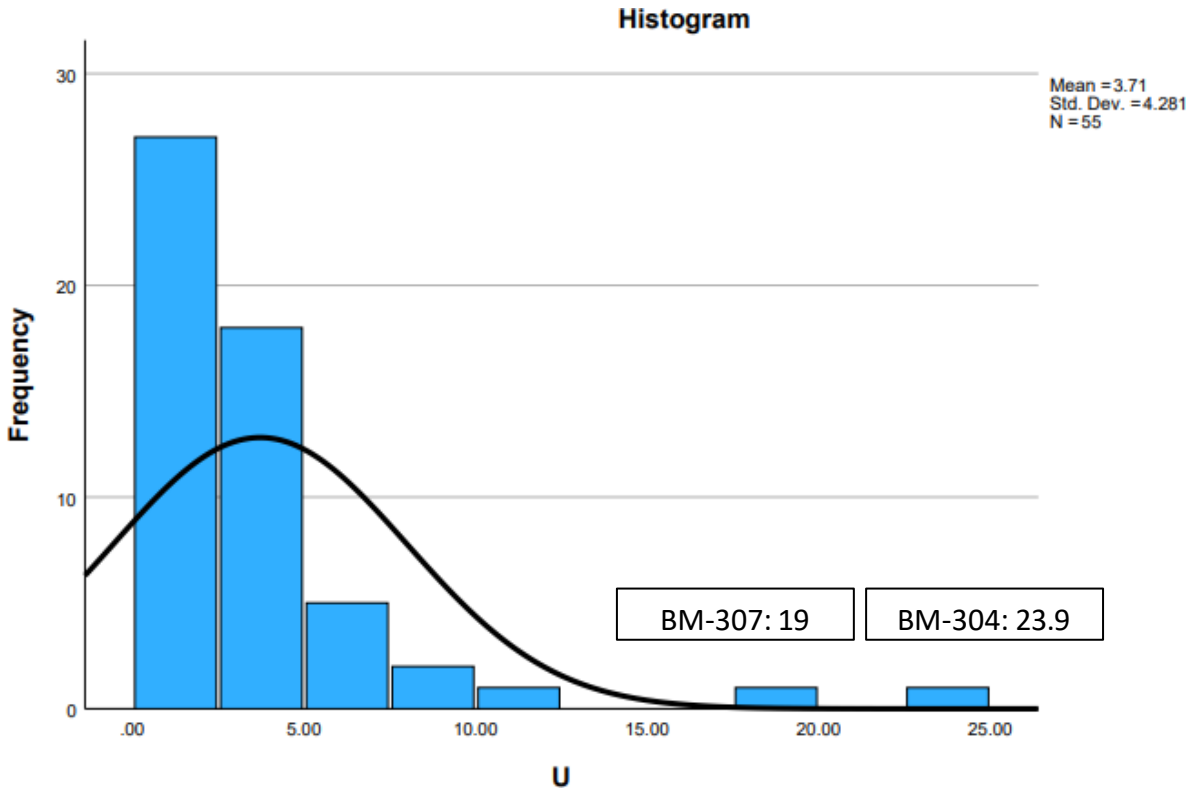
Histogram
Mean =3.71
Std. Dev. =4.281
N =55
Frequency
30
20
10
0
.00
5.00
10.00
15.00
20.00
25.00
U
BM-307: 19
BM-304: 23.9

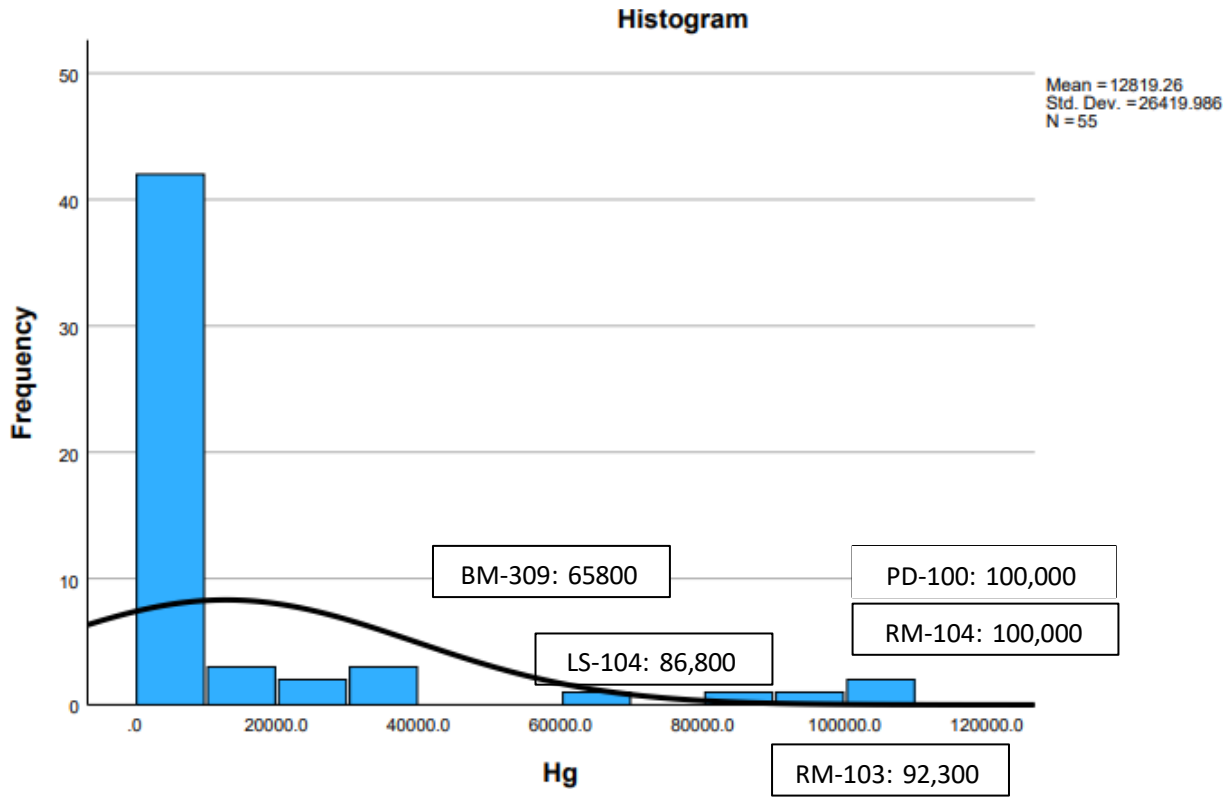
Histogram
Mean = 12819.26
Std. Dev. = 26419.986
N = 55
Frequency
50
40
30
20
10
0
.0
20000.0
40000.0
60000.0
80000.0
100000.0
120000.0
Hg
BM-309: 65800
LS-104: 86,800
PD-100: 100,000
RM-104: 100,000
RM-103: 92,300

Appendix 2

Number of outliers	Unimodal with Outliers	Bimodal with outliers
1	V, Cr, Co, Sr, Sn, Cs, Pr, Sm, Lu, Hf, Ta, W	Ge, Tm, Yb, Tl,
2	Zr, Nb, Mo, Sb, Ba, Ce, Tb, Pb, U	Zn, Th
3	Nd, Eu, Gd, Dy,	
4	As, Rb, La	Ga, Y,
5		Hg
6	Ho,	
7	Er	

Unimodal 1 outlier	Unimodal 2 outliers	Unimodal 3 outliers	Unimodal 4 outliers	Unimodal 5 outliers	Unimodal 6 outliers: Holmium	Unimodal 7 outliers: Erbium
Vanadium :BM-304: 680	Barium MM-100: 13700 MM-105: 9260	Neodymium CM-400 53.6 BM-100: 47.3 RM-100: 37.6	Arsenic BM-300: 2000 BM-308: 1620 BM-307: 877 BM-304: 572		RM-105: 1.27	BM-303: 3.67
Tungsten MM-105: 337					BM-303: 1.24	RM-105:3.25
Chromium : RM-100: 260	Zirconium BM-303: 688 CM-400: 302				CM-400: 1.04	CM-400
Cobalt : MM-105: 188		Europium CM-400: 3.08 RM-100: 2 RM-105: 1.87			RM-100: 0.8	RM-101: 2.41
Cesium RM-100: 97.4	Niobium BM-303: 210 CM-400: 56.6		Rubidium RM-100: 143 RM-101:118 RM-103:84 RM-104: 71		RM-101: 0.8	RM-103: 2.28
Tantalum BM-303: 17.60					RM-103: 0.8	RM-100: 1.93
Hafnium: BM-303: 16.80	Antimony BM-300: 159 BM-307: 78.1	Gadolinium RM-105: 8.35 CM-400: 7.99 RM-100: 5.77				RM-104: 1.86
Praseodymium BM-100: 13.4						
Samarium CM-400: 9.9	Cerium BM-100: 139 CM-400: 111		Lanthanum BM-100: 86.1 CM-400: 53.9 RM-100: 35.3 RM-101: 33			
Lutetium : BM-303: .68		Dysprosium RM-105: 7.45 CM-400: 6.24				
Tin BM-303: 15	Molybdenum					

	: BM-307: 91 BM-303: 47	BM-303: 5.91				
	Lead					
	MM-105: 97 BM-303: 55					
	Uranium					
	BM-304: 23.9 BM-307: 19					
	Terbium					
	CM-400: 1.10 RM-105: 1.4					

Bimodal 1 outlier	Bimodal 2 outliers	Bimodal 3 outliers	Bimodal 4 outliers	Bimodal 5 outliers	Bimodal 6 outliers	Bimodal 7 outliers
Thallium BM-307: 21.6	Zinc MM-105: 250 BM-304: 200		Gallium CM-400: 19 RM-100: 18 RM-101: 17 RM-103: 15	Mercury PD-100: 100,000 RM-104: 100,000 RM-103: 92,300 LS-104: 86,800 BM-309:65,800		
Germanium BM-304: 14.6	Thorium RM-103: 12.2 RM-101: 11.4		Yttrium RM-105: 34.5 BM-303: 31.8 CM-400: 28.9 RM-100: 21.8			
Ytterbium BM-303: 4.33						
Thulium BM-303: .61						

REE	RM	Bp2	MM	CM	BM
Y Yttrium:	RM-100: 20.4, RM-101: 21.8, RM-103: 20.1, RM-105: 34.5			CM-400: 28.9,	BM-303: 31.8
La Lanthanum:	RM-100: 35.3, RM-101: 33			CM-400: 53.9,	BM-100: 86.1
Ce Cesium:	RM-100: 97.4, RM-101: 15.1, RM-103: 10.7				
Pr Praseodymium:	RM-100: 8.69, RM-101:8, RM-103: 7.59 RM-105: 8.68			CM-400: 12.5	BM-100: 13.4
Nd Neodymium:	RM-100: 35.9, RM-101: 29.8, RM-103: 27.7, RM-104: 23.8, RM-105: 37.6		MM-201: 16.2	CM-400 53.6	BM-100: 47.3
Pm					
Sm Samarium:	RM-100: 7.5, RM-101: 6, RM-103: 5.32, RM-104: 4.53 RM-105: 9.3,			CM-400: 9.9	BM-100: 5.5, BM-303: 4.12
Eu Europium:	RM-100: 2, RM-101: 1.07 RM-105: 1.87,			CM-400: 3.08	
Gd Gadolinium:	RM-100: 5.77, RM-101: 4.39,	Bp2-404: 2.55	MM-201: 2.58	CM-400: 7.99	BM-100: 3.03 BM-303: 4.18

	RM-103: 3.78, RM-104: 3.11, RM-105: 8.35				
Tb Terbium:	RM-100: 0.8, RM-101:0.7, RM-103: 0.6, RM-104: 0.5, RM-105: 1.4,	Bp2-404: 0.4	MM-201: 0.4	CM-400: 1.10	BM-303: 0.9
Dy Dysprosium:	RM-100: 4.31, RM-101: 4.42, RM-103: 3.86, RM-104: 3.18 RM-105: 7.45,	Bp2-404: 2.40	MM-201: 2.41	CM-400: 6.24	BM-303: 5.91
Ho Holmium:	RM-100: 0.8 RM-101: 0.8, RM-103: 0.8, RM-104: 0.6 RM-105: 1.27	Bp2-404: 0.4	MM-201: 0.5	CM-400: 1.04	BM-303: 1.24
Er Erbium:	RM-100: 1.93, RM-101: 2.41, RM-103: 2.28, RM-104: 1.86 RM-105: 3.25,	Bp2-404: 1.20	MM-201: 1.30, MM-200: 1.12	CM-400: 2.79	BM-303: 3.67
Tm Thulium:	RM-101: .35, RM-103: .34 RM-105: 0.4,			CM-400: .35	BM-303: .61
Yb Ytterbium:	RM-100: 1.7, RM-101: 2.37, RM-103: 2.25, RM-104: 1.9, RM-105: 2.47	Bp2-404: 1.1	MM-200: 1.1 MM-201: 1.2	CM-400: 2.25,	BM-303: 4.33
Lu Lutetium:	RM-100: 0.23 RM-101: .35,		MM-201: 0.2, MM-202: 0.2,	CM-400: .34	BM-303: .68

	RM-103: .34, RM-104: 0.3, RM-105: 0.4,		MM-200: 0.2, MM-103: 0.2		

Sample location	Enriched in:
Cm-400	Er, Ho, Dy, Gd, Eu, Sm, Nd, Pr, Ce, La, Y, Tb, Nb, Zr, Ga
BM-303	Lu, Dy, Yb, Tm, Er, Ho, Y, Pb, Ta, Hf, Zr, Nb, Mo, Sn
RM-105	Dy, Er, Tb, Gd, Eu, Sm, Y, Ho, Nd
RM-100	Ho, Gd, Eu, Sm, Cs, Rb, Ga, Cr
RM-103	Ho, Er, Rb, Ga, Th, Hg
RM-101	Er, Ho, Y, Rb, Ga, Th
BM-307	U, Tl, Sb, As, Mo
BM-304	U, As, Ge, Zn, V
MM-105	Pb, W, Ba, Zn, Co
BM-100	Pr, Ce, La, Nd
RM-104	Ho, Hg, Rb
MM-100	Ba, Sr
BM-300	Sb, As
BM-308	As, Ge
PD-100	Hg
LS-104	Hg

Vita

Eduardo Lee Zuniga was born in El Paso, Tx, To Eduardo B. and Debbie R. Zuniga. Raised in the agricultural town of Clint, Tx with an older sibling. Growing up in a rural agricultural town Eduardo (Eddie) Fostered an appreciation for the outdoors and nature. Both parents were teachers, His Dad was a high school chemistry teacher while his Mom was an 8th grade reading teacher. In this setting and environment his thirst for knowledge and outdoors grew into an interest in geological sciences. Acquiring two associate degrees from El Paso Community College (EPCC) one in geological sciences and the other in Multi-Disciplinary Sciences, he went on to pursue a Bachelor of science in Geology from the University of Texas at El Paso (UTEP). This was not the end of his education, he continued to pursue a Master of Science in Geology from UTEP and a master's in education from Western Governors University. Throughout his educational career he would maintain a position on the Dean's list and become a member the Alpha Chi National Honors society. His research history consists of several directed study and independent research starting at EPCC with mentor Robert Rohbaugh, he studied fault structures in the Hueco Mountains. His other research: he mapped Several areas around the southwestern United states, assist graduate students mapping a vertical and horizontal amalgamation of cross bedded structures in Gypsum Valley, map vertical walls in Big Bend National Park using a Gigapan system and Drones. He also helped EPCC with their drone program and Gigamacro system, where he created virtual educational tools. For the master's in education research, his thesis focused on experiential learning, and he used a guided hike to complete his research. Eddie Zuniga is a local community geology guide for organizations such as Celebration of our Mountain, Geo-ventures, Insights Museum, and his own personal outdoor guide business, Natural High Outdoor Guide.

Contact information: elzuniga@miners.utep.edu